Tools for Studying Metabolism in the Human Gastrointestinal Microbiome

---

A Dissertation

Presented to

The faculty of the School of Engineering and Applied Science

University of Virginia

In partial fulfillment

Of the requirements for the degree

Doctor of Philosophy

By

Thomas James Moutinho Jr.

August 2021

APPROVAL SHEET

This

Dissertation

is submitted in partial fulfillment of the requirements
for the degree of

Doctor of Philosophy

Author: Thomas James Moutinho Jr

This Dissertation has been read and approved by the examing committee:

Advisor: Jason Papin, PhD

Advisor:

Committee Member: Jeffery Saucerman, PhD

Committee Member: Kristen Naegle, PhD

Committee Member: Philip Bourne, PhD

Committee Member: Sean Moore, MD

Committee Member:

Committee Member:

Accepted for the School of Engineering and Applied Science:

Jennifer L. West, School of Engineering and Applied Science

August 2021

“Biology is chaos. Biological systems are the product not of logic but of evolution, an inelegant process. Life does not choose the logically best design to meet a new situation. It adapts what already exists...The result, unlike the clean straight lines of logic, is often irregular, messy.”

- Author: John M Barry

Abstract

The human gastrointestinal (GI) microbiome is a complex ecosystem consisting of trillions of microorganisms. The microbial life present in the gut contributes significantly to human physiological processes, health, and well-being. Conversely, disturbances in the GI microbiome have been correlated with a broad array of diseases, having a particularly strong connection to the brain, immune system, cardiovascular system, and GI tract. With a high exposure to external factors, the GI microbiome can be rapidly influenced by drugs, diet, and life-style. There is a need for an improved understanding of GI microbial communities for applications in medical diagnostics and treatments. In this dissertation I worked to advance three distinct tools for the study of GI microbiomes. In aim 1, I identify biomarkers for Parenteral Nutrition Associated Cholestasis in neonatal intensive care unit (NICU) infants using 16S sequencing data and fecal metabolomics. This aim is the first step in work to develop a point-of-care diagnostic tool to expand precision medicine in the NICU. Leveraging systems biology to understand clinical microbiome data and developing a mechanistic understanding of pathophysiology requires advanced research tools. In aim 2, I design and develop a computational tool to aid in the procedural generation of organism-specific metabolic network reconstructions that explicitly accounts for uncertainty in the datasets utilized for the building process. An essential aspect of this tool relies on an alteration to the structure of these models for enhanced representation of the biological evidence for the resulting network. In aim 3, I developed an *in vitro* culture device for the pairwise co-culture of microbes to study contact-independent microbial interactions. The co-culture plate allows bacterial growth curves to be generated for two microbial cultures that are physically separated by a semipermeable membrane while interacting via diffusion. Contact-independent interactions are important for understanding the mechanisms that influence how microorganisms interact in communities. This dissertation covers the design and development of three different tools for the study and leveraging of the human GI microbiome to improve the treatment of associated diseases.

Acknowledgements

Although this section does not exhaustively articulate the gratitude I feel for all of the people who have impacted my life, I would like explicitly thank many of the people who have impacted me over the years.

To my mentor, Jason Papin, thank you for your unyielding optimism and for all of your support on and off for the past 9 years.

To my committee, Jeff Saucerman, Kristen Naegle, Sean Moore, and Philip Bourne, thank you for your support and guidance throughout my graduate studies. I greatly appreciate all of the advice and effort you provided over the years.

To the Papin Lab, Laura, Matt J, Anna, Matt B, Glynis, Phil, Edik, Kris, Bonnie, Greg, Maureen, Lillian, Deb, Joe, and Dawson, thank you for your thoughtful input on my work over the years. I am grateful to have worked alongside each of you.

To all of my friends, thanks for all of the wonderful adventures and memories.

To all of the undergraduates I mentored over the years, thank you for helping me to develop my teaching and leadership skills.

Will Guilford and Brian Helmke, thank you for teaching me all about pedagogy during my time TAing for each of you.

To my parents, Tom and Michelle, thank you for your consistent support and love over the years, I never could have achieved any of this without you.

To my siblings, Jennifer and Joe, thank you for navigating life with me; it has been a crazy ride so far.

To the rest of my extended family, thanks for all of you support, guidance, and love.

Thank you to my in-laws, Kristine and Jamie, you make Virginia feel like home.

Finally, thank you to my wife, Melissa, and pup, Sebago. You have been an absolutely essential grounding point for me over the years.

Table of Contents

Table of Figures

Table of Tables

Chapter 1 Introduction

1.1 The Human Gastrointestinal Microbiome

The human body harbors trillions of microorganisms that form complex ecosystems called microbiomes (1,2). Microbial ecosystems reside on all bodily surfaces that are exposed, directly or indirectly, to the external environment. The skin, lungs, gastrointestinal tract, and vagina all have distinct microbial ecosystems (3–7). The organisms, or microbiota, present in these ecosystems are primarily bacteria, archaea, and fungi (8–10). The remaining abiotic components that are present along with the resident microbiota, such as metabolites, sum up to be defined as the microbiome (11). Currently the study of human microbiomes is primarily focused on bacterial populations living on the human body (12,13). However, there are additional fields of study focused on the other types of microorganisms present, while also including viruses (8–10,14). The communities of bacteria living on the human body are commonly measured in several ways: the total weight of resident microbes ranges from 2-4 kilograms, the number of individual cells is roughly equivalent to the number to human cells with nuclei, and the amount of non-human genetic material is roughly 150 times greater than the human genome (1,15,16). However, it has been proposed that the gastrointestinal microbiota should be considered an independent human organ, due to how essential it is to human physiology (17–20). Therefore, perhaps the most important lens through which we can measure human associated microbiota is grounded in the health promoting physiological contributions provided by the resident microbiota (8,10,21–28).

There are several exceptionally important functions that the GI microbiota contributes to human physiology. Three of the most important functions are colonization resistance against GI pathogens, training of the immune system, and the production of valuable metabolites (26). Colonization resistance is an emergent property of a robust microbial community present in the GI tract (27). Just as a healthy ecosystem is resistant and resilient to invasion, the human GI microbiota is best

able to resist colonization from foreign microbes when there is sufficient diversity and ecological stability (27,29). The GI microbiota has an exceptionally intimate connection to the immune system. The current understanding is that the immune system directly samples the GI microbiota resulting in proper regulation of autoimmunity (30). Additionally, the immune system plays in important role in regulating the community composition primarily via mucus composition and anti-bacterial peptides (29). Finally, the GI microbiota aids in the digestion of fiber in the colon while producing essential metabolites. Short-chain fatty acids are the primary example of metabolic byproducts from the GI microbiome that have a significant impact on the human body; they are an energy source for colonocytes that also provide important anti-inflammatory signaling (31–37). Examples of other physiologically important metabolic byproducts that are produced by the GI microbiota include several essential amino acids, vitamins, and neurotransmitters (31,38).

Human microbiomes can readily be altered by exposure to the external environment (39). The fact that human microbiomes can be influenced by external factors is a double-edged sword from a medical point of view. Although we can quickly resort microbial communities to improve health outcomes, such as fecal microbiota transplants for the effective treatment of *C. difficile*, there are also many aspects of daily life that have an enormous impact on the composition and functions of the GI microbiota (40). These aspects include sleep, stress, diet, therapeutics, and exercise (39,41,42). The GI microbiota also contributes to the production of detrimental compounds such as TMAO and enterotoxins (43). It has been shown that there are measurable negative health outcomes that result from the disruption of the GI microbiome due to infection, genetic factors, poor diet, or other deleterious life-style choices (41,42). The GI microbiome is an aspect of human physiology that can be rapidly changed to either promote or negatively impact overall health at a systems-level.

1.2 Gaps in medical knowledge about the GI Microbiome

Over the past several years there has been an explosion in the number of correlations identified that link various diseases with disturbances in the GI microbiome (43,44). There are two major classifications that each of these correlative links will ultimately fall into: (a) correlative biomarkers that can be leveraged to diagnose disease, and (b) governing causal mechanisms that drive the disease in question. Both classifications require an improved understanding to create accurate diagnostic tests and, with greater difficulty, to characterize the mechanisms with the GI microbiome that are driving a disease. Improved understanding of both of these two areas of research will improve the treatment of several difficult diseases that are currently on the rise across the globe.

There are several existing types of treatments that have demonstrated utility in the treatment of human disease, in the case when the GI microbiota is causally linked. The most promising treatment that has recently become common in clinical practice is the fecal microbiota transplant (FMT) for the direct treatment of *C. difficile* infection. FMTs have been found to be impressively successful compared to other treatment options (40). Other probiotic treatments similar to FMTs have also been shown to be clinically relevant, such as the use of Lactobacilli for the treatment of inflammatory bowel disease (IBD) (45). Another related treatment option is to alter nutritional inputs to alter community composition and increase diversity. There is a growing body of research exploring how various types of fiber influence the composition of resident microbiota. This type of intervention is largely relevant for chronic diseases such as cardiovascular disease, IBD, colorectal cancer, depression, and obesity (46). The final important aspect of microbiome research in medicine involves understanding how drugs interact with the GI microbiome (47). Improvements in antibiotic usage may result in a reduction in the prevalence of *C. difficile* infections; the use of broad-spectrum antibiotics disrupts the GI microbiota providing an opportunity for *C. difficile* to flourish and begin producing toxins (48,49). Additionally, there are

examples of drugs that have been metabolized by the liver being converted into toxic metabolites by resident microbes (43,47).

The need for more advanced analysis techniques has become obvious with the advent of large complex datasets that are now available for studying the GI microbiome. The precise perturbation of a GI microbiota *in situ* is a daunting task that requires a great deal of mechanistic understanding of how microbial communities function. Currently, existing treatments are either utilized as a last resort (e.g. FMTs), or are particularly nonspecific and unreliable (e.g. generic probiotic supplements). Bioinformatics and systems biology have both developed in part to help solve complex medical challenges related to diagnosing disease earlier and more accurately, while also improving understanding of the causative factors driving disease. Specifically, for the GI microbiome, there is a great deal of interest in utilizing systems biology to understand how metabolites and drugs flow through microbial communities in order to understand how to precisely alter the community to induce an intended affect (50).

1.3 Systems biology: Applying advanced mathematics to complex biological systems

Biological systems are composed of interacting components that are typically governed by simple rules, but result in complex emergent behaviors. Systems biology aims to understand how perturbations impact complex biological systems for targeted manipulation of a system, diagnosis of why a system is behaving a certain way, or predicting how a system will change as a result of a specific perturbation. The goals for systems biology are achieved via the collection of high-throughput data, advanced statistics, and quantitively modeling (51). The methods and models utilized to study biological data are based on and designed for vast sets of biological observations. Combining different forms of biological data is an essential aspect of understanding biological systems, in part, due to the innate uncertainty associated with each type of data. Reference databases have become absolutely essential for all aspects of analyzing biological data. There are two broad applications of systems biology that are

particularly relevant to this dissertation: machine learning, and quantitative network modeling of biological systems. When combined, these two methods provide a path forward for studying the governing mechanisms of human associated microbiota.

Machine learning that has been tailored to systems biology data is a field of study grounded in advances statistical techniques that leverage computational power to make high-dimensional data more human interpretable and to establish the variables in a dataset that contribute most to the classification of samples into known experimental groups. Unsupervised machine learning provides a variety of tools for determining classifications based on similarity across samples within a dataset and supervised learning utilizes known experimental groups to determine a small set of variables that are the primary drivers that differentiate the groups (52).

Quantitative network modeling includes many different variations, notably: signaling, regulatory, and metabolic network modeling (51). All three involve data that represents the connections (edges) between components (nodes). The relationships among components in a system are particularly important because it is this information that allows for the modeling systems-level emergent behavior. For metabolic network the three high-throughput dataset that are most common are genomics, transcriptomics, and proteomics (51,53). These data are utilized to determine how phenotypic data can be mechanistically explained. When studying metabolism within a cell, it can be helpful to incorporate known biochemical structure when analyzing high-throughput data. Known biochemical structure includes the process of how a gene is translated into a protein, the stoichiometry of biochemical reactions that are catalyzed by enzymes, and the thermodynamics of biochemical reactions (51). Each additional layer of information can help to contextualize and intelligently connect different types of high-throughput data. Genome-scale metabolic network reconstructions (GENREs) are an example of a type of model that is capable of contextualizing a larger array of data types (54,55). GENREs are increasingly being used to understand microbial communities (56,57).

In the case of studying microbial communities, machine learning is an essential tool for determining the microbial species, and metabolites that show the greatest difference among experimental or disease groups. Quantitative network modeling can be utilized to gain a better understand of how the key actors in a community are metabolizing environmental compounds. An existing gap in the study of metabolism in microbial communities is a lack of data for the mechanisms that govern how microbes interact with one another.

1.4 Clinical diagnostic technology and precision medicine

Precision medicine was born from the advent of genomics. An overarching goal of personalized medicine is to maximize an individual's health outcomes by intervening sooner to ultimately prevent serious disease (58,59). Therefore, an essential aspect of personalized medicine is rapid and accurate diagnostics tools that allow for preventative medicine. Currently, medical teams in the NICU rely on precision medicine. Genetic information, collected from blood samples, is a form static precision medicine because the patient's genome is a source of unchanging information (60). Whereas, constant monitoring of metabolic markers in the blood is an example of dynamic precision medicine. Both aspects contribute to precisely treating each infant to maximize health outcomes. However, diseases still remain to be diagnosed via exclusion, thus necessitating more precise diagnostics and mechanistic understanding. Systems biology and advanced statistics provide a path forward toward personalized medicine that is grounded in the analysis of readily available biological materials, such as blood, stool, urine, and DNA. The study of human waste products has gained interest due to advancements in data collection technologies, such as metabolomics and genomics (61,62). Stool samples provide research with a glimpse of the microbiome present in the GI tract of an individual. However, analysis of these samples can be difficult due to their complexity. Nevertheless, it has been shown that certain microorganisms and metabolites are correlated with disease (63). A better understanding of these correlations may provide medical teams with additional diagnostics for personalized medicine.

1.5 Constraint-based Computational Modeling: Utilizing Optimization to Understand Biological Systems

Systems biology can take many forms, one of these is constraint-based computational modeling (CBM). CBM leverages mathematical optimization and linear algebra to computationally represent biological systems. One class of CBMs are genome-scale metabolic network reconstructions (GENREs) are quantitative biological models of metabolism that are structured to leverage mathematical optimization to represent all known biochemical reactions that occur in a cell (51,64). The biochemical reactions that are thought to occur in an organism are represented in a hypergraph network by explicitly accounting for all of the reaction stoichiometries and metabolite conversions at an elemental level. Each reaction consists of metabolites that are composed on their constituent elements with an associated structure. These data can be utilized to perform Flux Balance Analysis (FBA), an optimization technique that, in its most basic form, allows a researcher to maximize the production of a certain set of metabolites. Most commonly for prokaryotes, the set of metabolites selected to be maximally produced represent cellular biomass and thus growth (64). The resulting output data is the metabolic flux distribution through the network, an indication of the reactions that are required for optimal growth of the organism in a given growth condition. This type of model can also be utilized to have different objective functions, aside from maximizing growth, that provide the researcher with the ability to explore different aspects of a metabolic network.

GENREs have been shown to accurately determine the reactions that are actively catalyzed by an organism during exponential growth phase (64). However, accurate reaction flux values are dependent upon building a GENRE that contains the reactions that are catalyzed by an organism. The building process of a GENRE is a difficult task that requires genomic data to be annotated based on reference databases to determine a set of reactions that are thought to be catalyzed by an organism (64). Other functional data is then utilized to further improve the GENRE to increase the network

accuracy when recapitulating the associated phenotypic data (64). For the study of microbial communities and microbe-microbe metabolic interactions, there is a great need for more advanced methods of quickly building accurate GENREs. Additionally, GENREs offer a means for contextualizing other forms of data, such as transcriptomics, proteomics, and metabolomics. Since each node in a GENRE represents a biochemical reaction, there are several ways of determining which reactions are actively catalyzed in a given condition. Each genomics, transcriptomics, and proteomics provide information about the presence enzymes. Metabolomics provides an opportunity to determine the metabolites that are present and thus are a measure of the functional output of an organism. However, when accounting for associated uncertainty, the knowledge of which reactions are active in an organism remains under-constrained; therefore necessitating a quantitative representation of the resulting uncertainty when building a GENRE.

1.6 Experimental data collection

The optimal combination of computational modeling and sophisticated *in vitro* biological data is an important step forward for understanding biological systems. A thorough understanding of the limitations involved with computational modeling in tandem with advanced *in vitro* techniques is important for establishing a functional understanding of how a biological system behaves. An essential aspect of computational modeling and understanding complex biological mechanisms is grounded in the acquisition of *in vitro* biological data. For studying microbial interactions that occur within microbial communities, such as the GI microbiome, it has been shown that pairwise interactions provide a great deal of information about how higher-order interactions occur (65). Therefore, generating experimental data about how pairs of different microorganisms interact is a valuable for building computational models to represent microbial communities. Although there are many new high-throughput datatypes, there remains a need for elegant experimental design to best align the data collected with the innate assumptions that constrain the computational techniques available for analysis. In order to study the

metabolic cascade of compounds through a microbial community, there is a need for better culturing techniques that allow for researchers to determine how pairs of microbial species may interact within a community.

1.7 Dissertation Specific Aims: A Preview

A unique characteristic of engineering is that we aim to identify problems that can be solved through the elegant design of tools. It is an incremental process of improving upon existing technologies/tools while maintaining an understanding of the constraints and objectives when designing the optimal solution. If a tool is ever to be utilized and ultimately have a positive impact on the world, the engineer designing it must account for not only quality of the tool, but also costs associated with building and using the tool. In this dissertation, I identified three problems in studying the GI microbiome and designed tools to attempt to solve these problems.

In Chapters 2 and 3, I discuss the first aim of my dissertation. I identify biomarkers for Parenteral Nutrition Associated Cholestasis (PNAC) in neonatal intensive care unit (NICU) infants using 16S sequencing data and fecal metabolomics. PNAC is a specific type of liver disease that often occurs in NICU infants that can be difficult to diagnose and treat quickly (66). In the first study presented in this chapter, we utilized 16S sequencing data from stool samples to determine the microbial genera that are highly associated with PNAC. In the second study presented in this chapter, we identified fecal metabolic biomarkers for the early detection of PNAC that may provide medical teams with an indication that an infant is beginning to develop PNAC before the standard clinical metric is detected in the blood. Finally, we calculated the expected accuracy of a diagnostic tool using a small set of fecal metabolites to predict infants at risk of developing PNAC.

In Chapter 4, for my second aim, I design and develop a tool to aid in the procedural generation of GENREs while explicitly accounting for the uncertainty in the source genetic annotation data utilized

for the reconstruction process. This method is called CANYUNs (**C**onstraint-based **A**nalysis **Y**ielding reaction certainty and **U**sage across metabolic **N**etworks) and relies on a novel form for Flux Balance Analysis (FBA) and an altered model structure. The structural changes made to the resulting GENREs are intended to connect the network reconstruction directly to the source biological data utilized during building. We validate the performance of CANYUNs using aerobic and anaerobic growth data across an array of carbon and nitrogen sources for *E. coli* K-12 and benchmarked its performance against a manually curated *E. coli* GENRE.

In Chapter 5, for my third aim, I developed an *in vitro* culture device for the pairwise co-culture of microbes to generate contact-independent microbial interaction data. The design of the co-culture growth plate allows for the generation of bacterial growth curves for two microbial cultures that are physically separated by a semi-permeable membrane while interacting via diffusion. Contact-independent interaction determined with the co-culture plate provides a tool for understanding the different types of mechanisms that influence how microorganisms interact in communities. We validated the performance of the co-culture plate under expected usage conditions. Finally, to demonstrate its utility, we use the co-culture plate to generate contact-independent interaction growth curves for *P. aeruginosa* and *B. cenocepacia*, two pathogens found to interact when infecting patients with cystic fibrosis.

In the final chapter, I conclude this dissertation with a discussion of the broader impacts of the work I was involved with during my PhD career and explore my thoughts on the future work that will follow.

Chapter 2 Microbiota changes in twins discordant for parenteral nutrition associated cholestasis

Thomas J. Moutinho Jr*[5], Suchitra K. Hourigan, MD*[1,2,3,4], Andrew Berenz, MD[6], Jason Papin, PhD[5], Pallabi Guha, MD[1,4], Lois Bangiolo, MD[1], Sandra Oliphant, RN[7], Marina Provenzano, MA[2], Raj Baveja, MD[8], Robin Baker, MD[8], Thierry Vilboux, PhD[2], Shira Levy, MA[1,2], Varsha Deopujari, MD[1,2], James Nataro, MD[7], John E. Niederhuber, MD[2,4,7], Sean R. Moore, MD[7]

***Joint first authors**

1. Inova Children's Hospital
2. Inova Translational Medicine Institute
3. Pediatric Specialists of Virginia
4. Johns Hopkins School of Medicine
5. Department of Biomedical Engineering, University of Virginia
6. Department of Pediatrics, Rush Medical College
7. Department of Pediatrics, University of Virginia
8. Fairfax Neonatal Associates

Published work in Journal of Pediatric Gastroenterology and Nutrition; 2020

2.1 Abstract

Parenteral nutrition associated cholestasis (PNAC) causes significant morbidity in the NICU. Infection with gut-associated bacteria is associated with cholestasis but the role of intestinal microbiota in PNAC is poorly understood. We examined the composition of stool microbiota from premature twins discordant for PNAC as a strategy to reduce confounding from variables associated with both microbiota and cholestasis. Eighty-four serial stool samples were included from four twin sets discordant for PNAC. Random Forests was utilized to determine genera most discriminatory in classifying samples from infants with and without PNAC. In infants with PNAC, we detected a significant increase in the relative abundance of Klebsiella, Veillonella, Enterobacter and Enterococcus ($P<0.05$). Bray-Curtis dissimilarities were significantly different ($p<0.05$) from infants with and without PNAC. Our findings warrant further exploration in larger cohorts and experimental models of PNAC to determine if a microbiota signature predicts PNAC, setting the stage for interventions to mitigate liver injury.

2.2 Introduction

Parenteral nutrition (PN) is an essential component of nutritional support for premature infants yet is frequently complicated by its association with liver disease. Preterm infants are at increased risk of developing PN associated cholestasis (PNAC) due to immaturity of the hepatobiliary system compounded by lack of enteral feeding (67), with cholestasis often persisting after PN cessation (68). Thus PNAC causes significant morbidity in the neonatal intensive care unit (NICU) and beyond (69). Clinical factors associated with PNAC include low birth weight, longer duration of PN, delayed enteral nutrition, antimicrobial administration, gram-negative infections, necrotizing enterocolitis and, gastrointestinal malformations (66).

Altering the composition of PN and lipid sparing strategies to prevent or alleviate the development of cholestasis has been partially successful (70). More recently, studies have focused on the role of the intestinal microbiota in the development of PNAC. PN has been associated with an altered intestinal microbiota (71), although this can be difficult to separate from the effect of lack of enteral nutrition on the microbiota. Evidence also suggests that cholestasis may be related to the composition of the microbiota (72,73). Bile acids, diminished in cholestasis, normally have an antimicrobial effect on the microbiota; conversely, the intestinal microbiota metabolizes and biotransforms bile acids (73). In adults, perturbations in the intestinal microbiota have been associated with worsening liver function, cirrhosis, and primary biliary cholangitis, with dysbiosis worsening as liver disease progresses (74,75).

In a prior study of infants with short bowel syndrome receiving PN, infants who developed PN-associated liver disease displayed less diverse microbiota and a higher abundance of pathogenic bacteria (76). Moreover, infection with gram-negative bacteria, including *Escherichia coli* urinary tract infections or *Klebsiella* septicemia, has been associated with the development of cholestasis (74–78).

Early enteral feeding has been shown to be the most effective maneuver to prevent the development of cholestasis (79); however, initiation of enteral feeding in the NICU is often restricted by clinical factors. Other targets to decrease the burden of PNAC in the NICU are needed and the intestinal microbiota provides a compelling target. Due to methodological challenges in comparing infants with different genetics, diets, and environments, little is known about changes in the intestinal microbiota associated with PNAC in NICU patients. Therefore, the goal of this study was to investigate intestinal microbiota composition from serial stool samples of premature twins discordant for PNAC.

2.3 Methods

Subjects and sample collection

Subjects were chosen from a larger cohort in two ongoing neonatal microbiome studies from level IV NICUs at Inova Fairfax Hospital, Virginia (IRB approval #15-1945) and the University of Virginia (IRB approval #18244). Neonates with an anticipated length of stay over 5 days were recruited. Detailed maternal, pregnancy and delivery data were collected. While in the NICU infants had stool collected at least twice a week and frozen at -80°C within 12 hours. Detailed data regarding feeding, medications and health status were collected.

Twin sets were selected for discordance for PNAC, i.e., twin pairs simultaneously receiving PN but only one twin developed PNAC. Selected subjects were admitted to the NICU for prematurity only; no subject developed necrotizing enterocolitis. Subjects were not included from the larger cohort if they were singletons, had cholestasis from causes other than PNAC, were admitted to the NICU for causes other than prematurity, had congenital abnormalities or developed necrotizing enterocolitis. PNAC was defined as a direct bilirubin level of ≥1mg/dL, deemed to be caused by PN by the treating physician, with no other apparent causes for cholestasis (80). Tests conducted to screen for other causes of cholestasis included a right upper quadrant ultrasound, Alpha-1 Antitrypsin deficiency testing, urine CMV PCR, urine culture and thyroid stimulating hormone; specific tests conducted varied for each cholestatic subject.

Twin sets were chosen as a strategy to reduce potential confounding variables associated with both the microbiota and cholestasis including age, intrauterine environment, genetics (although the environment has been shown to dominate the shaping of the microbiome more than genetics (81)) and maternal breast milk.

DNA extraction and 16S ribosomal RNA gene sequencing

Whole stool samples were stored at -80°C until DNA extraction. Prepped samples were loaded on the EZ1 Advanced (Qiagen, Valencia, CA) using the EZ1 Tissue Kit and the Bacterial DNA Extraction protocol card. Samples were cleaned and concentrated using the DNeasy PowerClean Cleanup kit (Qiagen, Valencia, CA).

Sequencing libraries were prepared using a Nextera XT kit (Illumina, San Diego, CA) using a modified Illumina 16S Metagenomics Sequencing Library Preparation protocol for analysis of hypervariable region V4. Each sample was sequenced on the Illumina MiSeq with paired-end reads of 301bp. Sequencing of negative controls of lysis buffer and positive controls of *Staphylococcus aureus* (Strain NCTC 8532, ATCC, VA) and *Escherichia coli* (Strain NCTC 9001, ATCC, VA) were included. The sequence data are being deposited in NCBI Sequence Read Archive (SRA).

16S ribosomal RNA gene analysis

Sequence analysis was performed using DADA2 (version 1.6.0) (82,83). The forward read was truncated to 200 base pairs and reads with ambiguous 'N' bases, and >2 expected errors were filtered out. Chimeras were removed. Taxonomy was assigned using the Ribosomal Database Project's naïve Bayesian classifier (84) with RDP training set 16. Resulting sequence variant counts (SVs) and taxonomic assignments were analyzed using several R packages: Phyloseq (v. 1.22.3), Vegan (v. 2.4.6), GGplot2 (v. 2.2.1), and mice (v. 2.46.0) (85,86). Ultralow abundance SVs (<2 raw reads and present in <5% of samples) were removed. Missing values in the metadata were imputed using mice. Benjamini-Hochberg corrected Wilcoxon rank sum tests were used to compare the alpha diversity, and genus relative abundances. A

PERNANOVA (Adonis test in the Vegan R package) was used to compare the sample clusters displayed in the non-metric multidimensional scaling (NMDS) ordination plot.

Random Forest model generation

The R package AUCRF (v. 1.1) was used to generate a Random Forest (RF) model to classify the samples according to the disease state of the individual each sample was sourced from. Relative SV counts, agglomerated to the genus taxonomic level were used to train the RF. During the creation of an optimal RF, 5-fold cross validation with 20% of the data left out for validation was used to assess the fit of the model. The forest used has 1000 trees with a node split (mtry) of 2, and the classes were manually weighted to account for the imbalance between the PNAC and non-PNAC classes. Features were selected by maximizing model accuracy and minimizing the features required for classification. All code is available on Github (https://github.com/Tjmoutinho/PNAC_microbiome).

2.4 Results

Demographics and clinical characteristics

A total of 84 serial stool samples were included from 4 twin sets discordant for PNAC. Twins ranged from 25 to 31 weeks gestational age (mean = 27 weeks). All twin sets were delivered by emergency Cesarean Section. Each twin set has one subject that was diagnosed with PNAC for part of the sampling period. Birth weights did not differ between twins who did and did not develop cholestasis ($P >> 0.05$, Wilcoxon rank sum test); see birth weights in Supplementary Table 2.1. There was no significant difference in antibiotic exposure between twins who did and did not develop cholestasis. Both members from one twin set (Twin set 3) were treated for sepsis, with negative blood and urine cultures, and hence had more days of antibiotic use than the other twin sets. No other subjects were diagnosed with sepsis or an infection; all blood cultures drawn on all subjects during the study were negative. Twins who developed cholestasis trended towards being on PN longer than their sibling without cholestasis (Table 2.1) due to slower tolerance of advancement of enteral feeds or less satisfactory weight gain, although this difference

was not significant; however cholestasis in the affected twin in all twin sets developed while both twins were still on PN. When enteral feeding was started, all subjects received maternal breast milk. Demographic and clinical characteristics of twin sets are listed in Table 2.1. The range of peak cholestasis in the twins with PNAC was 1.9–10.1mg/dL, mean=5 mg/dL; see hepatic function panel values for subjects in Supplementary Table 2.2.

Table 2.1: Demographic and clinical characteristics of twin sets.

Twin Set	Twin with cholestasis	Gestational age at birth	Twin Type	Sex	Days on PN (Twin A/Twin B)	Days of Antibiotics Use (Twin A/Twin B)
1	A	28w3d	Di-Di	Female/Female	24/15	2/2
2	A	31w3d	Mono-Di	Male/Male	14/11	0/0
3	B	25w1d	Di-Di	Male/Female	20/31	11/9
4	A	25w1d	Mono-Di	Female/Female	26/12	2/5

Di-Di = Dichorionic/Diamniotic. Mono-Di = Monochorionic Diamniotic

PNAC stool samples were different from non-PNAC samples; there were five significantly differentially abundant genera driving this difference.

All samples were classified by the clinical PNAC diagnosis at sampling. PNAC and non-PNAC samples cluster separately ($p < 0.001$, PERMANOVA; Figure 2.1A). There were five statistically significant differentially abundant genera between PNAC and non-PNAC samples ($p < 0.05$, corrected Wilcoxon rank-sum; Figure 2.1B). PNAC was associated with increased levels of gram-negative bacteria *Klebsiella, Veillonella* and *Enterobacter*, increased levels of *Enterococcus* and decreased levels of *Escherichia/Shigella*. *Klebsiella*, *Enterococcus*, and *Veillonella* have the highest median relative abundances and tend to be more abundant in PNAC samples. Alpha diversity (Shannon index) was not significantly associated with PNAC. In several subjects, the alpha diversity increased with age, but this was not seen in all individuals (Figure 2.1C). Five genera dominating most samples (*Staphylococcus, Escherichia/Shigella, Klebsiella, Veillonella, Enterococcus*) consisting of two phyla (Proteobacteria and Firmicutes) (Figure 2.1D).

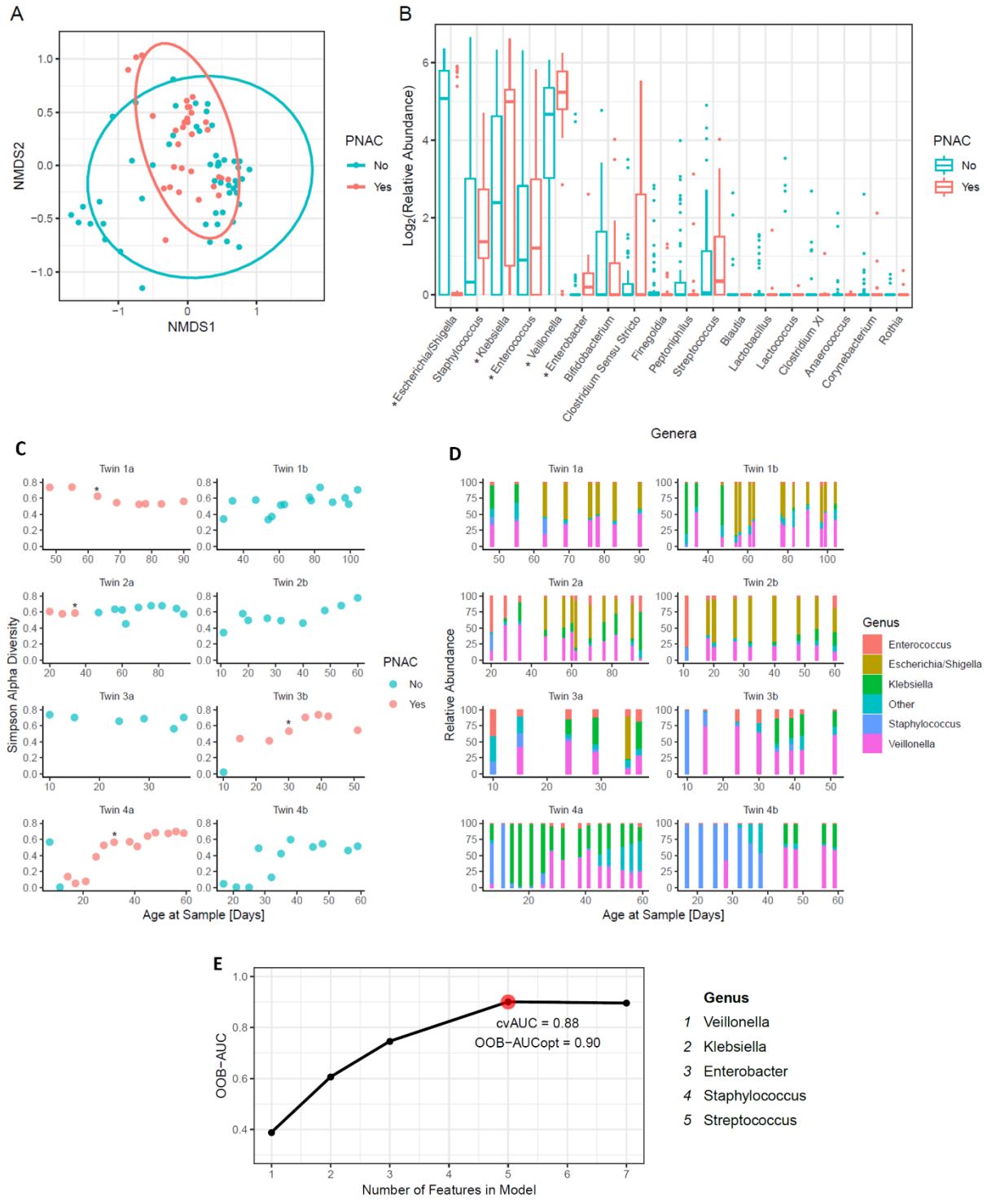

Figure 2.1: Microbiota 16S rRNA gene sequence data.

(A) Microbiota 16S rRNA gene sequence data is visualized using NMDS (Bray-Curtis) to compare samples. The PNAC samples cluster is different from the non-PNAC samples cluster (p< 0.001, PERMANOVA). (B)

Differentially abundant taxa in samples with and without PNAC are starred (*) (Benjamini-Hochberg corrected p-value<0.05). (C) Alpha diversity (Shannon Diversity Index) was not significantly different between PNAC vs non-PNAC. The sample with the greatest direct bilirubin level per subject is starred (*). (D) Relative abundance of microbial genera is displayed for each sample. (E) AUCRF was used to select the optimal random forest model with the lease number of predictive features. The optimal RF model generated for classifying the microbiota samples had an accuracy of 90%. Using 5-fold cross validation, with a 1/5 of the samples for a validation set, the average accuracy was 88%, indicating that the optimal model was not over fit to the dataset. The five microbial features (genera) used in the optimal RF model are displayed. Each feature is listed in order of descending importance to the model.

Random Forest model predicts PNAC based on relative abundance of specific genera.

Feature reductions was performed using AUCRF (Area Under the ROC Curve Random Forest) to identify the microbial features that were predictive of PNAC vs. non-PNAC samples. Feature reduction involved starting with all the genera with at least one non-zero median value as seen in Figure 2.1A. The optimal RF model consisted of five genera and predicts sample diagnosis with 90% accuracy (Figure 2.1E). Five-fold cross validation indicated that the model was not overfit to the dataset. The high predictive capability of the optimal RF model indicates that there is a strong microbial signature associated with PNAC.

2.5 Discussion

We detected significant differences in the stool microbiota of premature twins discordant for PNAC. Specifically, the relative abundance of genera differed, including increased levels of gram-negative bacteria Veillonella, Klebsiella, and Enterobacter in infants with PNAC. This finding is intriguing given well known associations of gram-negative infections in neonates and the development of cholestasis (77,78) and raises the question of whether increased intestinal colonization alone, rather than frank infection, with these microbes is sufficient to provoke cholestasis. Indeed, increased intestinal *Enterobacteriaceae* (74) has been described in adults with cirrhosis, whereas increased Klebsiella and Veillonella has been described in adults with primary biliary cholangitis (75). A predominance of Enterobacteriaceae has also been identified in infants with short bowel syndrome and PN-associated liver disease (76). The actual

407 species and strains associated with PNAC will need to be identified in future studies, using techniques
408 such as shotgun metagenomic sequencing.

409 The extent to which these changes in the relative abundance of genera occur prior to cholestasis
410 versus a result of cholestasis cannot to be answered in this pilot study because cholestatic subjects from
411 two twin sets (1 and 2) developed cholestasis before the first stool sample was collected. However, in one
412 twin set (4) the subject who developed PNAC displayed an increase in *Veillonella* abundance relative to
413 their non-PNAC twin at the same time point. This question is of the utmost importance to answer, due to
414 the significant potential utility of being able to identify which infants might be susceptible to PNAC before
415 clinical evidence of PNAC develops. Early interventions to mitigate the development of PNAC could then
416 be initiated in at risk infants, e.g., early enteral feeding and the use of fish oil-based lipid emulsions (70).
417 While this approach would be difficult to test in human neonates, gnotobiotic models of PNAC might offer
418 one path forward for testing whether specific gram-negative bacteria are predictive, or even causal, in the
419 development of PNAC (87).

420 Certainly, the ability to predict the development of cholestasis based on a microbiota signature
421 would be powerful. In our study, a predictive model of PNAC was created based on five genera, providing
422 a method for identifying informative microbial signatures using RF. This model needs to be further trained
423 and tested on larger datasets to ensure that it remains valid in a broader population of at-risk infants. In
424 addition, testing it in at-risk infants who have not yet developed PNAC will be imperative. If increased
425 levels of certain gram-negative bacteria are found to be causal or compounding in PNAC, targeted
426 interventions such as antibiotics, probiotics, or fecal microbiota transplantation could be investigated.

427 Limitations of this study include the small number of infant twin pairs. However, this limited
428 sample size is offset somewhat by the use of discordant twin pairs, potentially reducing confounding from
429 the intrauterine environment, age, genetics and maternal breast milk and rigorous analysis of serial stool

samples. An additional limitation is that tests used to exclude other causes of cholestasis in each cholestatic subject were not homogeneous and were dependent on the clinical situation.

In conclusion, we found marked differences in the diversity and relative abundance of stool microbiota in infants who developed PNAC versus twin controls, most notably an increase in gram-negative bacteria Veillonella, Klebsiella, and Enterobacter. This finding warrants further exploration in larger cohorts and experimental models to determine if signals in the microbiota are predictive of PNAC, thereby providing a basis for interventions to mitigate the development of PNAC in vulnerable infants.

Acknowledgements

The authors thank Kristy and Roger Crombie for their generous philanthropic donation toward this project in loving memory of their daughter Anna Charlotte.

Research reported in this publication was supported in part by the National Center for Advancing Translational Sciences of the National Institutes of Health under Award Number UL1TR003015 (Moore, Hourigan) and the National Institute of Child Health and Human Development under Award Number K23HD099240 (Hourigan). The content is solely the responsibility of the authors and does not necessarily represent the official views of the National Institutes of Health.

2.6 Supplement

Supplementary tables are available in the published version of this manuscript:

Moutinho TJ Jr*, Hourigan S*, Berenz A, Papin JA, Guha P, Bangiolo L, Oliphant S, Baveja R, Baker R, Vilboux T, Levy S, Deopujari V, Nataro J, Niederhuber J, Moore SR. Gram-negative Microbiota Blooms in Premature Twins Discordant for Parenteral Nutrition-associated Cholestasis. Journal of Pediatric Gastroenterology and Nutrition. (2020).

Chapter 3 Stool metabolome early predictors of infants who will develop parenteral nutrition associated cholestasis

Thomas J. Moutinho Jr.[5], Jason A. Papin[5], Deborah A. Powers[5], Shira Levy MA[1,2], Rajiv Baveja MD[7], Isabel Hefner[1], Masouma Mohamed[1], Alaa Abdelghani MD[1], Robin Baker MD[7], Sean R. Moore MD[6], Suchitra K. Hourigan[1,2,3,4]

1. Inova Children's Hospital
2. Inova Translational Medicine Institute
3. Pediatric Specialists of Virginia
4. Johns Hopkins School of Medicine
5. Department of Biomedical Engineering, University of Virginia
6. Department of Pediatrics, University of Virginia
7. Fairfax Neonatal Associates

Submitted to Journal of Pediatric Gastroenterology and Nutrition in August of 2021

3.1 Abstract

Parenteral nutrition associated cholestasis (PNAC) in the Neonatal Intensive Care Unit (NICU) can cause significant morbidity and associated healthcare burdens. While certain clinical factors can be used to predict which infants may be more likely to develop PNAC, the current standard diagnostic measurement is the detection of elevated direct bilirubin levels in the blood. Noninvasive markers in early life that predict which infants are at risk of developing PNAC would be beneficial, enabling the earlier implementation of liver protective strategies. Stool samples are currently an underutilized resource in the NICU with the potential to be used for diagnostic purposes. We demonstrate in our analysis that the stool samples that we collected and analyzed using metabolomics have predictive potential in diagnosing PNAC before the standard clinical metric presents in the blood. Based on the data we collected, it may be possible to develop into a simple point-of-care diagnostic test to provide NICU clinicians with an additional tool for early identification to catalyze intervention for infants at risk for PNAC. A diagnostic such as this could enable clinicians to confidently optimize caloric nutrition with PN for infants at low risk of developing PNAC and enable earlier detection of infants at risk of developing

life-threatening cholestasis which can be proactively mitigated with alterations to the administered parenteral nutrition.

3.2 Introduction

Through poorly understood mechanisms, a subset of neonates receiving parenteral nutrition (PN) develop liver damage and ultimately parenteral nutrition associated cholestasis (PNAC). PNAC is characterized by an elevated level of direct bilirubin in the blood that can only be detected once there is decreased bile flow through bile ducts. The incidence of PNAC exceeds 50% of infants born less than 1000 grams, and 85% of infants requiring PN for longer than 14 weeks (69). Liver injury persists even after cessation of PN, representing a significant health and economic burden (68). Recently, alternative PN lipid emulsions sourced from fish (Omegaven®) or a mixture of plant and fish lipids (Smoflipid®) have been shown to limit the progression and injury from PNAC (70,88). However, due to a variety of factors that may include cost, insurance limitations, and the requirement for a second IV line, these potentially protective lipid formulations are not yet utilized for all infants in the NICU (89).

We, and others, have shown an intriguing association between the development of PNAC and a differential composition in the gut microbiome (71–73,90). These findings suggest that there are detectable changes in the stool that may predict PNAC. There is a great need for identifying safe and effective biomarkers in infants to aid in diagnosing disease in the NICU (62). Stool and urine samples, although non-invasive and with minimal risk to the infant, do not currently play a role in diagnostic protocols in the NICU. It is well known that the urine and stool can contain valuable information about physiological processes (61,62). However, stool and urine remain an untapped resource for diagnostic applications in the NICU.

Infants in the NICU are an ideal patient population for expanding upon precision medicine due to their tightly regulated nutritional sources, treatment administration, and consistent monitoring. We

believe that stool and urine samples have an integral role to play in monitoring the health of NICU infants. We hypothesize that it will be possible to identify liver injury before bilirubin levels in the blood show signs of PNAC by utilizing metabolites present in stool samples. These data will provide medical teams with valuable information for making clinical decisions involving PN formulations and preventative treatments. It is important to maximize infant nutrition and minimize the occurrence of liver injury, while also accounting for healthcare costs and additional challenges associated with hepatoprotective lipid emulsions. In this study, our aim was to identify the metabolites that are highly associated with the development of PNAC before direct bilirubin level elevate above the clinical threshold for diagnosing PNAC.

3.3 Results

This analysis included 60 infants: 23/60 (38%) of subjects were female, 10 (17%) identified as Hispanic or Latino, and 10 (17%) identified as Black or African American. The infants in this study were selected from a patent study encompassing 202 individuals. The mean gestational age at birth was 30 weeks (range 23-39 weeks). A total of 200 serial stool samples were collected and analyzed with Liquid chromatography - Mass Spectrometry (LC-MS) to measure the stool metabolome. Additionally, 327 serial stool samples underwent 16S ribosomal RNA gene sequencing. Across all subjects, the mean gestational age was 30 weeks (range 23-39 weeks) and 23 (38%) infants were female. All of the infants received PN with Intralipid as the lipid emulsion with a total of 19 (32%) developing PNAC during the study. All infants were verified to have no other causes of cholestasis.

We collected relevant clinical data for all infants enrolled in this study, including but not limited to their gestational age at birth, birth weight, number of days of PN before developing PNAC, information about antibiotics, and calculated metrics such as birth weight percentile adjusted for gestational age. Among the clinical metrics measured, only birth weight and the number of days of PN before occurrence

of PNAC are statistically different between the disease and control groups (Figure 3.1A; $p < 0.05$). However, in our cohort we found that infants with a birth weight percentile greater than 40% and a birth weight greater than 1.1 kilograms did not develop PNAC. These clinical criteria are consistent with known clinical risk factors (Figure 3.1B). Since PN administration is associated with the development of PNAC, we inspected the relationship further in our cohort to better understand how PNAC is impacted by the amount of time an infant is on PN. We found a positive correlation between PNAC diagnosis and the amount of time an infant receives PN before diagnosis. Additionally, there is a noticeable increase in the rate of PNAC diagnosis after 20 days of PN administration for an individual.

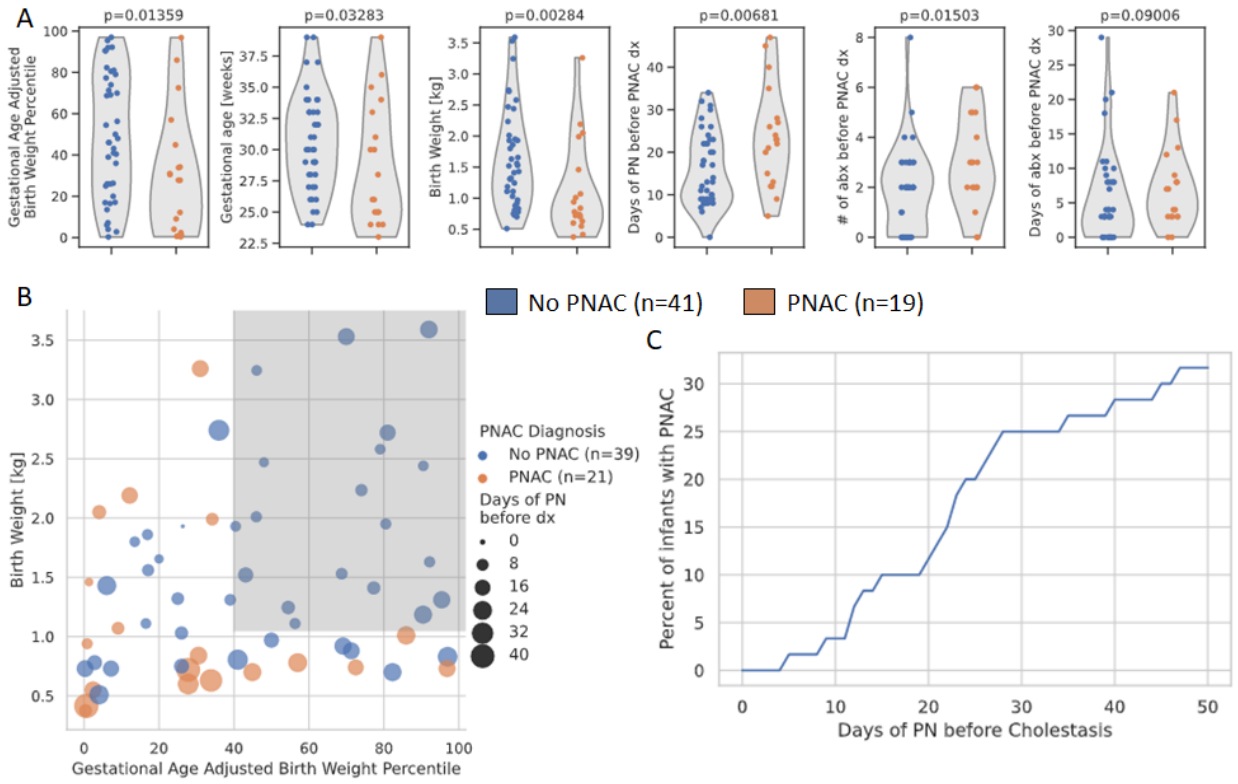

Figure 3.1: Clinical characteristics of infants with and without PNAC.

A) Continuous clinical variables were tested for a statistically significant difference between the control and PNAC groups using a Wilcoxon rank sum test. We determined that all six variables are statistically different except for the number of days of antibiotics an infant received before developing PN cholestasis (p-value < 0.05). For the control distribution, we used the total number of days on PN or antibiotics administered to those infants never diagnosed with PNAC. B) The comparison of two clinical metrics reveals that there are simple thresholds that classify infants in our cohort as high or low risk. Infants born

above the 40th weight percentile (adjusted for gestational age) and also weigh greater than 1.1 kg at birth are at a low risk of developing PN cholestasis compared to the rest of the infants. C) PNAC diagnosis is correlated with the amount of time an infant receives PN. There is a noticeable increase in incidence of PNAC at greater than 20 days of PN indicating that there may be clinical benefit in transitioning infants away from Intralipid PN before this critical time point.

Bacterial taxa correlate with PNAC, but lack predictive potential in this cohort

Within this cohort of NICU infants, we identified several microbial taxa that are statistically different between the disease and control groups ($p < 0.05$). Among these taxa, the Enterobacteriaceae family is present at greater abundance in the stool samples with high associated direct bilirubin levels in the blood (Figure 3.2A). However, the three known genera within the Enterobacteriaceae family all demonstrate an opposite trend with high abundance in the control group (Figure 3.2B). The unknown genera within the Enterobacteriaceae family show a higher abundance in samples from infants with PNAC (Figure 3.2C). Although this result is consistent with our previous work (90), more research is needed to identify the primary Enterobacteriaceae genera that are present at elevated levels in infants with PNAC. Finally, at the species level, *Veillonella dispar* appears to be at an elevated relative abundance in infants with PNAC (Figure 3.2D). It is important to note that none of these microbes show a strong predictive value for determining infants at risk of developing PNAC, all are simply correlated with elevated levels of direct bilirubin.

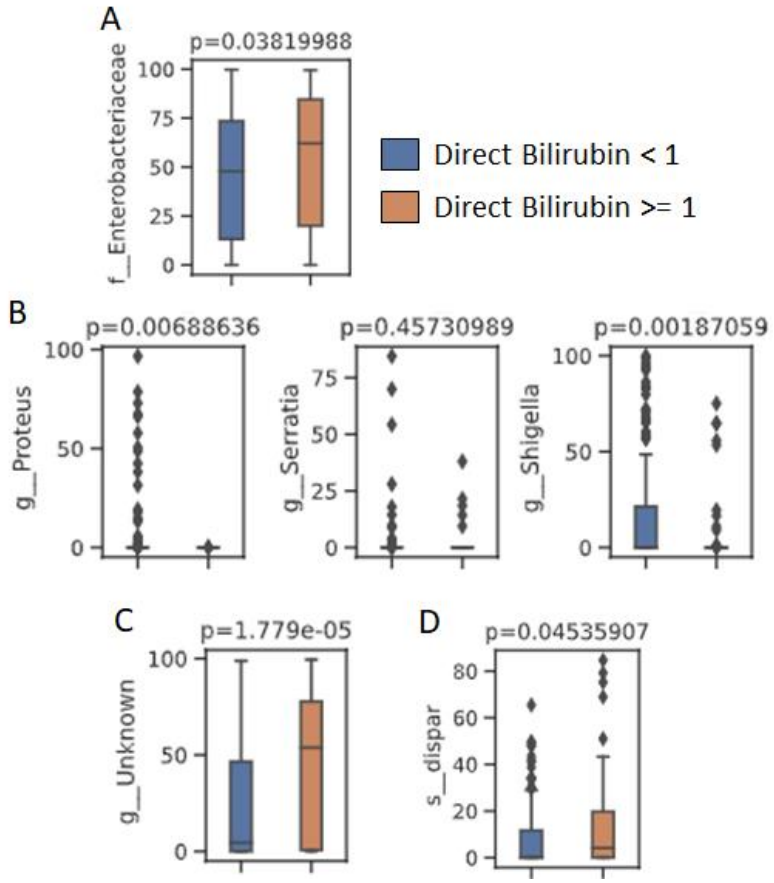

Figure 3.2: Microbiota composition correlated with direct bilirubin levels.

A) The infants in our cohort have microbiota that are primarily dominated by Enterobacteriaceae. Infants with high direct bilirubin levels have statistically higher relative abundance of Enterobacteriaceae ($p < 0.05$). B) There are three known genera within the family Enterobacteriaceae that do not align with the statistical trend at the family level. C) However, there are several Enterobacteriaceae with unknown genera in our study. Within this unknown group we see the driving signal for the significant difference at the family level ($p < 0.05$). D) Finally, at the species level, we have one significantly different microbe, Veillonella dispar*. Within these data we were unable to identify any predictive potential for the diagnosis of PNAC.*

The stool metabolome contains valuable biomarkers for infants at risk of PNAC

Among the 19 infants in our cohort who developed PNAC (Figure 3.3A), there were nine for which we were able to collect stool samples from before they were diagnosed with PNAC. These infants represent our most valuable case study individuals for identifying the biomarkers that are early predictors of PNAC. These samples were of particular interest because they provide us with a glimpse into the metabolites that might have the greatest predictive potential for diagnosing PNAC before the

gold standard clinical metric. We first identified over 100 statistically different metabolites when comparing the disease group to the control group ($p < 0.05$). We then utilized the case study samples to identify biomarkers with predictive potential for classifying infants at risk of developing PNAC. For metabolites that were found to be more abundant in PNAC samples, we selected only those that had scaled intensities in greater than 90% of the case study samples above the median value of the PNAC distribution (Figure 3.3B). This provided us with a subset of metabolites that represent those which have the greatest potential to be early predictors for the risk of developing PNAC (Table 3.1). For the metabolites that negatively correlated with disease, we selected PNAC biomarkers by identifying those with scaled intensities in greater than 90% of all the case study samples falling below the median value of the disease distribution.

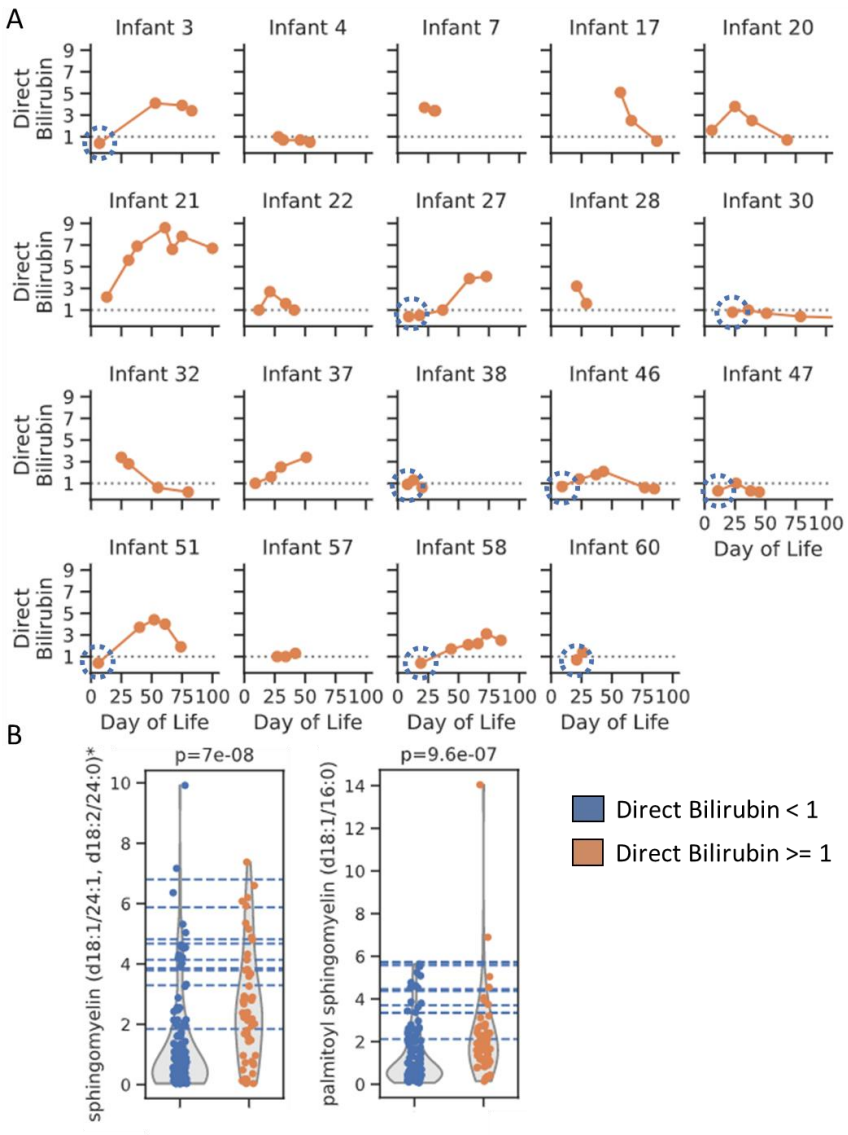

Figure 3.3: Metabolomics data and predictive biomarker selection.

A) There are 60 infants in this study; 19 were diagnosed with PNAC. We collected 200 fecal samples with accompanied metadata. The samples from each infant are plotted on an individual plot. The clinical direct bilirubin threshold, used to diagnose PNAC, is displayed with a dashed gray line on each panel. There are 6 cholestatic infants for which we were able to collect fecal samples before direct bilirubin levels were above the diagnostic threshold of 1 mg/dL. The samples that were collected before the direct bilirubin level increased above the diagnostic threshold are particularly important for identifying metabolites that are predictive of the development of PNAC before the current clinical metric. The nine samples for which the direct bilirubin levels were below the clinical threshold were used in this study as case study samples for filtering statistically significant metabolites to identify biomarkers with the greatest predictive potential. B) The y-axis displays the scaled intensity for each metabolite. We performed Mann Whitney U tests to assess statistical significance of each metabolite between the samples with direct bilirubin below the clinical threshold and above. The case study samples were

excluded from the statistical analysis and plotted as dashed blue lines across the boxplots. We selected biomarkers based on statistical significance ($p < 0.05$) and consistency among the case study samples.

We identified a total of 28 metabolites that are positively correlated with an increase in direct bilirubin levels (Table 3.1) and 29 metabolites that are negatively correlated with an increase in direct bilirubin levels (Figure S3.1). The biomarkers elevated in PNAC samples provide a glimpse into the pathophysiology that may be governing the disease. Although these biomarkers have predictive value based on the six case study infants, they require additional validation that can only be provided via a more rigorous targeted metabolomics study.

Table 3.1: Biomarkers positively correlated with PNAC.

We identified 28 biomarkers that are statistically significantly elevated in samples with an associated direct bilirubin level greater than 1 mg/dL, while all six case study samples have values that are above

the median value of the elevated group. The total set of biomarkers is displayed with their associated p-values.

Metabolite	P-value
1-(1-enyl-palmitoyl)-GPE (P-16:0)*	0.001125
1-linoleoyl-GPC (18:2)	3.64E-07
1-oleoyl-2-linoleoyl-GPC (18:1/18:2)*	9.41E-05
1-oleoyl-GPC (18:1)	6.42E-07
1-palmitoyl-GPC (16:0)	0.000506
1-stearoyl-2-linoleoyl-GPC (18:0/18:2)*	0.026087
1-stearoyl-GPC (18:0)	1.6E-05
2-palmitoyl-GPC* (16:0)*	0.01854
2-stearoyl-GPE (18:0)*	6.07E-06
behenoyl sphingomyelin (d18:1/22:0)*	2.33E-07
hydroxypalmitoyl sphingomyelin (d18:1/16:0(OH))	0.005053
lignoceroyl sphingomyelin (d18:1/24:0)	1.23E-06
methyl-4-hydroxybenzoate sulfate	0.005453
palmitoyl dihydrosphingomyelin (d18:0/16:0)*	7.19E-06
palmitoyl sphingomyelin (d18:1/16:0)	3.05E-06
sphingomyelin (d17:1/16:0, d18:1/15:0, d16:1/17:0)*	3.25E-07
sphingomyelin (d18:0/18:0, d19:0/17:0)*	1.39E-05
sphingomyelin (d18:1/14:0, d16:1/16:0)*	4.71E-09
sphingomyelin (d18:1/17:0, d17:1/18:0, d19:1/16:0)	3.99E-07
sphingomyelin (d18:1/20:0, d16:1/22:0)*	8.71E-08
sphingomyelin (d18:1/20:1, d18:2/20:0)*	9.07E-09
sphingomyelin (d18:1/21:0, d17:1/22:0, d16:1/23:0)*	1.55E-08
sphingomyelin (d18:1/22:1, d18:2/22:0, d16:1/24:1)*	1.34E-08
sphingomyelin (d18:1/24:1, d18:2/24:0)*	1.56E-07
sphingomyelin (d18:2/16:0, d18:1/16:1)*	2.59E-05
sphingomyelin (d18:2/23:0, d18:1/23:1, d17:1/24:1)*	1.66E-06
sphingomyelin (d18:2/24:1, d18:1/24:2)*	4.45E-08
tricosanoyl sphingomyelin (d18:1/23:0)*	4.48E-07

While individual biomarkers are useful, a comparison of metabolites based on general classifications provides a measure of uniqueness for each of the biomarkers. For example, there are 1000 known metabolites detected across all samples in this study with a total of 19 sphingomyelin metabolites. We determined that 18 of the 19 known sphingomyelin metabolites are biomarkers for high direct bilirubin levels in the blood. Aside from sphingomyelin metabolites, we classified the PNAC biomarkers into nine other groups (Table 3.2). There are several other classifications of membrane lipids that are at greater abundance in PNAC samples indicating a general dysregulation of lipid metabolism in the liver of GI tract. Several primary and secondary bile acids were identified to be lacking in PNAC samples, validating well-known pathophysiology. Long-chain carnitines are also lacking in PNAC samples.

Table 3.2: All Biomarkers determined.

We classified each biomarker into 10 groups. Among all of the sphingomyelin molecules in the known set of metabolites detected, we identified 95% of them to have biomarker potential for early prediction of PNAC.

	Biomarker Classification	Number of Biomarkers	Total in Dataset	Percent SS Biomarkers
1	Sphingomyelins	18	19	95%
2	GPC Phosphatidylcholines	2	13	15%
3	GPC Lysophospholipids	4	5	80%
4	GPE Lyso-lipids	2	8	25%
5	Primary Cholic Bile Acids	4	17	24%
6	Secondary Cholic Bile Acids	3	28	11%
7	Vitamin A & Carotene diols	3	4	75%
8	Long-chain Carnitines (>= 10 carbons)	13	23	57%
9	Proline dipeptides	4	5	80%
10	Misc. (Vitamin E, N-acetylglutamate)	4	--	--
	Total statistically significant biomarkers:	**57**	--	--
	Total idetified metabolites in dataset:	--	**1000**	--

The biomarkers presented in Table 3.1, Table 3.2, and Figure S3.1 are directly applicable to the clinical setting. They have the potential to help diagnose the development of PNAC before any clinical markers of cholestasis, as opposed to diagnosing the disease after liver damage has already occurred. Three of the biomarkers have particularly high correlation with direct bilirubin levels while being present at exceptionally high levels in the first samples regardless of direct bilirubin levels (Figure 3.4). These characteristics are ideal for predictive biomarkers that will provide early detection of infants at risk for developing PNAC.

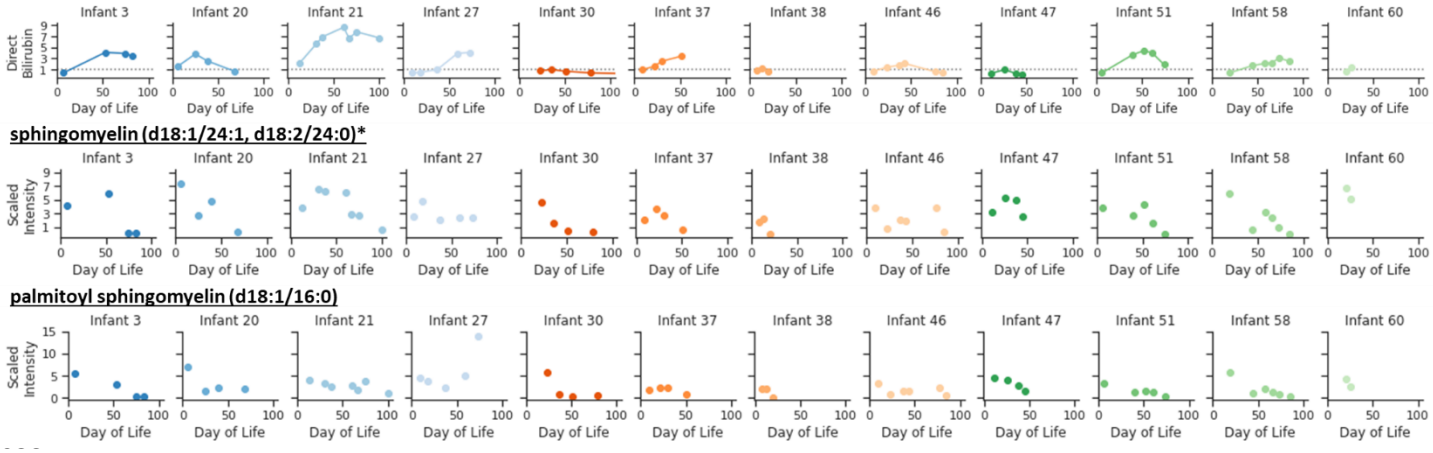

634 ***Figure 3.4: Biomarkers correlated with direct bilirubin while maintaining predictive potential.***

635 *We identified three biomarkers demonstrating particularly high correlation with direct bilirubin levels,*
636 *except for the notable difference of being at high abundance in the first stool sample collected from each*
637 *of the infants. We restricted this analysis to the infants that have some recovery from PNAC with reduced*
638 *direct bilirubin levels.*

639 Predicting PNAC before elevated direct bilirubin levels is of particular interest because bilirubin in
640 the blood indicates that impaired bile flow has already occurred. Ideally, identifying the infants at greatest
641 risk of developing PNAC would provide clinicians with a tool to prevent PNAC through known
642 interventions. Additionally, determining infants at low risk of developing PNAC would allow for those
643 infants to continue receiving the standard care regimen. Birth weight and birth percentile (adjusted for
644 gestational age) are the most important predictors of infants at risk of developing PNAC (Figure 3.5A).
645 When including metabolic biomarkers, we are able to achieve greater than 75% overall predictive
646 accuracy with 5-fold cross-validation when classifying samples as control or PNAC (Figure 3.5B). The top
647 five biomarkers determined to be the most predictive are all sphingomyelins and make up 50% of the top
648 20 most predictive biomarkers. Birth percentile and birth weight again demonstrate their predictive utility
649 while accounting for the metabolic biomarkers. Other important biomarkers in these random forest
650 models include several long-chain carnitines and bile acids (Table S3.1).

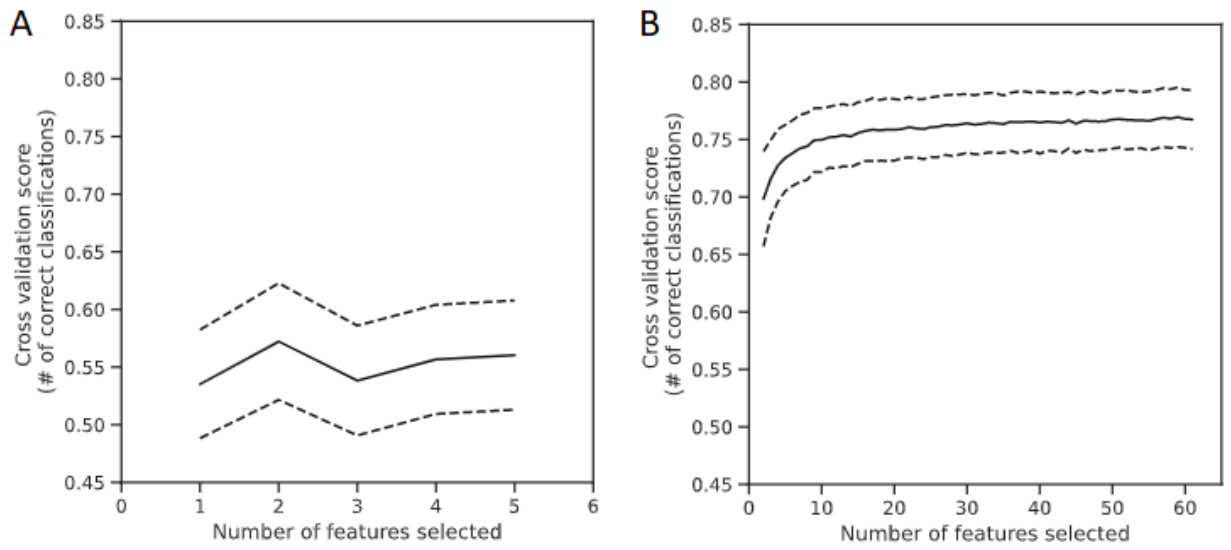

Figure 3.5: Random forest machine learning with five-fold cross-validation.

A) We performed feature reduction random forest machine learning to determine the minimal set of clinical metrics that provide the greatest predictive potential in our cohort. The optimal random forest consists of 2 clinical metrics and has an average 5-fold cross-validation overall accuracy of 57%. Birth weight percentile adjusted by gestational age and birth weight each contribute significantly to this model. B) When we include the 58 biomarkers that we identified to have predictive potential, we are able to generate a set of random forest models with greater than 75% cross-validation accuracy on average. The second set of models also demonstrates that the two previously identified clinical variables maintain predictive potential when in the context of the stool biomarkers. These models utilize all of the metabolomics samples in this study and classify samples as high or low bilirubin levels, therefore they do not predict if an infant will develop PNAC from the first stool sample collected.

With predictive potential demonstrated using 5-fold cross-validation with a set of random forest machine learning models, we next calculated the classification accuracy within our cohort using simple criteria that would be possible to implement in the clinic. The ideal implementation of these biomarkers in the clinic would be a simple point-of-care diagnostic that provides the medical teams with additional information about an infant's GI health. This ideal scenario requires basic thresholds to be applied to a small set of metabolites that are present in the stool in the first weeks of life. Additionally, low birth weight and birth percentile both provide valuable information about PNAC risk in our cohort, while existing as well-known variables associated with PNAC. In a clinical setting clinical metrics recorded at birth are valuable to categorizing infants into risk-level groups. In our cohort, infants born greater than 40th

672 percentile and greater than 1.1kg were at significantly lower risk for developing PNAC. We placed all other
673 infants in a high-risk group for the following analysis of biomarkers that may provide the most robust
674 discriminatory accuracy between infants that will or will not develop PNAC (Figure 3.6). We found that
675 the 12 best biomarkers, selected from our complete set of 57, are all sphingomyelin metabolites. Each of
676 these metabolites has a classification accuracy of the infants in our study between 79-88%. It is essential
677 to note that the reported accuracies require proper validation via an independent dataset. However,
678 accurate classification within our cohort while maintaining high correlation with direct bilirubin levels in
679 the blood over time provides a high level of confidence that these biomarkers hold potential for robust
680 prediction of infants that are at risk of developing PNAC.

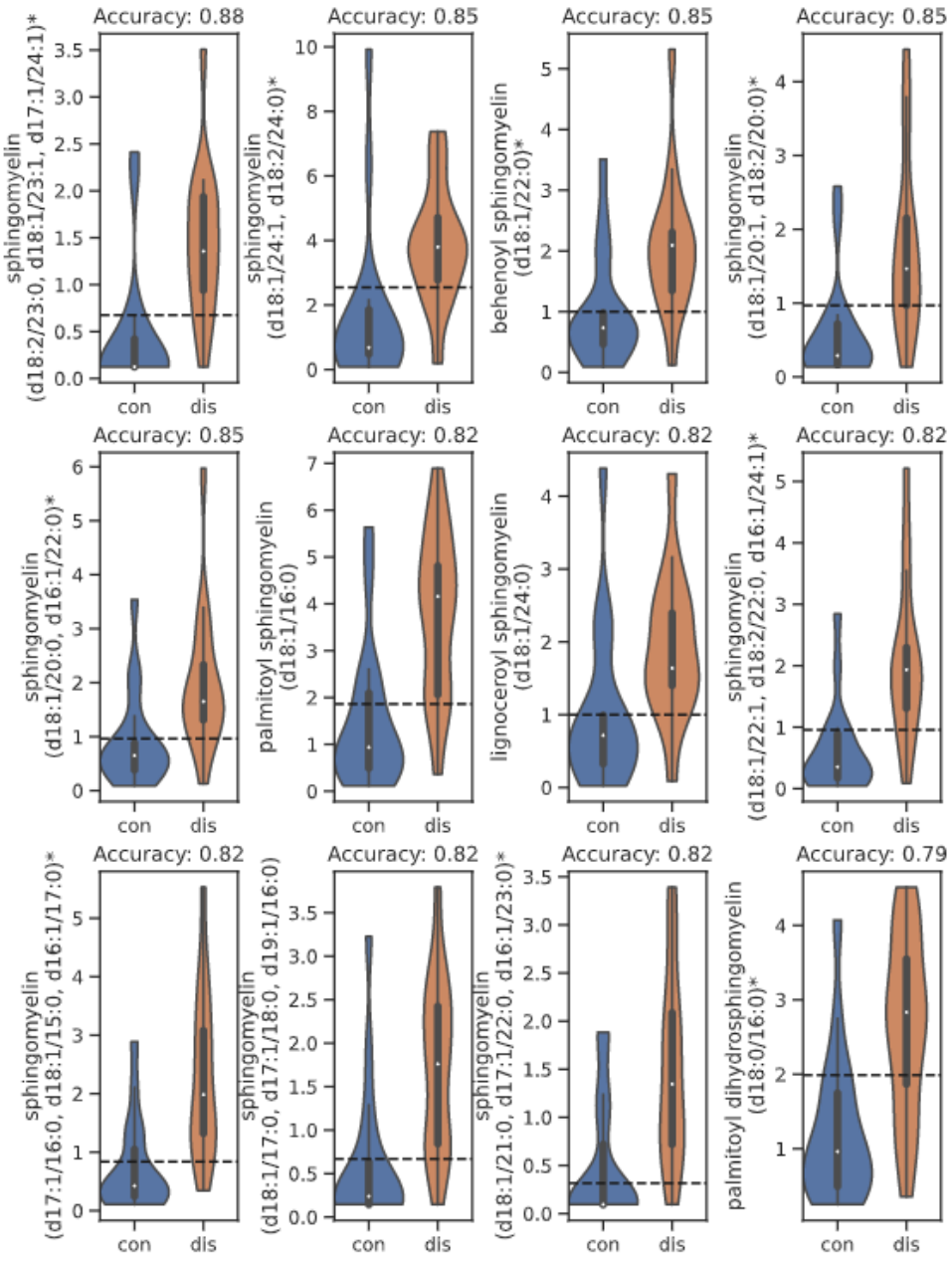

Figure 3.6: Biomarkers with the strongest discriminatory accuracy.

This analysis includes only the infants that fall outside of the low risk group identified in Figure 3.1 with a birth weight percentile above 40% and birth weight above 1.1 kg. Additionally, we reduced the number of stool samples to only include the first sample for each infant. There are 12 metabolites from our complete set of 57 that demonstrate particularly accurate discriminatory potential within our cohort. These metabolites range from being 88% to 79% accurate at classifying the infants in our cohort based on only the first fecal sample that was collected for each infant. Although these accuracies are not properly validated with independent data, they demonstrate that there are several metabolites present in NICU stool samples that have predictive capabilities. All 12 of these metabolites are various types of sphingomyelin.

692 Although there are 12 metabolites that each are able to individually discriminate between the
693 disease and control groups in our cohort, it is important to guard against overfitting and assess a more
694 robust strategy that may be implemented in the NICU. To improve the robustness of this calculation, we
695 assessed the accuracy of classification when using all 12 metabolites simultaneously with an ensemble
696 approach. A majority-vote ensemble classifier for our cohort provides an overall accuracy of 85% which
697 demonstrates consistency in the alignment across the 12 metabolites identified to be the optimal
698 candidates for a rigorous follow-up validation study (Figure 3.7).

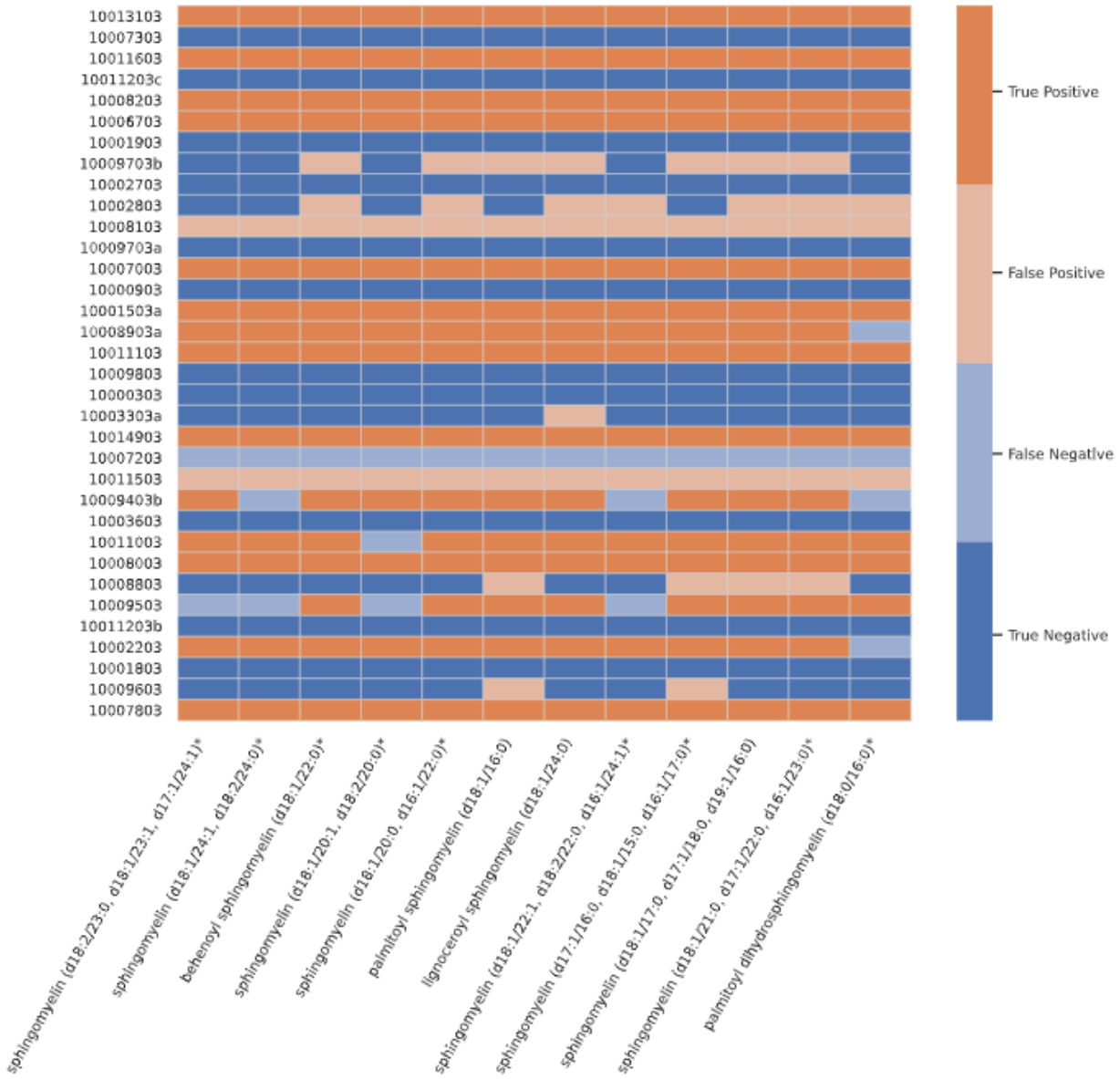

Figure 3.7: The 12 best biomarkers show high agreement across our cohort.

There is one infant in particular that contributes the majority of false negatives across all 12 metabolites. Among the infants we see only false positive classifications when using an ensemble majority vote across the 12 metabolites. There were 4 false positives based on majority vote and 1 false negative resulting in an overall accuracy of 85%.

3.4 Discussion

Parenteral nutrition associated cholestasis is a common disease that is in part the result of a clinical intervention required for infant survival. Advancements in precision medicine in the NICU may

allow medical teams to improve treatment plans and ultimately health outcomes. A key challenge in the NICU is the lack of access to frequent blood samples to run consistent diagnostic tests. We hypothesized that infant stools, currently treated as waste, have significantly diagnostic potential in the NICU. Our key findings in this study were threefold. We found that basic clinical variables that are recorded at birth provide discriminatory potential for classifying NICU infants based on their risk level. Secondly, there is a measurable difference between infants with and without PNAC in the gastrointestinal microbiota. Finally, we found that there are 57 metabolites present in stool samples that have predictive value in identifying infants at increased risk of developing PNAC. Several of the biomarkers identified, specifically a reduction in bile acids in PNAC infants, were validated based on known pathophysiology. Notably, there were 12 sphingomyelin lipids that demonstrated significant predictive value in our cohort and are the most promising metabolites to move forward with for future validation of a diagnostic test.

This prospective study was limited by the size of our cohort. With a specific focus on Intralipid, there were few infants that were not switched to a different lipid emulsion to improve health outcomes after developing PNAC. This limitation contributed to the lack of robust validation of the predictive modeling and thus requiring future studies to explore governing mechanisms and a more accurate calculation of predictive accuracy.

Precision medicine in the NICU has profound potential due the regimented control of the infants' nutritional intakes and treatment adherence. Our results demonstrate that clinical variables recorded at birth along with frequent testing for biomarkers in the stool would provide an accurate and effective method for measuring an infant's tolerance for the standard PN lipid emulsion. We have proposed a set of simple diagnostic criteria for classifying infants based on their expected risk level for developing PNAC. The clinical and metabolic variable we identify in this study could be developed into a simple point-of-care diagnostic test to provide NICU clinicians with an additional tool for early identification to

catalyze intervention for infants at risk for PNAC. The early identification of PNAC before elevated direct bilirubin levels in the blood would allow NICU medical teams to take early action to limit the occurrence of liver damage in this vulnerable population. The most likely course of action would involve switching an infant at risk of PNAC to a hepatoprotective lipid emulsion. This precise diagnostic plan would allow medical teams to proactively optimize for infant health outcomes, while also helping the NICU to account for other competing objectives, such as cost. Additionally, frequent monitoring of the stool may enable clinicians to confidently optimize caloric nutrition with PN for infants at low risk of developing PNAC, a known enhancer of health outcomes.

Sphingomyelin in the stool appears to be the most predictive signature for the risk of PNAC. This lipid plays a role in inflammatory signaling in the GI tract, tight junction maintenance, and the metabolism of nutrients present in the GI tract (91,92). Additionally, there are several known connections with GI diseases such as ulcerative colitis and GI hyperpermeability (91,93). Finally, there are also connections to the GI microbiota. Sphingomyelin has been shown to play a role in the physiology of how probiotics interact with the intestinal lining (45).

The diagnostic potential that resides in biological samples that are currently treated as waste in the NICU is immense. Our results demonstrate that stool samples contain measurable biomarkers that are predictive of disease. In the NICU there is a constant need for more information to help treat and take care of premature infants. Stool and urine represent two additional sources of valuable information that have previously been out of reach due to the complexity of identifying effective biomarkers for disease. However, with the advent of advanced metabolomics and systems biology, there is a new opportunity to advance diagnostic procedures in the NICU past blood tests and monitoring of vitals. PNAC is only one of many devastating diseases in the NICU that may, someday, be diagnosed using stool samples.

3.5 Methods

Sample collection and processing:

After informed consent from parents, infants in the NICU were enrolled before 5 days of life in a longitudinal microbiome study (Western IRB approval# 20210065). Serial stool samples were collected from infants in the NICU up to twice weekly and flash frozen at - 80 °C. Infants were monitored for the development of cholestasis (direct bilirubin >1mg/dL), and the cause of cholestasis was noted as assessed by the treating physicians. Clinical data was collected including gestational age, birth weight, antibiotic use, infections and length of time on PN.

To prepare feces for metabolomic analysis, frozen samples were lyophilized and then resuspended at a 50:1 (50 µL deionized water for every 1 mg of feces weight) ratio for homogenization as previously described (94). The homogenates were subjected to automated biochemical extraction and analysis by liquid chromatography and high-resolution tandem mass spectrometry (LC-MS/MS) on Metabolon's Global Platform, as previously described (95–97). Raw data were extracted, peak-identified, and processed by Metabolon using proprietary software (94,98,99). In brief, metabolites - were identified by comparison to library entries of purified standards or recurrent unknown entities. Metabolon maintains a dynamic and proprietary biochemical reference library of more than 4,500 known metabolites (based on authenticated standards) and more than 2,000 novel metabolites (without an identified chemical structure); each library entry contains the retention time/index (RI), mass to charge ratio (m/z), and spectral data (including MS/MS fragmentation). Biochemical identifications are based on three criteria: retention index within a narrow RI window of the proposed identification, accurate mass match to the library ± 10 ppm, and the MS/MS forward and reverse scores between the experimental data and authentic standards. The MS/MS scores are based on a comparison of the ions present in the experimental spectrum to the ions present in the library spectrum. Three types of controls were included: a pool of small portions of each experimental sample serving as a technical

replicate throughout the platform run; extracted water samples (process blanks); and a cocktail of standards spiked into every analyzed sample allowing instrument performance monitoring.

327 serial stool samples underwent 16S rRNA gene sequencing at Ubiome or the Inova core research lab. Samples were sequenced using NextGen sequencing technology with 150 base pair paired end reads.

Metabolomics Data

Metabolon pre-processed the LC-MS data to identify metabolites present in our samples. Additionally, they normalized the raw ion intensity data by scale to set the median of each metabolites equal to 1. All missing values are imputed with the minimum scaled intensity value.

Statistical analysis:

We analyzed the clinical metadata for each infant enrolled in the study as well as the metabolomics data for each of the fecal samples.

We performed Mann Whitney U tests for all comparisons in this study. All distributions were confirmed to be non-normal using the Shapiro-Wilk test. Stool metabolites significantly associated with later development or protection from PNAC were assessed using Mann Whitney U Tests and random forest machine learning.

Data processing and Machine Learning:

We utilized QIIME and DADA2 to process the 16S data. We processed the metabolomics data using Python and jupyter notebooks. We generated the machine learning models using Scikit Learn in Python. All python scripts and data are available upon request.

3.6 Supplement

A

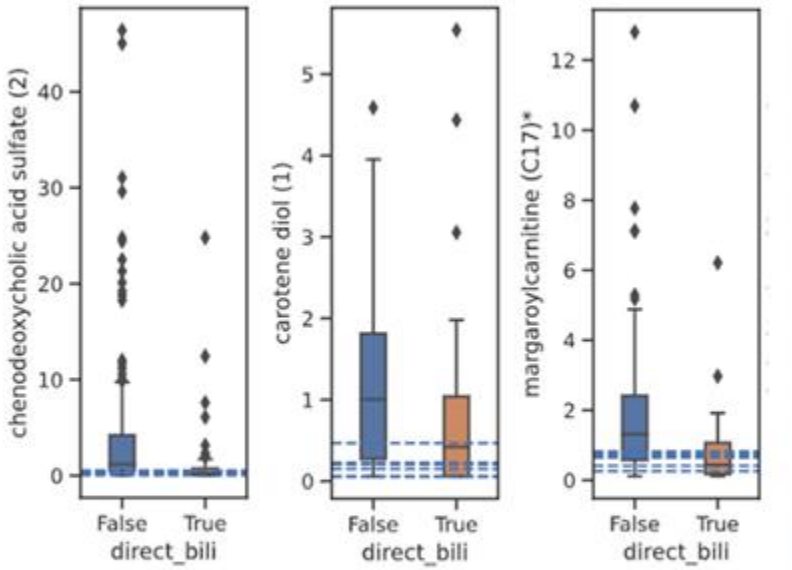

B

Metabolite	P-value
1-carboxyethylisoleucine	0.024751
3-dehydrochenodeoxycholate	0.000277
3-hydroxyoleoylcarnitine	7.24E-05
alpha-tocopherol	0.029013
carotene diol (1)	0.000249
carotene diol (2)	0.000594
chenodeoxycholate	8E-05
chenodeoxycholic acid sulfate (2)	5.67E-07
cholate	3.09E-06
cholate sulfate	2.63E-09
cyclo(gly-pro)	0.007341
cyclo(his-pro)	0.040203
cyclo(leu-pro)	0.002625
cyclo(pro-sulfo-tyr)*	0.003588
dihomo-linolenoylcarnitine (C20:3n3 or 6)*	5.76E-06
docosahexaenoylcarnitine (C22:6)*	9.01E-09
eicosenoylcarnitine (C20:1)*	2.7E-09
hyocholate	2.19E-06
linoleoylcarnitine (C18:2)*	0.040458
lithocholic acid sulfate (2)	2.61E-05
margaroylcarnitine (C17)*	7.63E-08
myristoleoylcarnitine (C14:1)*	0.043701
myristoylcarnitine (C14)	0.014157
N-acetylglutamate	0.001154
oleoylcarnitine (C18:1)	0.001148
palmitoleoylcarnitine (C16:1)*	0.000578
palmitoylcarnitine (C16)	1.7E-05
pentadecanoylcarnitine (C15)*	4.11E-07
retinol (Vitamin A)	0.032567
undecenoylcarnitine (C11:1)	0.021953

Figure S3.1. We identified the metabolites that are statistically significantly elevated in samples with an associated direct bilirubin level less than 1 mg/dL, while all six case study samples have values that are below the median value of the elevated group. A) The values of the six case study samples are displayed with the blue dashed lines. We have displayed three representative metabolites from the total set found. B) The total set of potentially protective metabolites are displayed with their associated p-values. The 6 case study samples are not included in either group when performing the Wilcoxon rank sum test for each metabolite.

Chapter 4 Quantifying cumulative phenotypic and genomic evidence for procedural generation of metabolic network reconstructions

Thomas J. Moutinho Jr.[1], Benjamin C. Neubert[1], Matthew L. Jenior[1], Jason A. Papin[1]

[1] University of Virginia, Department of Biomedical Engineering

Submitted to PLOS Computational Biology; July 2021

4.1 Abstract

Genome-scale metabolic network reconstructions (GENREs) are valuable tools for understanding microbial community metabolism. The process of automatically generating GENREs includes identifying metabolic reactions supported by sufficient genomic evidence to generate a draft metabolic network. The draft GENRE is then gapfilled with additional reactions in order to recapitulate specific growth phenotypes as indicated with associated experimental data. Previous methods have implemented absolute mapping thresholds for the reaction automatically included in draft GENREs; however, there is growing evidence that integrating annotation evidence in a continuous form can improve model accuracy. There is a need for flexibility in the structure of GENREs to better account for uncertainty in biological data, unknown regulatory mechanisms, and context specificity associated with data inputs. To address this issue, we present a novel method that provides a framework for quantifying combined genomic, biochemical, and phenotypic evidence for each biochemical reaction during automated GENRE construction. Our method, Constraint-based Analysis Yielding reaction Usage across metabolic Networks (CANYUNs), generates accurate GENREs with a quantitative metric for the cumulative evidence for each reaction included in the network. The structure of a CANYUN GENRE allows for the simultaneous integration of three data inputs while maintaining all supporting evidence for biochemical reactions that may be active in an organism. CANYUNs is designed to maximize the utility of experimental and

annotation datasets and to ultimately assist in the curation of the reference datasets used for the automatic reconstruction of metabolic networks. We validated CANYUNs by generating an *E. coli* K-12 model and compared it to the manually curated reconstruction iML1515. Finally, we demonstrated the use of CANYUNs to build a model by generating an *E. coli* Nissle CANYUN GENRE using novel phenotypic data that we collected. This method may address key challenges for the procedural construction of metabolic networks by leveraging uncertainty and redundancy in biological data.

4.2 Introduction

Complex microbial communities play an important role in human physiology (100–104). Genome-scale metabolic network reconstructions (GENREs) have been shown to precisely model the functional capabilities of microbes and their interactions in communities (24,56). A GENRE is a constraint-based mathematical model structured to combine various forms or biological data to gain an improved mechanistic understanding of metabolism (105). This form of modeling explicitly accounts for biochemical thermodynamics and stoichiometry to represent the physical constraints that govern cellular metabolism. Methods used to generate GENREs are progressively being automated to reduce time and resource requirements with the goal of modeling the vast number of unique species and strains that reside in human associated microbiota (106–109). However, there remains a need for advancements in the procedural generation of GENREs to improve utilization of uncertainty in the source biological data.

The foundational data that procedurally generated GENREs are built upon is a universal biochemical reaction network with associated reference genetic annotation data for sequence-to-reaction mapping. When building an organism specific GENRE, a genome is annotated with precise biochemical reactions. The annotation process typically involves a threshold of sequence alignment that is used to determine if a sequence is similar enough to the reference sequence to justify annotation with the associated biochemical function (110). The data used to build GENREs is incomplete and subject to uncertainty, necessitating gapfilling of the metabolic network generated via genetic data alone. Gapfilling is the process of adding biochemical reactions with low or no evidence to a GENRE based on functional phenotypic growth data and the cellular biomass requirements. The resulting accuracy of the curated GENRE is then calculated by how well it recapitulates the phenotypic growth data utilized for training. There are additional methods for further assessment of model quality involving other data types, such as gene essentiality data, and separate validation data (111). Recent methods have

demonstrated that utilizing gene annotation alignment scores in a continuous way can help to improve gapfilling results (107,112).

A curated GENRE consists of a set of reactions that have biological evidence suggesting that they are catalyzed by the organism. When a GENRE is procedurally generated the remaining error is commonly dominated by false growth calls; this indicates that these models over-predict the metabolic capabilities of an organism. Additionally, annotation alignment scores, universal biochemical network source data, and annotation reference data are all often left out from published GENREs (113,114). Without the source sequence-to-reaction data used to generate a GENRE, the reactions that are included in the curated GENRE lack explicit indication of what type of biological evidence was used to justify inclusion.

Phenotypic growth data used for gapfilling is not treated the same as context specific data is treated when used to contextualize a GENRE. For example, transcriptomics data can be used to gain insight into how metabolic flux may occur in an unknown growth condition (54,115). Phenotypic growth data provides a similar type of context specific data compared to transcriptomic data, yet it is utilized build a metabolic network rather than contextualize the existing universal metabolic network. From a biological point of view, it is an over simplification of an organism specific metabolic network to ignore the existence of gene regulation during the GENRE building process (116). The practice of including all genetic data in the functional GENRE and then gapfilling remaining essential reactions with phenotypic data results in an over-constrained assessment of the biological system under investigation (107). There is a need for additional flexibility in the structure of GENREs to better account for uncertainty in biological data, unknown regulatory mechanisms, and context specificity associated with data inputs.

In this study, we present a novel method for contextualizing a manually curated universal metabolic network through the simultaneous integration of genetic annotation data, and phenotypic

886 growth data. Our method, Constraint-based Analysis Yielding reaction Usage across metabolic Networks
887 (CANYUNs), procedurally generates a GENRE by explicitly quantifying the combined biological evidence
888 for the inclusion of reactions in the resulting network. CANYUNs utilizes a continuous weighting for each
889 reaction in a curated universal metabolic network to quantify the evidence provided by the biological
890 data that is used during the reconstruction process. Rather than gapfilling a draft network by leveraging
891 phenotypic data, CANYUNs determines the reactions required for computational growth in each known
892 growth condition separately to quantify the cumulative evidence for each reaction. The cumulative
893 evidence generated for each reaction during the CANYUNs training process is subsequently used to
894 determine the reactions that are included in the final GENRE. The resulting CANYUNs model consists of
895 the universal metabolic network and associated reference annotations, organism specific genetic
896 alignment scores, phenotypic growth data, and certainty values associated with each reaction included
897 in the curated network.

898 4.3 Results

899 Constraint-based Analysis Yielding reaction Usage across metabolic Networks (CANYUNs)

900 The model training process in CANYUNs is designed to capture and quantify the cumulative
901 experimental and genomic evidence for the inclusion of biochemical reactions in a procedurally
902 generated GENRE. CANYUNs simultaneously utilizes phenotypic growth data, genomic annotation
903 evidence, and universal biochemical network data making it distinct from existing reconstruction
904 methods that first reconstruct a draft metabolic network using genomic data and then gapfill additional
905 reactions to match model predictions with phenotypic experimental data. CANYUNs maintains a direct
906 connection with all annotation evidence used during model building to help facilitate future model
907 curation.

908 We built a curated universal biochemical network by combining the reactions from the CarveMe
909 universal network (107) and reactions from the manually curated *E. coli* K-12 model, iML1515 (117).

When metabolite formulas did not match, we used the iML1515 formulas to maximize the number of mass-balanced reactions in the final universal network. For additional curation, we used an optimization method to check the network for generation of free-mass (see Methods). In short, we created intracellular sink reactions for each intracellular metabolite in the network and closed all exchange reactions to ensure the network did not have access to any extracellular metabolites. We then maximized the sum of flux through all sink reactions to identify any metabolites produced due to mass-imbalanced reactions or mass-generating loops. We curated the universal network by manually removing reactions that were contributing to free-mass generation. The reactions removed during this process fell into two categories: reactions that were mass-imbalanced, and reactions that were biologically infeasible due to missing energy metabolites. Using this optimization-based method, we were able to more rigorously identify free-mass generation in the network compared to simply checking each reaction for mass-balance.

We utilized BLASTp to align the genome of the target organism with reference sequences in the CarveMe sequence-to-reaction dataset. We used the sequence alignment bitscores for *E. coli* K-12 genes and the CarveMe dataset to then generate reaction bitscores using the published method (107). We subsequently used a step-wise linear transformation to convert the reaction bitscores to reaction weights that fall between -1 and 1 to use during linear optimization and flux balance analysis. We developed a novel formulation of flux balance analysis called, Data Guided Flux Balance Analysis (dgFBA) specifically for CANYUNs. This optimization equation minimizes the sum of flux through all reactions with low or no genetic evidence while simultaneously maximizing the sum of flux through all reactions with substantial genetic evidence. The degree to which a reaction is minimized or maximized is linearly determined by the reaction weights. During a dgFBA optimization, flux is required through the biomass reaction to represent growth. Importantly, dgFBA allowed us to determine the flux-carrying reactions (FCRs) in each experimental growth condition by setting the exchange reactions to represent the specific

growth media conditions. By tracking the flux-carrying reactions for each growth condition, we were able to then calculate the ratio of growth conditions in which a reaction carries flux and determine reaction Certainty Values (CVs) for each FCR indicating confidence in the presence of each biochemical function in the target organism.

In the final stage, all flux-carrying reactions across the experimental growth conditions are used to generate an organism-specific CANYUNs model (Figure 4.1A). The resulting network is processed further by selectively removing a single reaction, or a small set of reactions, to further improve the overall accuracy of the model and adjust the type of error remaining. For validation of CANYUNs, we generated an automatic GENRE for *E. coli* K-12 leveraging phenotypic nutrient utilization data obtained from EcoCyc and compared it to iML1515 (117–119).

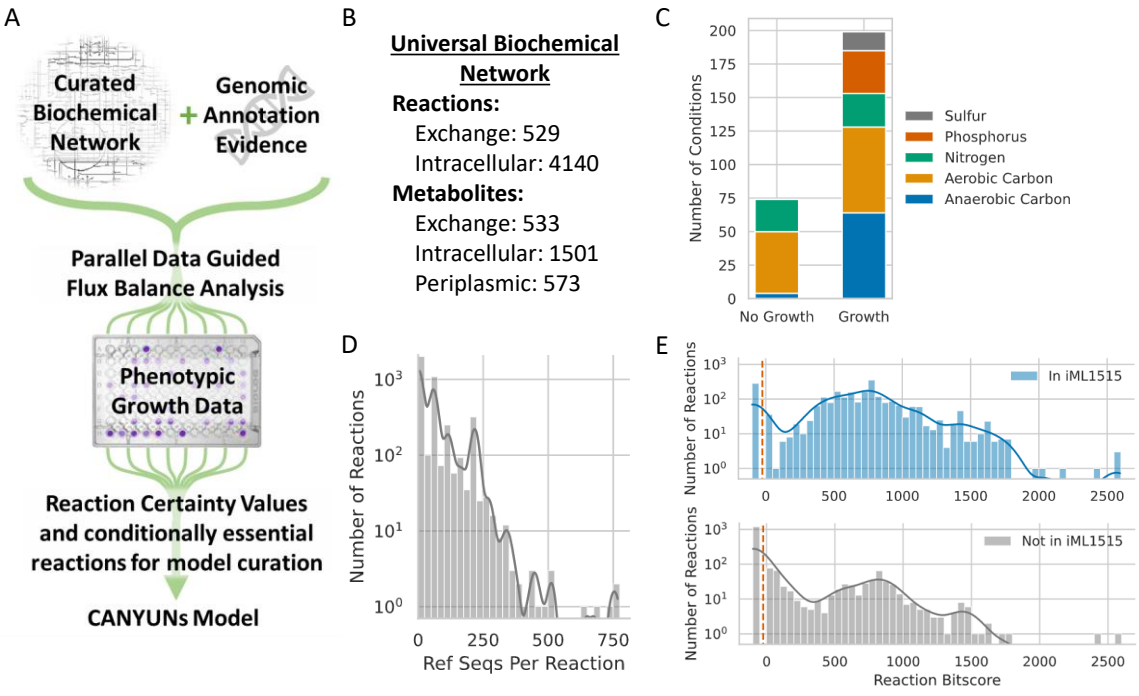

Figure 4.1:The CANYUNs pipeline integrates genomic, phenotypic, and biochemical data to quantitatively identify reactions that are likely catalyzed by an organism.

A) Genomic annotation data and phenotypic growth data for a specific organism are used to influence the flux distribution through a curated universal biochemical network to build an organism-specific

metabolic network model. Parallel growth simulations using Data Guided Flux Balance Analysis for each known experimental growth condition allows for a model building process that is not influenced by the order in which growth conditions are integrated. This process allows for the explicit quantification of Reaction Certainty Values, determined by the ratio of times a reaction carries flux across all of the condition-specific solutions to the total number of conditions. B) The universal biochemical network used in this study consists of reactions from the CarveMe dataset as well as novel reactions added from the manually curated E. coli *metabolic network, iML1515. C) The phenotypic data used in this study includes Biolog minimal media growth data from ~275 different conditions. D) The sequence to reaction dataset used to calculate reaction annotation evidence consists of over 4,000 reactions with 1 to 800 sequences associated with each reaction. E) The distribution of reaction bitscores for* E. coli *K-12 shows that there are reactions in the universal network with high evidence that are not included in iML1515. There are also many reactions with low evidence that are not included in iML1515, as expected. The annotation evidence generated for* E. coli *K-12 shows that there are 1,460 reactions in the universal biochemical network that have no genetic evidence associated with them, 260 of these reactions are in iML1515 and 1,200 of them are not.*

Data Guided Flux Balance Analysis

The reaction bitscores for *E. coli* K-12 were calculated directly from BLASTp sequence alignment bitscores using a previously published method (107). One third of reactions in the universal network have a bit score of 0 and the rest range from 1 to 2,500 (Figure 4.2A). A typical bitscore threshold for assigning a reference enzymatic metabolic function to the query sequence(s) is between 200 and 500 (120–122). The level of confidence in a functional call increases with the value of the bitscore, yet small changes in a sequence can result in large functional changes. Bitscores below the threshold also contribute information about the protein in question, values that are just shy of the threshold may still have the same function as the reference protein; however, scores that fall far short of the threshold suggest that the protein in question does not have the function of the reference.

We designed dgFBA to account for some of the uncertainty inherent in setting a threshold for assigning function to a given protein by utilizing reaction weights that are a function of the reaction bitscores. The reaction weights influence the reactions that carry flux in the optimization solution. Genomic annotation data must be transformed to a range of values that are compatible with dgFBA. The transformation function used in this study is graphically displayed in Figure 4.2B. This function can be adjusted based on the user's preferences. In this study we selected a bitscore threshold of 500 based on

a sensitivity analysis that demonstrated that model accuracy was insensitive to values between 200 and 500 (Figure 4.2B).

FCRs in a dgFBA solution are a result of complex interactions among the reaction weight values, media condition, and flux demands (i.e. biomass). Flux is maximized through reactions with a bitscore above 500 and minimized through reactions below 500. However, the degree of maximization and minimization depend upon the value of the bitscore. The low evidence reactions that are included in the final flux solution are likely essential for flux through biomass and can be thought of as gapfilled reactions that maintain their genomic annotation evidence (Figure 4.2E and 4.2F). Utilizing the reaction bitscores in this way allows for additional flexibility with reactions near to the bitscore threshold of 500 where the reaction weight is equal to zero. Reactions with weights near to zero are much less impacted by the dgFBA objective function and therefore are influenced far greater by thermodynamic requirements.

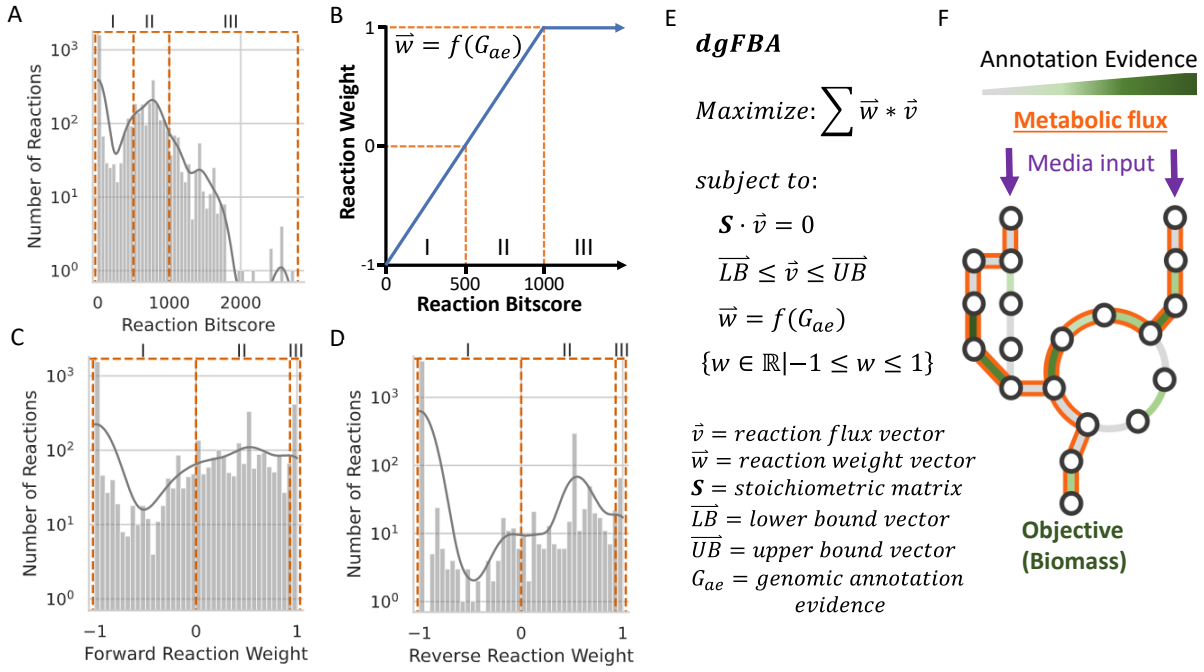

Figure 4.2: Data Guided Flux Balance Analysis.

A) Distribution of reaction bitscores for E. coli *K-12. B) This is a visual representation of the transformation function for calculating the reaction weights based on reaction bitscores. The reaction bitscore of 500 is an important value because it corresponds with zero in the weight space. C) Distribution of the calculated weights for forward reactions. D) The distribution of weights for reverse reactions shows that there are far fewer reactions that allow flux in both directions or only in the reverse direction. E) Data Guided Flux Balance Analysis optimization problem. Reactions with a positive weight are maximized and reactions with a negative weight are minimized proportional to the value of the weight. F) Toy network example demonstrating the flux-carrying reactions that would result from the pictured annotation evidence distribution and media inputs.*

Data Guided Flux Balance Analysis can be compared to parsimonious enzyme usage flux balance analysis (pFBA) to demonstrate how flux through the network changes with additional layers of information. The objective of pFBA is to uniformly minimize the sum of flux across all reactions, while maintaining flux through the biomass reaction (123). Since dgFBA maximizes the weighted flux through reactions with genetic evidence the flux distribution is consistently different from the pFBA flux distribution. However, the two optimization problems remain similar because the majority of reactions in the universal network do not have genetic evidence and are thus minimized in a dgFBA problem, just as they are in a pFBA problem. We compared dgFBA to pFBA to quantify how much impact the genetic data has on the flux distribution for each solution. We generated a separate pFBA and dgFBA flux solution for each known *E. coli* K-12 growth condition. We used two metrics to verify that dgFBA results in more reactions carrying flux, while also increasing the number of reactions that have associated annotation evidence (Figure 4.3A and 4.3B). We found that across all 199 growth conditions, the average number of FCRs for dgFBA was 305, which was 45 reactions greater than the average for pFBA solutions. We expected dgFBA to identify less parsimonious solutions than pFBA due to the influence imparted on the solution from the annotation evidence. It is important to note that the number of FCRs for the dgFBA solution in a single condition was always greater than the number of FCRs in the corresponding pFBA solution by at least 10 FCRs. A second important verification was to ensure that dgFBA also identifies solutions that contain a greater proportion of FCRs that have associated annotation evidence. We found that the average number of FCRs with annotation evidence greater than

or equal to our reaction bitscore threshold of 500 in dgFBA solutions was nearly 20% greater than the pFBA solutions.

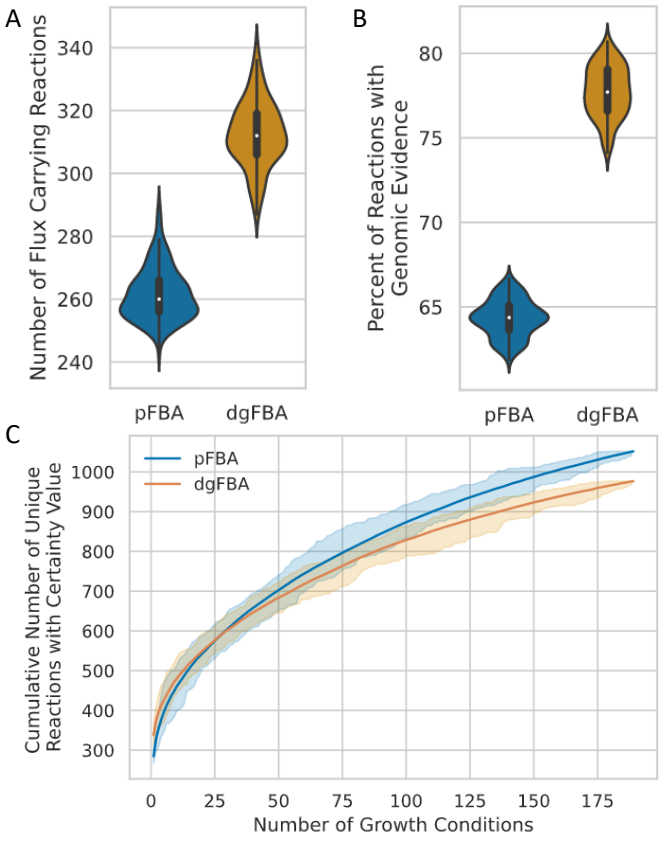

Figure 4.3: Data Guided Flux Balance Analysis breaks parsimony and identifies fewer unique reactions required for simulated growth on all experimental growth conditions.

A) The number of FCRs in each growth condition is visualized for parallel pFBA and dgFBA to quantify the degree to which dgFBA breaks parsimony. B) The number of reactions with bitscores above 500 that carry flux in a dgFBA solution is greater than the number in a pFBA solution. C) The cumulative number of unique FCRs identified by dgFBA is fewer than pFBA. The complete range in number of unique FCRs is indicated by the shaded regions.

To assess FCRs across all of the known growth conditions, we generated rarefaction curves each consisting of 10,000 samples to measure the full distribution of unique permutations of growth conditions that could be used to generate a GENRE. The x-axis displays the number of growth conditions used to calculate the total number of unique FCRs found (Figure 4.3C). The shaded regions show the minimum and maximum values sampled for each number of conditions included. The small range

between the minimum and maximum indicates that there is minimal advantage to optimizing for the minimum number of growth conditions that provide the maximum training value. Each individual growth condition adds unique reactions to the cumulative set of unique FCRs. However, the asymptotic shape of the average curves indicates that the total number of valuable unique minimal growth conditions may not be far beyond 200 conditions. The number of unique FCRs identified by dgFBA across all growth conditions is fewer than pFBA, indicating that there is a core set of FCRs with genetic evidence that dgFBA preferentially identifies over pFBA (Figure 4.3C). These data indicate that dgFBA performs as intended, reactions with genetic evidence preferentially carry flux even when there is a more parsimonious path which results in a diversion of flux away from extraneous reactions that are more parsimonious but lack sufficient genetic evidence.

Certainty Values Determine the Reactions Included in a CANYUN GENRE for *E. coli* K-12

The CANYUNs pipeline involves generating a dgFBA solution for each of the known growth conditions using the curated universal metabolic network. During the process of recording the FCRs for each condition, the directionality of each flux value is used to specifically determine the cumulative evidence for each reaction specific to direction. We proceeded to calculate a reaction certainty value for each reaction in the universal metabolic network based on the set of FCRs from each growth condition. The Certainty Value (CV) for a reaction is the ratio of the number of times the reaction carries flux in a growth condition over the total number of known growth conditions. A CV indicates the cumulative experimental evidence for the presence of the biochemical function in an organism-specific metabolic network. Using the *E. coli* K-12 genome and phenome, we calculated 690 reactions with CVs greater than zero in the forward direction (Figure 4.4A), and 127 reactions with CVs greater than zero in the reverse direction (Figure 4.4B). There are 45 reactions common to the two sets of reaction CVs (Figure 4.4C).

We built an *E. coli* K-12 specific GENRE that consists of the reactions identified to have CVs greater than zero, including only the reaction directionalities specifically with CVs. Reversible reactions that receive a CV above zero in only one direction were set to only allow flux in that direction. We simulated growth in each of the known growth conditions using the resulting cumulative model to determine the baseline performance of the model. The draft metabolic reconstruction, at this point, had an overall accuracy of 80% with a strong bias toward false positive growth calls (Figure 4.4D). To improve the model accuracy, we calculated the conditionally essential reactions for each of the conditions predicted to allow for growth, including false growth predictions. A comparison across the sets of conditionally essential reactions revealed reactions that, when removed, would provide a net benefit for improving the overall accuracy of the adjusted model. We identified that with the removal of a single reaction, RuBisCO, the number of false positives was reduced by 38 conditions and the number of true positives was only decreased by 7 conditions. RuBisCO was manually selected for removal because it had the maximum net benefit of 31 conditions and the least annotation evidence. All of the other candidate reactions for removal are plotted based on their net benefit to accuracy from removal versus their annotation evidence (Figure 4.4E). This process could be repeated for further alteration of the model. Although RuBisCO is an obvious reaction that should not have been included in the universal metabolic network before generating reaction CVs, this result demonstrates that there are reactions that may require manual removal from the universal metabolic network based on additional biological knowledge aside from there being no annotation evidence or contribution to mass-generating loops. However, CANYUNs allowed for rapid identification of reactions that may be improperly included during the process of procedural generation of a CANYUN GENRE.

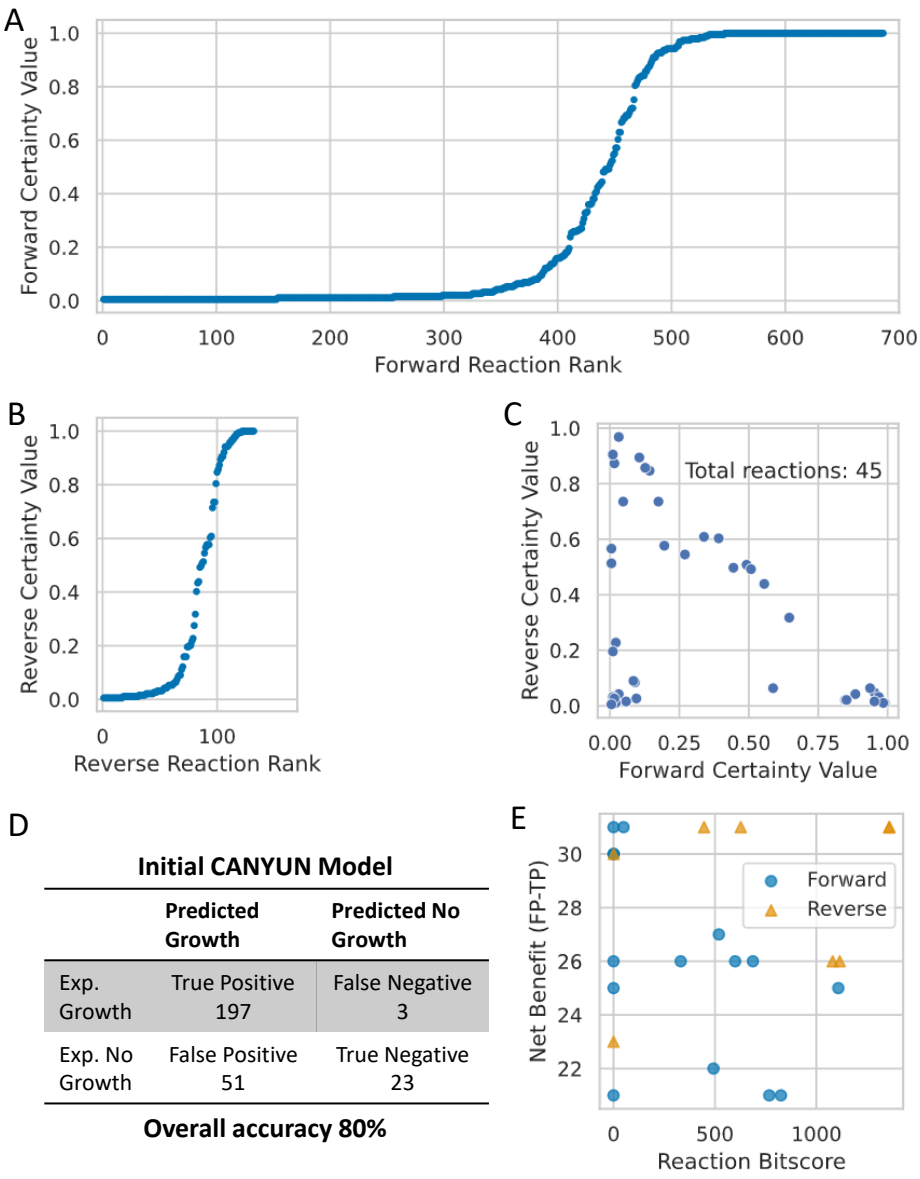

Initial CANYUN Model

	Predicted Growth	Predicted No Growth
Exp. Growth	True Positive 197	False Negative 3
Exp. No Growth	False Positive 51	True Negative 23

Overall accuracy 80%

Figure 4.4: **E. coli *K-12 CANYUNs model generation and draft processing.***

A) Ranked scatter plot of forward reaction Certainty Values. B) Reverse reaction Certainty Values. C) Certainty values for reversible reactions that carry flux in both directions. D) Initial accuracy of CANYUNs model before processing. E) Conditionally essential reactions allow for the user to identify reactions that can be selectively removed from the resulting model that improve the overall predictive accuracy. The net benefit refers to the number of false positives that will be correct minus the number of true positives lost due to removing a given reaction. RuBisCO is the forward reaction in the top left corner of the plot with maximum net benefit and minimum genetic evidence.

CANYUNs more accurately recapitulates phenotypic data

The final *E. coli* K-12 model from the CANYUNs pipeline can be compared with two automatically generated models using CarveMe and the manually curated model iML1515 to benchmark and validate its performance. Using the same input biochemical and genetic data as the CANYUNs model, we generated a CarveMe model without using phenotypic data to establish how subsequent gapfilling impacts the model accuracy (Figure 4.5A). The gapfilled CarveMe model that we generated had an overall accuracy of 76%, a 24% improvement over the untrained model (Figure 4.5B). The training process results in nearly all of the false negative predictions being corrected, as can be expected. The manually curated reconstruction, iML1515, was not specifically curated for all of the known growth conditions used to train the CarveMe model and the CANYUN model, but it remains a valuable point of comparison as the best representation of *E. coli* K-12 metabolism that is currently available. Our *E. coli* K-12 CANYUNs model shows the highest overall accuracy, while maintaining a balance in type 1 and type 2 error. The distinction between false positives and false negatives is notable because false negatives represent an opportunity to selectively add an organism-specific reaction to the universal model that directly corrects the issue. However, correcting false positive errors involves finding reactions to remove or adjust that result in minimal negative impacts to the rest of the model. CANYUNs provides a method for selectively adjusting the balance of error based on user preferences during the construction of the GENRE.

A **CarveMe Model without Gapfilling**

	Predicted Growth	**Predicted No Growth**
Exp. Growth	True Positive 100	False Negative 96
Exp. No Growth	False Positive 30	True Negative 39

Overall accuracy 52%

B **CarveMe Gapfilled Model**

	Predicted Growth	**Predicted No Growth**
Exp. Growth	True Positive 197	False Negative 3
Exp. No Growth	False Positive 62	True Negative 12

Overall accuracy 76%

C **iML1515**

	Predicted Growth	**Predicted No Growth**
Exp. Growth	True Positive 158	False Negative 41
Exp. No Growth	False Positive 28	True Negative 46

Overall accuracy 75%

D **CANYUN Model**

	Predicted Growth	**Predicted No Growth**
Exp. Growth	True Positive 189	False Negative 10
Exp. No Growth	False Positive 13	True Negative 61

Overall accuracy 92%

Figure 4.5: The E. coli CANYUNs Model performs better than iML1515 and CarveMe when simulating growth on all known phenotypic data.

A) The CarveMe model without gapfilling has a base accuracy of 52%. B) The CarveMe model we trained using all of the phenotypic data performs with an accuracy of 76%. However, there is a strong bias toward false positive predictions. C) The manually curated E. coli *K-12 model, iML1515, was not trained using all of the growth conditions. However, it performs with 75% accuracy while maintaining a relatively even split between false positive predictions and false negative predictions. D) The CANYUNs model we generated performs with 92% accuracy. The increased accuracy is primarily due to an improvement in true negative prediction rate.*

CANYUNs more accurately identifies the reactions present in iML1515

It is possible to generate a CANYUNs model using pFBA instead of dgFBA; in this case no genetic data incorporated to influence the flux distribution of the solution for each growth condition. The most parsimonious solution is determined for each condition. In doing so, we are able to establish a more precise understanding of how the inclusion of genetic annotation evidence impacts the discovery of reactions when compared to the manually curated *E. coli* K-12 model, iML1515. We did not expect the CANYUNs reactions to align perfectly with iML1515 since the manual curation process did not include all of the growth conditions used to train the CANYUNs model. However, since the sequence-to-reaction

dataset used to generate annotation evidence does not include all of the sequences used to build iML1515, we were able to track the FCRs that CANYUNs identifies without annotation evidence, yet are confirmed to be *E. coli* K-12 reactions by the iML1515 model. The 'Likely additions' category (Figure 4.6A and 4.6B) represents a set of reactions from the CANYUNs model with genetic annotation evidence (bitscore above 500) that are not present in iML1515 and cannot be validated using this comparison, but they may represent reactions that could be added to iML1515 to improve alignment with the phenotypic data. We demonstrate that the dgFBA CANYUNs model has 12% greater alignment with iML1515 at the reaction level, compared to the pFBA CANYUNs model (Figure 4.6C). The discovery accuracy is calculated as the number of FCRs that are identified by CANYUNs while lacking sufficient annotation evidence yet that were included in the iML1515 model. The dgFBA CANYUN model has a discovery accuracy of 62%, 24% greater than the pFBA CANYUN model. CANYUNs accurately identifies reactions that should be included in the *E. coli* K-12 metabolic network validated by the most recent manually curated reconstruction, iML1515.

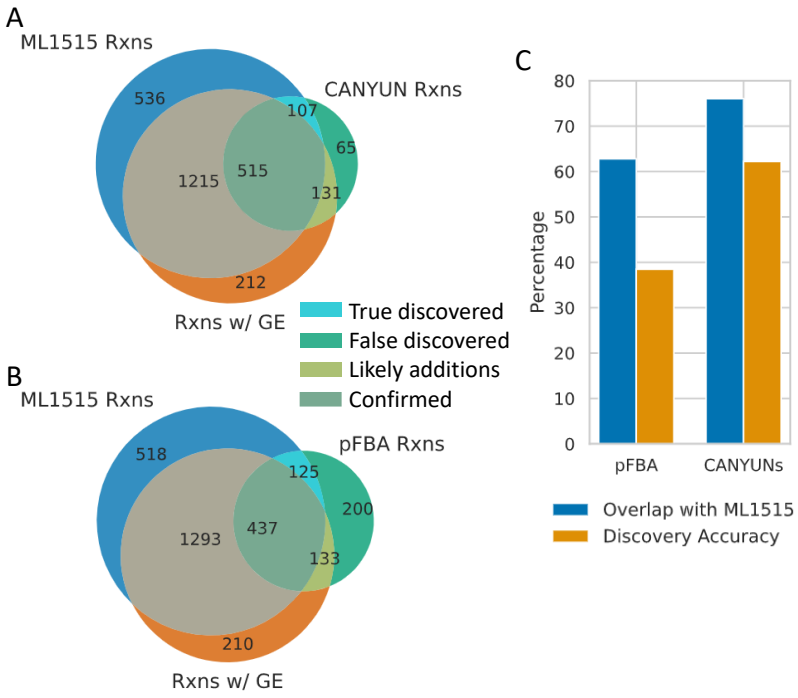

Figure 4.6: CANYUNs reaction certainty values accurately identify reactions found in iML1515.

The manually curated metabolic network, iML1515, provides a point of comparison to determine if CANYUNs accurately identifies reactions that should be included in a final model. A) By comparing our CANYUNs model with iML1515, we were able to place reactions into four categories. FCRs with genetic evidence and in iML1515 (confirmed), FCRs without genetic evidence in iML1515 (true discovered), FCRs with genetic evidence not in iML1515 (likely additions), and FCRs without genetic evidence and not in iML1515 (false discovered). The total amount of genetic evidence that is used to generate a CANYUNs model influences the accuracy of the FCRs. B) When we use pFBA instead of dgFBA in the CANYUNs pipeline, there are far more reactions that lack genetic evidence and are not in iML1515. C) The percent overlap of FCRs with reactions present in iML1515 increases from 62% when no genetic evidence is used (pFBA) to 76% overlap when all of the available genetic evidence is used.

A further analysis of the reaction CVs demonstrates that the accuracy of reaction inclusion in a CANYUN GENRE correlates positively with the magnitude of the reaction CV. The percent overlap with iML1515 improves rapidly when the bottom 30 reactions with the lowest certainty values are ignored. Overall, dgFBA provides a noticeable benefit over pFBA; however, there is a set of about 50 core reactions that are accurately identified with both optimization methods. We found that dgFBA strongly outperforms pFBA and CarveMe when evaluating the discovery accuracy. The performance of CANYUNs is in part explained by the reduced total number of discovered reactions compared to CarveMe. That

number represents a significant advancement when considering the process of manually validating the reactions with insufficient annotation evidence by searching for the appropriate gene-protein rule to add to the sequence-to-reaction dataset.

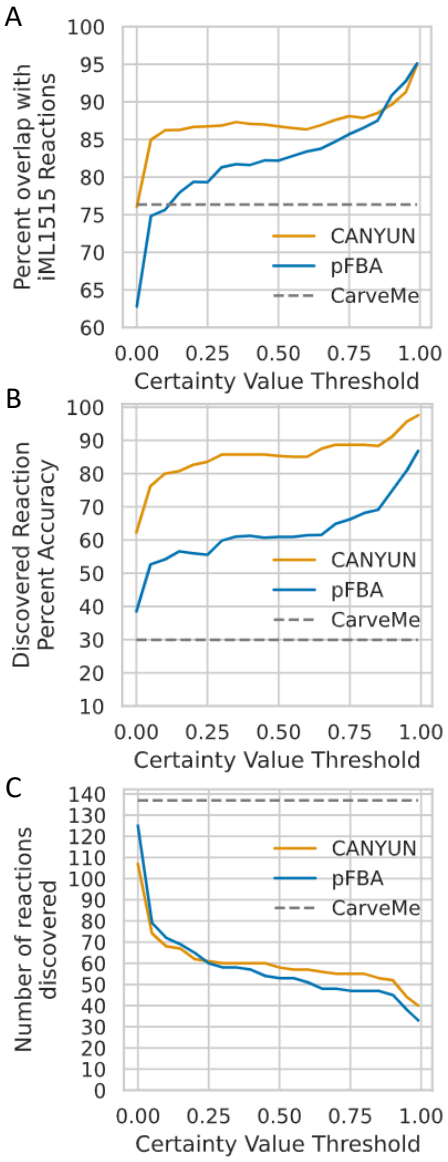

Figure 4.7: Reaction Certainty Values correlate with accurate reaction inclusion and comparison with CarveMe.

A) The percentage of reactions identified by CANYUNs that align with the iML1515 model correlates with the associated certainty value. All reactions with a certainty value greater than or equal to 0.99 have a 94% chance of being in the iML1515 model. B) The accuracy of discovered reactions, confirmed by iML1515, increases with the certainty values assigned using CANYUNs. C) Although the accuracy of the

discovered reactions increases with the certainty value, there is a significant drop in the number of reactions with the increase.

CANYUN GENRE for the probiotic strain: *E. coli* Nissle

We built a novel model of the *E. coli* Nissle metabolic network to demonstrate the application of CANYUNs and to provide an example representation of a CANYUN GENRE with all accompanying source data. Although Nissle has significant clinical relevance and is similar to *E. coli* K-12, there are no published Nissle metabolic network reconstructions that currently exist and are freely available. Nissle is a probiotic strain that has demonstrated measurable impacts on colonization resistance against human gastrointestinal pathogens (124–126). Additionally, it is important to note that several studies demonstrate that the metabolism of Nissle is phenotypically different from K-12. We generated novel phenotypic growth data for *E. coli* Nissle using Biolog Phenotype MicroArray 96-well growth plates. We performed growth assays for the carbon source plates, PM1 and PM2A, in both aerobic and anaerobic growth conditions. We found that the metabolic consumption profile of Nissle is 9% different from K-12 (Figure 4.8A and S2). There are 25 media conditions in which Nissle and K-12 do not align out of a total of 285. Nissle is able to grow in 16 conditions in which K-12 is not, in the other 9 conditions K-12 grows with Nissle does not. All inconclusive results for K-12 were treated as no growth conditions. Data for K-12 anaerobic growth in the PM2A plate does not exist on Ecocyc. All data is displayed in the Supplement (Figure S4.1 & S4.2 and Table S4.1).

We generated a CANYUN GENRE using the same input data discussed in Figure 4.1, although with the Nissle specific annotation evidence and our set of phenotypic growth experiments. The final model that we generated had an overall accuracy of 92%, with no false positive error. There are 18 false negative conditions that could be fixed by adding organism-specific reactions to the model. There were 481 reactions that received CVs and had high genetic evidence, indicating that they are likely to be actively catalyzed by Nissle during exponential growth. Additionally, in the process of building the Nissle model, we identified 114 reactions that have low genetic evidence, yet were included in the model with

CVs greater than zero. There were an additional 5 spontaneous reactions included. We assessed CVs associated with the 114 low evidence reactions to determine their rank of importance for future curation of the datasets used to generate this model. There were 34 reactions within the set that have no reference sequences and thus have unknown genetic evidence (Figure 4.8D). Finally, there were 80 reactions that had both low genetic evidence and CVs greater than zero (Figure 4.8E). The reactions with bitscores closer to 500 and high CVs have a high cumulative evidence indicating that they should be assessed further to determine the appropriate reference sequences that should be added to the dataset used to generate this model.

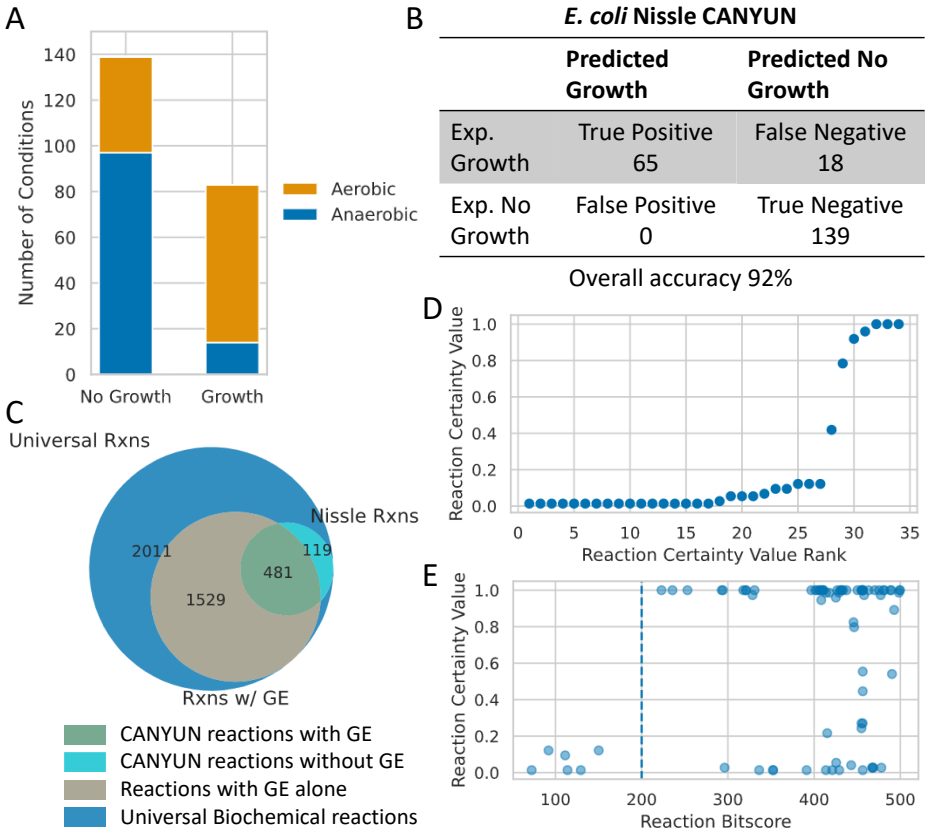

Figure 4.8: E. coli Nissle Model.

A) Phenotypic data used to build the model. B) The final accuracy of the model is 92% with no false positive predictions. C) Model reaction classes. The sequence-to-reaction dataset used to generate genetic evidence bitscores includes 3,017 reactions with associated sequences. D) Reactions that receive certainty values, but do not have reaction bitscores. E) Reactions with Certainty Values and low bitscores

(below 500). There are 80 reactions represented on this plot. Reactions with a high certainty value and a bitscore above 200 are likely candidates for additions to the sequence-to-reaction database.

4.4 Discussion

Introduced here is a procedural reconstruction method for the generation of CANYUN GENREs that accurately recapitulate phenotypic training data and select appropriate reactions to represent the biochemical capabilities of a target organism. CANYUNs leverages a novel form of FBA, dgFBA, to direct flux through the universal metabolic network during model building and curation resulting in a GENRE that is structural different from manually curated GENREs. Cumulative evidence for inclusion of a given reaction in a CANYUN GENRE is explicitly quantify during the reconstruction process. Existing methods rely heavily on genetic data to estimate the metabolic capabilities of an organism. CANYUNs fills a separate niche, it produces procedurally generated GENREs that include functional data such as phenotypic growth data as an integral step in the curation protocol. Maintaining a strong connection with all source data allows CANYUNs to guard against information loss that can occur. Most importantly, a core objective of CANYUNs is to leverage the uncertainty innate to the biological data used during the reconstruction process to generate a GENRE built upon continuous data inputs. This aspect of CANYUN GENREs differs from the presence of absence of reactions in other GENREs. The structure of CANYUN GENREs allows for the uncertainty across biological data to be managed via redundancy. Each type of data provides various benefits while mitigating associated error.

There is an existing paradigm in the field of constraint-based modeling: a GENRE can be either a reconstruction of a model depending upon the context in which it is utilized. CANYUNs formalizes a structure that highlights the important differences between a reconstruction and a model. Through this lens, a CANYUN GENRE can be viewed as a reconstruction when assessing all of the evidence that is utilized to identify organism specific reactions. A CANYUN GENRE can be viewed as a model when utilizing only the reactions that acquire CVs. The conceptual framework underlying this distinction is

grounded in the idea that phenotypic growth data should be utilized to contextualize the genetic and biochemical data, rather than determine the absolute inclusion or exclusion of reactions from a GENRE. By accepting that an organism specific GENRE is simply a contextualized version of the underlying universal metabolic network, there is additional flexibility that can be leveraged for future curation of the GENRE with additional biological data or expansion of the source data. This concept is the core difference between CANYUN GENREs and other GENREs generated using existing methods.

The technical characteristics that make a CANYUN GENRE unique from other methods revolve around a consistent connection to source data and management of associated uncertainty in the source data. CANYUN GENREs are structured to facilitate future curation by ensuring that all source data is an integral part of the model. As seen in Figure 4.8C, a CANYUN GENRE consists of four classifications of reactions: Universal biochemical reactions, reactions with GE and no CV, reactions with GE and a CV, and reactions with a CV and no GE. Each class of reaction has an associated continuous spectrum that indicates how much evidence has contributed to the reaction being in that class. Universal biochemical reactions have a spectrum of reference sequences (Figure 4.1D). Reactions with only GE have the reaction bitscore which is positioned on a continuous spectrum. Reactions with only a CV have the magnitude of the CV that represents the cumulative phenotypic and biochemical evidence associated with the reaction. Finally, reactions with a CV and GE have the most complex array of associated evidence including: genetic, phenotypic, and biochemical.

Procedural generation methods benefit from existing manually curated GENREs via their contribution to the universal biochemical network and the associated sequence-to-reaction reference dataset. Manually curated versions of foundational data provide the base on which procedural generation methods can be built upon. It has been shown that, procedurally generated GENREs benefit from manually curated data inputs (107). For example, ensuring that all reactions in the universal biochemical network are mass-balanced and that there are no mass-generating loops in the network

eliminates the need for further thermodynamic-based curation of the resulting GENREs (107,127). The high specificity required for the annotation of metabolic enzymatic function with accompanying thermodynamic and stoichiometric directionality is relatively unique to GENREs and thus a limiting factor in the building process. Reaction directionality is a simple, yet important aspect of curating GENREs. Often sequence annotation databases do not include specific information about reaction directionality. Directionality can become particularly important when a reaction is thermodynamically unfavorable in a certain direction. Improper directionality assignments can lead to free mass-generation and improper assignment of catalytic function. Our method provides a way to quantify reaction evidence specific to directionality by calculating CVs specific to the direction of the flux through reactions. This level of specificity provides more control over the model's behavior.

Genetic data is the base on which GENREs are built, yet not all genetic information is required to represent the metabolic network for an organism. Due to gene regulation and other aspects of metabolic control theory that are exceptionally challenging to incorporate into a GENRE, it is important to keep in mind that genetic data, with all associated uncertainties, is simply an imperfect lens through which an organism specific model can begin to take shape. Functional phenotypic data, when paired with a stoichiometrically accurate universal metabolic network, provides information for contextualizing the underlying genetic data. This conceptual framework provides the flexibility required for passively allowing unknown gene regulation across differing growth conditions to influence the building process. The core assumption in this conceptual model is that thermodynamic efficiency, both stoichiometric and enzymatic, is the primary governing objective at the cellular level. This is technically achieved during the prediction of growth by utilizing only the reactions with CVs for flux balance analysis. All other reactions with genetic evidence alone did not demonstrate their activity during the training of the model and are thus not active for growth predictions.

A core focus of this study was the need for better curation of source data used for procedurally generated GENREs. Curation of these datasets is far more useful for future model generation, opposed to the curation of specific models. The curation of specific models, separate from the source datasets, can result in thermodynamic inconsistences among models that make it difficult to simulate metabolic interactions. This method lays the groundwork for data-driven expansion of the sequence-to-reaction dataset by quantifying phenotypic evidence for the inclusion of sequences slightly below the functional bitscore threshold (in this study 500). With enough phenotypic data from an array of organisms, it would be possible to conservatively expand the reference dataset to propagate well-defined functional annotations to many more sequences and thus expand the ability to generate accurate models across a wide array of organisms. Additionally, CANYUN GENREs optimize for false negative predictions, thus specifically identifying areas of the universal biochemical network that need manual additions. Moving forward, CANYUNs may provide an additional starting point for analyses that provide more predictive capabilities. Nevertheless, CANYUNs provides solutions for several challenges in expanding genome-scale metabolic network reconstructions to model the vast array of microbes that exist in human associated microbial communities.

4.5 Methods

Universal metabolic network curation:

We started with the CarveMe universal model and added any new reactions from iML1515 to a universal metabolic network. Any metabolites with multiple formulas were altered to maintain only the metabolite formula used in the iML1515 model. Metabolites with multiple formulas that are not in the iML1515 model were adjusted based on stoichiometric consistency across all reactions. The final universal metabolic network is available on Github.

We utilized the following optimization problem to determine if the universal metabolic network contained any thermodynamically infeasible mass generation. The problem maximizes flux through a set

of sink reactions that allow flux to leave the system from within the cellular or periplasm compartment. No metabolites are allowed to enter the system through exchange reactions. This algorithm provides an output of all reactions that are able to carry flux when no external metabolites are provided. The simultaneous maximization of flux through all sink reactions allows for a thorough evaluation of all possible mass generating loops.

$Free\ mass\ generation\ check\ optimization\ problem$

$Maximize: \sum \overrightarrow{v_{snk}}$

$subject\ to$

$$\boldsymbol{S} \cdot \vec{v} = 0$$

$$\overrightarrow{LB} \leq \vec{v} \leq \overrightarrow{UB}$$

$$\vec{0} \leq \overrightarrow{v_{snk}} \leq \overrightarrow{1000}$$

$$\vec{0} \leq \overrightarrow{v_{ex}} \leq \vec{0}$$

$\overrightarrow{v_{snk}} = Sink\ rxn\ flux\ vector$

$\boldsymbol{S} = stoichiometric\ matrix$

$\vec{v} =$ intracellular flux vector

$\overrightarrow{LB} = lower\ bound\ vector$

$\overrightarrow{UB} = upper\ bound\ vector$

$\overrightarrow{v_{ex}} = exchange\ rxn\ flux\ vector$

<u>CANYUNs Reconstruction Building Process:</u>

We utilized the sequence-to-reaction database provided in the CarveMe publication. We aligned the unknown protein sequence fasta file with Diamond to calculate sequence alignment bitscores for each protein. We then calculated reaction bitscores for each reaction in the universal biochemical network utilizing the CarveMe method. For the CANYUN GENRE construction, the superset of all flux-carrying reactions determined using dgFBA for each of the know growth conditions are utilized to build a draft network reconstruction. The draft network reconstruction is processed to determine all of the

conditionally essential reactions for each of the draft model growth predictions (true and false positives). The reactions that are conditionally essential for more false positives than true positives are reactions that can be used to improve predictive accuracy. The reaction with the most leverage to improve model predictions is removed from the CANYUNs GENRE to create the final model. The model building process requires roughly 20 minutes from start to finish on an Intel Xeon processor with 4 cores.

CarveMe Model Generation:

We utilized CarveMe in a Windows 10 command line to generate a base model without gapfilling and a gapfilled model with all known growth conditions. All default parameters were used.

E. coli Nissle Data Collection and Model Generation:

We cultured *E. coli* Nissle in Biolog plates using a TECAN microplate reader. Optical density measurements were performed using a 600 nanometer wavelength. We used Biolog PM1 and PM2A plates. The cultures were started with an overnight culture in M9 4% glucose medium at 37 degrees Celsius from a single colony selection off an LB agar plate. The cells were centrifuged and washed with PBS three times and finally resuspended and diluted into the base Biolog inoculation fluid. The resulting OD of the Biolog inoculation fluid, after dilution, was calculated to be 0.01 OD.

We acquired the Nissle genome from EMBL. With this genome we implemented CANYUNs to calculate CVs and build an organism specific GENRE.

Code and Availability:

We utilized Python and Cobrapy for all aspects of this project. All code and data used is available on Github at github.com/Tjmoutinho/CANYUNs

4.6 Supplement

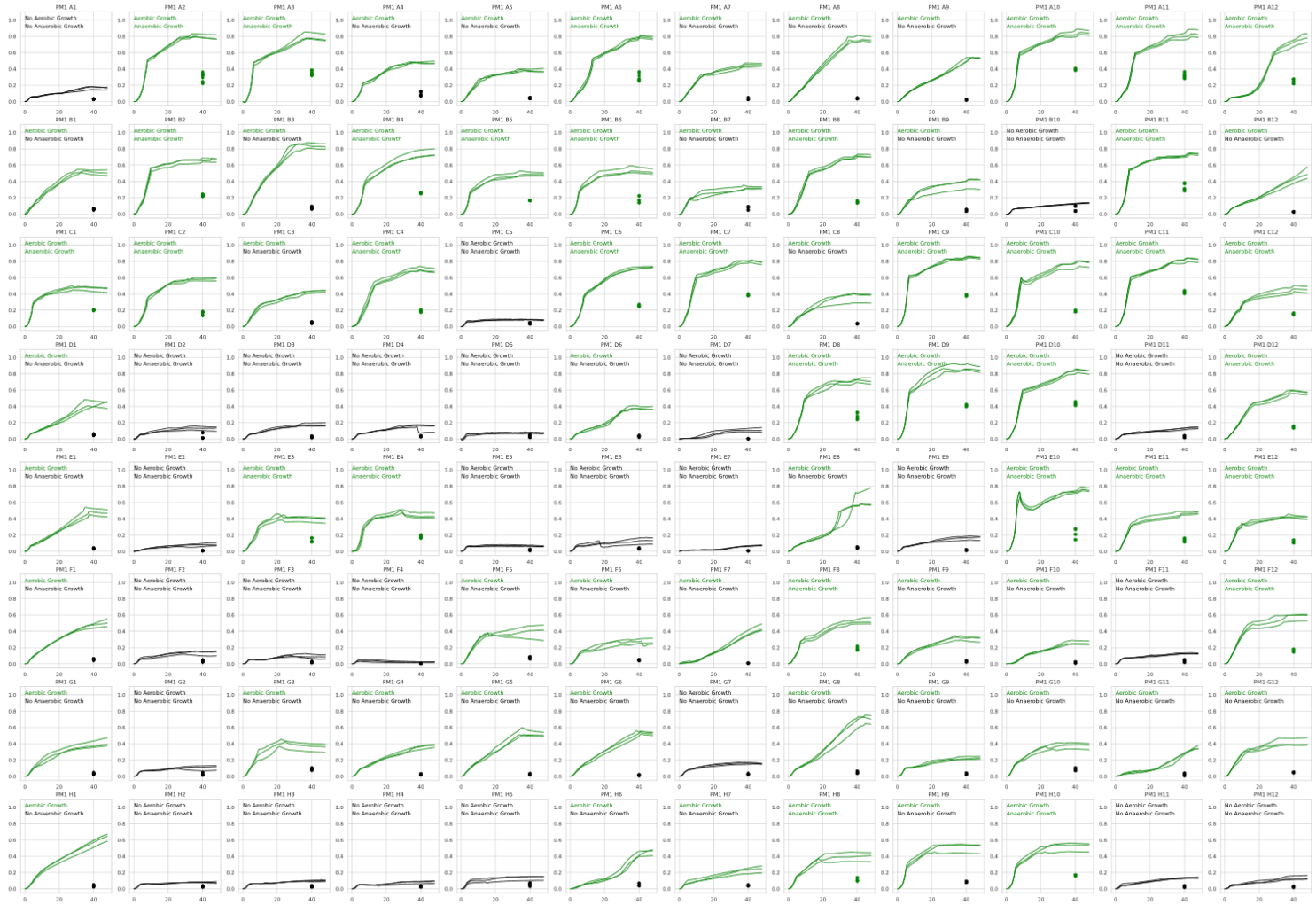

Figure S4.1: E. coli Nissle PM1 Biolog Growth Data. There are 70 aerobic growth conditions and 34 anaerobic growth conditions.

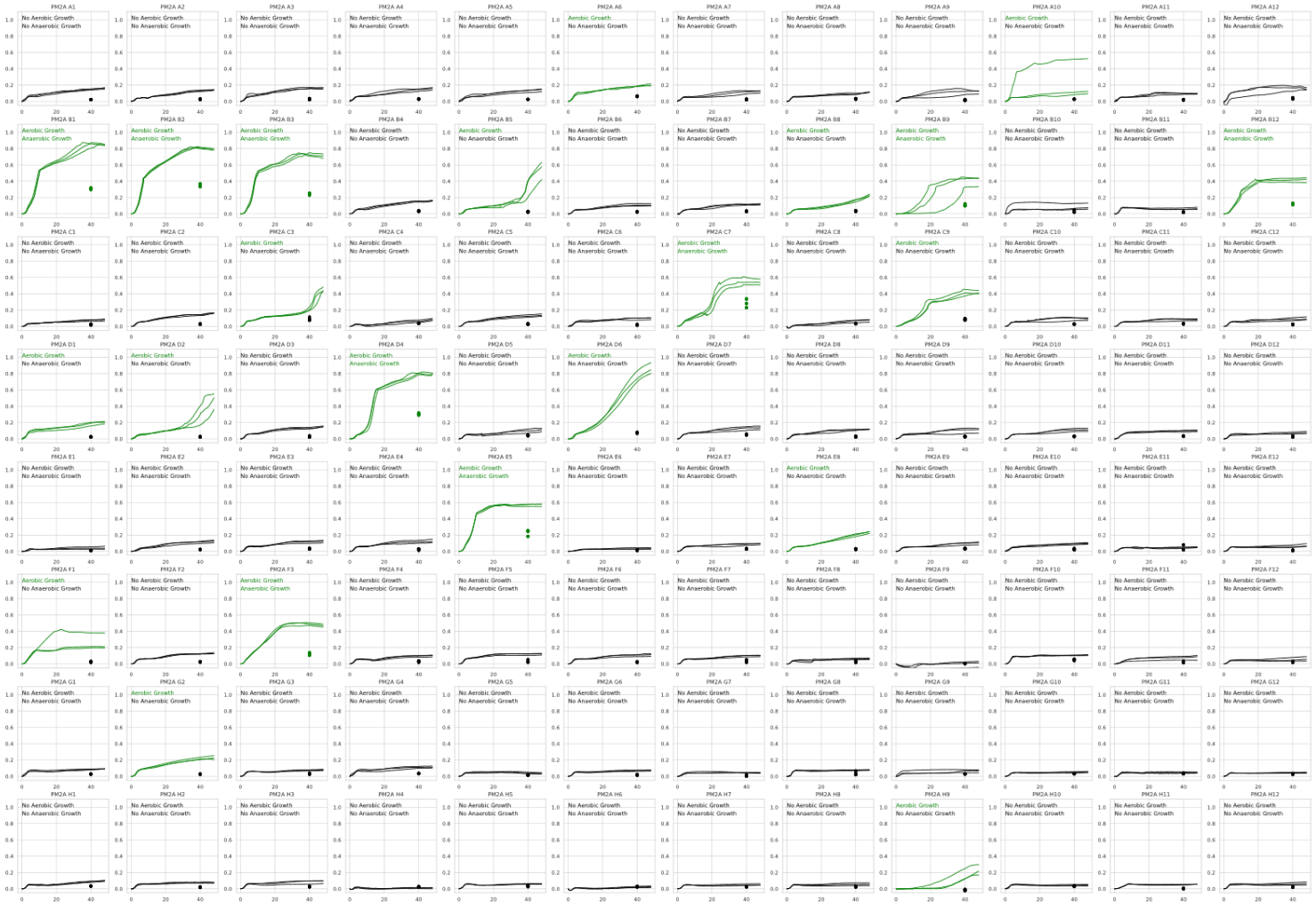

Figure S4.2: *E. coli* Nissle PM2A Biolog Growth Data. There are 22 aerobic growth conditions and 9 anaerobic growth conditions.

Supplemental Table 4.1: Difference in E. coli Nissle growth compared to *E. coli* K12. Anaerobic data for K-12 growth in Biolog plate PM2A was not available on EcoCyc.

Index	Metabolite Name	Biolog Plate and Well #	Culture Environment	*E. coli* K-12 Growth	*E. coli* Nissle Growth
1	Dulcitol	PM1 – A12	Aerobic	No Growth	Growth
2	L-Glutamic acid	PM1 – B12	Aerobic	No Growth	Growth
3	Glucuronamide	PM1 – H7	Aerobic	No Growth	Growth
4	N-Acetyl-D- Galactosamine	PM2A – B1	Aerobic	No Growth	Growth
5	D-Raffinose	PM2A – D1	Aerobic	No Growth	Growth
6	Salicin	PM2A – D2	Aerobic	No Growth	Growth
7	L-Alaninamide	PM2A – G2	Aerobic	No Growth	Growth
8	D-Lactitol	PM2A – C3	Aerobic	No Growth	Growth
9	L-Sorbose	PM2A – D4	Aerobic	No Growth	Growth
10	D-Arabinose	PM2A – B5	Aerobic	No Growth	Growth
11	D-Tagatose	PM2A – D6	Aerobic	No Growth	Growth
12	Arbutin	PM2A – B8	Aerobic	No Growth	Growth
13	β- Hydroxybutyric acid	PM2A – E8	Aerobic	No Growth	Growth
14	2-Deoxy- D-Ribose	PM2A – B9	Aerobic	No Growth	Growth
15	Laminarin	PM2A – A10	Aerobic	No Growth	Growth
16	M-Tartaric acid	PM1 – E2	Aerobic	Growth	No Growth
17	D-Fructose- 6-Phosphate	PM1 – E4	Aerobic	Growth	No Growth
18	Acetoacetic acid	PM1 – G7	Aerobic	Growth	No Growth
19	α- Ketobutyric acid	PM1 – D7	Aerobic	Growth	No Growth
20	α- Hydroxybutyric acid	PM1 – E7	Aerobic	Growth	No Growth
21	5-Keto-D- Gluconic acid	PM2 – E12	Aerobic	Growth	No Growth
22	D-Serine	PM1 – B1	Anaerobic	Growth	No Growth
23	D-Saccharic acid	PM1 – A4	Anaerobic	Growth	No Growth
24	L-Galactonic acid-γ- Lactone	PM1 – H9	Anaerobic	Growth	No Growth
25	Methylpyruvate	PM1 – G10	Anaerobic	Growth	No Growth

Chapter 5 Novel co-culture plate enables growth dynamic-based assessment of contact-independent microbial interactions

Thomas J. Moutinho Jr.[1], John C. Panagides[1], Matthew B. Biggs[1], Gregory L. Medlock[1], Glynis L. Kolling[1], Jason A. Papin[1]

1. Department of Biomedical Engineering, University of Virginia, Charlottesville, VA USA

Published in PLOS One; 2017

5.1 Abstract

Interactions between microbes are central to the dynamics of microbial communities. Understanding these interactions is essential for the characterization of communities, yet challenging to accomplish in practice. There are limited available tools for characterizing diffusion-mediated, contact-independent microbial interactions. A practical and widely implemented technique in such characterization involves the simultaneous co-culture of distinct bacterial species and subsequent analysis of relative abundance in the total population. However, distinguishing between species can be logistically challenging. In this paper, we present a low-cost, vertical membrane, co-culture plate to quantify contact-independent interactions between distinct bacterial populations in co-culture via real-time optical density measurements. These measurements can be used to facilitate the analysis of the interaction between microbes that are physically separated by a semipermeable membrane yet able to exchange diffusible molecules. We show that diffusion across the membrane occurs at a sufficient rate to enable effective interaction between physically separate cultures. Two bacterial species commonly found in the cystic fibrotic lung, *Pseudomonas aeruginosa* and *Burkholderia cenocepacia*, were co-cultured to demonstrate how this plate may be implemented to study microbial interactions. We have

demonstrated that this novel co-culture device is able to reliably generate real-time measurements of optical density data that can be used to characterize interactions between microbial species.

5.2 Introduction

There exists an extensive amount of interaction among microorganisms in microbial communities (128–130). An improved understanding of these interactions and their governing mechanisms in a physiologically relevant context will enable more informed treatment of polymicrobial infections and more precise modulation of microbial communities (131–133). Interactions between microbes are characterized using a variety of methods (134). Many interactions that take place within microbial communities are due to diffusible molecules such as cross-fed metabolites, quorum sensing molecules, and antimicrobial compounds (135,136). For example, muricholic acid, a microbe derived secondary bile acid inhibits *Clostridium difficile* taurocholic acid-mediated spore germination (137). Interactions mediated via diffusible molecules generally do not require the physical interaction of cells and are thus contact-independent (138–141). These interactions are challenging to characterize with existing approaches (139).

Common co-culture techniques include well mixed co-cultures (142), conditioned media exchange (143), agar plate colony assays (144,145), and membrane divided co-culture such as Corning ® Transwell ® co-culture plates (146). Each of these methods are limited in their ability to phenotypically characterize the growth dynamics of the microbes in co-culture. In a mixed co-culture it is challenging to measure the individual growth curves of the two species using high-throughput techniques. It is possible to use qPCR techniques to determine the relative abundance of each species; however, this is a technically and logistically challenging experimental technique requiring the development of specific primers for each species (147,148). Conditioned media exchange experiments are limited to unidirectional interactions which do not capture the dynamic response of cells to changing conditions (143). The Corning ® Transwell ® culture plates keep cells physically separate while allowing for contact-independent interactions, yet the horizontal membrane does not allow for the collection of optical density based continuous growth curve data for each culture.

Since the advent of semipermeable membrane-divided co-culture tools (149,150), to the best of our knowledge, this concept has never been interfaced with automated plate reader technology for the high-throughput continuous quantification of optical density-based phenotypic assessment of interacting cultures. Optical density of liquid bacterial cultures has been used for a multitude of phenotypic studies that aim to determine the relative changes in cellular growth subject to various environmental conditions (151–156). We present a novel co-culture plate with a vertically oriented membrane that maintains physical separation of two liquid cultures, yet allows for real-time contact-independent interactions across the membrane. The vertically oriented membrane allows for the co-culture plate to interface with a standard 96-well plate reader that is able to continuously monitor the optical density of both cultures on either side of the membrane. This culture tool is a simple, convenient, and inexpensive method for generating individual growth curves of two batch bacterial cultures as they interact across a membrane.

5.3 Materials and Methods

Strain Information

We used *Escherichia coli* (K12), *Pseudomonas aeruginosa* (PA14), and *Burkholderia cenocepacia* (K56-2) in this study.

Media Preparation

Lysogeny broth – Miller (LB) medium: tryptone (10g/L), yeast extract (5g/L), NaCL (10g/L), pH was adjusted to 7.0 with NaOH. In several experiments the LB media was diluted with 1x Dulbecco's Phosphate Buffered Saline (DPBS) (Gibco by Life Technologies). This dilution is indicated throughout the paper as the percentage of LB that is in the diluted media.

Sterilization Procedures

Before each experiment all parts of the co-culture plate were steam autoclaved at 121°C, 100kPa, for 60 minutes. The polycarbonate membranes (Isopore™ Membrane Filter, 0.1 µm VCTP; EDM

Millipore) were prepared by soaking in 70% ethanol for 10 minutes. For further description and rationale, see the Supplement. In a biosafety cabinet, the ethanol-soaked membranes were clamped between the wells and the assembly was left for 10 minutes to allow the ethanol to evaporate. For plate assembly protocol and visual aids, see the Supplement.

Counting of Colony Forming Units (CFUs)

CFUs were counted as previously reported (157). Briefly, a serial dilution down to 10^{-7} for each of the original cultures was prepared, 10 mL of each dilution was dripped onto LB agar plates and left to dry for roughly 10 minutes. The CFU plates were then incubated for the appropriate amount of time for visible colony growth. Colonies were then manually counted. Reported counts were done in quadruplicate (n=4).

Growth Curve Collection and Processing

Each well of the co-culture plate was loaded with 2 mL of media. Where appropriate, wells were inoculated at a calculated OD_{600} of 0.0005 with the bacterial strain specified. The co-culture plate was then placed into a Tecan Infinite M200 Pro, incubated at 37°C, shaken linearly at 3mm 450 rpm, and OD measurements were recorded at 600 nm every 5 minutes. All of the experiments were conducted in triplicate with biological replicates. The data from each experiment was exported as an Excel file and processed in MATLAB (R2014b; Mathworks). The growth curve plots consist of the average (bold line) displayed with the maximum and minimum values (as shaded regions around the average line). All growth experiments were conducted in triplicate. The MATLAB scripts used for all data processing are in the Supplemental Data.

Scanning Electron Microscopy (SEM)

Following an *E. coli* experiment with the co-culture plate, the polycarbonate membranes were fixed for 30 minutes with glutaraldehyde (2% by vol.). Followed by three 5-minute rinse steps in 1x DPBS. Samples were then dehydrated using increasing concentrations of ethanol, 10 minutes each in 30,

50, 70, 80, 90, 100, 100% (ethanol in water). The membranes were further dehydrated for 10 minutes in HMDS (hexamethyldisilazane; Sigma). Finally, the membranes were stuck to SEM stubs with adhesive carbon strips using the Phenom starter kit (Ted Pella, Redding, CA, USA) and sputter coated with gold using a SCD005 sputter coater (Bal-tec, Los Angeles, CA, USA). The final samples were imaged using a Sigma VP HD Field-emission SEM (Zeiss, Pleasanton, CA, USA) at 10,000x magnification through the University of Virginia Advanced Microscopy Facility.

Device Design and Machining

All of the parts for the co-culture plate were designed in SolidWorks 2015; all of these files can be found in the Supplemental. The files were exported as STL files and G-code was written for CNC machining. The aluminum parts were cut using a waterjet cutter and the holes were tapped by hand. The polypropylene wells were started using a waterjet cutter and finished using a milling machine. The polycarbonate was also cut using the waterjet cutter. All parts are designed to be able to be CNC machined without the use of a waterjet cutter. The silicone gaskets were made using a laser cutter (Universal laser Systems X-660 with a 50 watt CO_2 laser). For a detailed list of the parts please refer to the Supplement.

5.4 Results

Design and Description

The vertical membrane co-culture plate consists of eight co-culture chambers, each chamber is composed of two wells separated by a membrane that is replaced before each experiment. Each well is designed to hold 2 mL of culture and this 4 mL of total liquid in each chamber. All of the materials used for the body of the plate can be sterilized via autoclave. The outer dimensions and wells on the plate line up with the dimensions and wells of a standard Corning ® 96-well plate, allowing it to interface with any plate reader designed to read 96-well plates. Each of the co-culture wells lines up with two wells on

a 96-well plate, allowing for an internal technical replicate to be collected for each well to reduce noise (Figure 5.1A).

The well walls are machined polypropylene, bolted to a machined aluminum base. Clamped between the polypropylene wells and aluminum base are clear polycarbonate pieces acting as the bottom of the wells. A silicone gasket creates a liquid tight seal on the bottom edge of the wells. Additional silicone gaskets are adhered to the side ports in the well walls to create a seal against the membrane which is clamped between the wells. The location of the membrane is indicated in Figure 5.1B. Any type of membrane can be used in this plate; this point is discussed in the Materials and Methods section.

The base of the plate is composed of three separate parts. Each of the wells is first clamped onto the three base parts and these parts are subsequently clamped together horizontally after the membranes are in place. The dual clamping design allows for adequate force to be applied to create water tight seals both against the bottom of the wells and the sides where the membranes are placed. For further description of the design and machining of the plate, refer to the Supplement. Additionally, a video of the assembly process is provided, see the Availability section below.

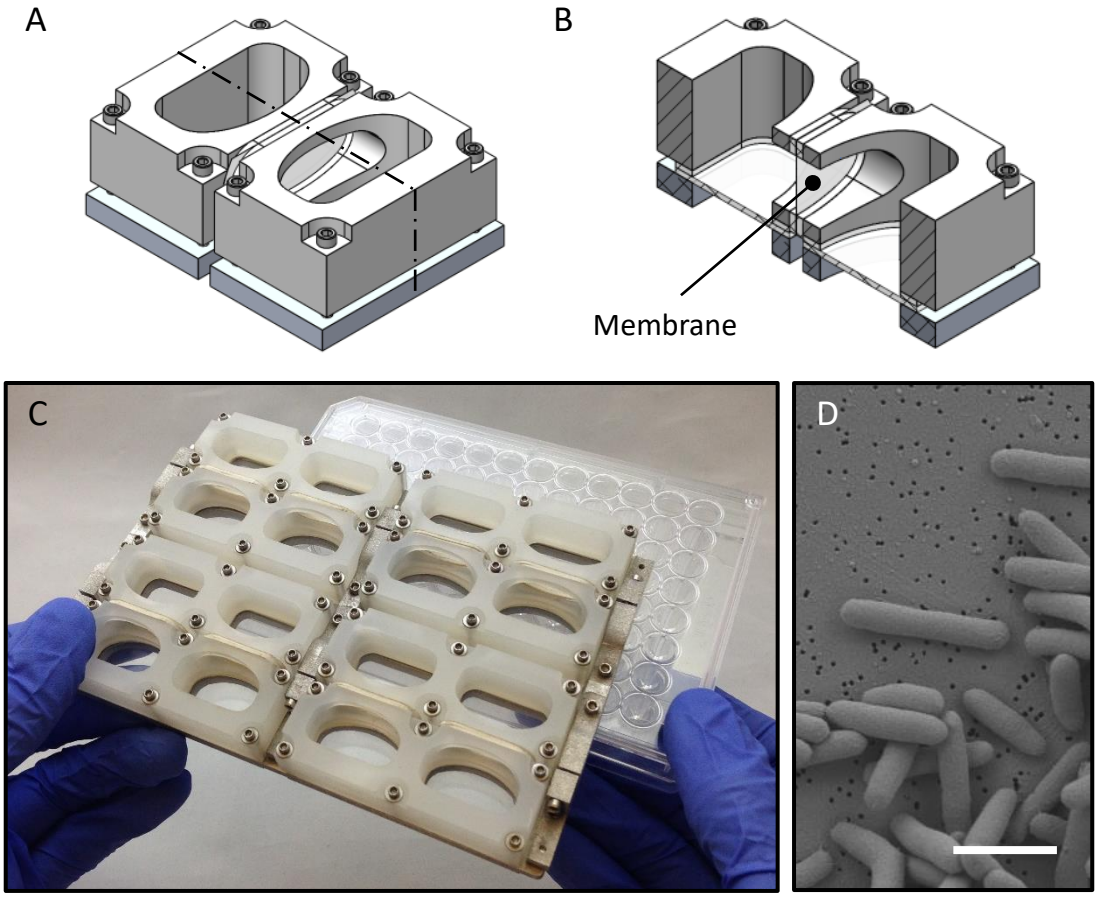

Figure 5.1. Co-culture plate design.

The co-culture plate consists of eight individual co-culture chambers. Each chamber consists of two wells that are able to hold liquid cultures that are physically separated by a semi-permeable membrane that allows for diffusion-mediated interactions. A representative isometric mechanical drawing of a single co-culture chamber is shown in (A), note it is composed of two wells. For a better view of the chamber, a cross-sectional view of it is shown in (B); the semi-permeable membrane is labelled. The co-culture plate composed of eight co-culture chambers has the same profile as a standard 96-well plate. Each well on the co-culture plate aligns with two wells of a 96-well plate and the culture volume is 2 mL per well (4 mL total per chamber) (C). An SEM image captures E. coli cells fixed on the surface of a polycarbonate membrane with 0.1 µm pores (D); the scale bar is 2 µm.

Validation

The co-culture plate was evaluated for basic functions to guide the interpretation of the data generated using this novel platform. First, we explored whether the rate of metabolite diffusion across the membrane would influence growth dynamics of a culture. Second, we confirmed that the membrane was a sufficient barrier to maintain physical isolation between wells. Finally, we

characterized interactions of a microbe with itself across the membrane, as a control for later multi-species co-cultures.

We characterized the impact that diffusion of metabolites across the membrane might have on growth characteristics. It was composed of four concentrations of two conditions, 'pre-mixed' and 'gradient' (Figure 5.2). The 'pre-mixed' condition is inoculated on one side of the membrane and has equal concentrations of LB (diluted with DPBS) on either side. The 'gradient' condition is also inoculated on one side of the membrane, but starts with all of the LB on the opposite side. Therefore, for growth to occur on the DPBS-inoculated side, the LB must diffuse across the membrane. The total quantity of LB provided between each condition was held constant. These two conditions were assayed at four different concentrations to demonstrate the observed behavior at various concentration gradients across the membrane, ranges of maximum optical density, and resulting population densities. We observe that there are only slight differences between the paired conditions at all four concentrations. These results indicate that the essential metabolites in LB are able to diffuse across the membrane at a sufficiently rapid rate to allow *E. coli* to grow similarly to the control case.

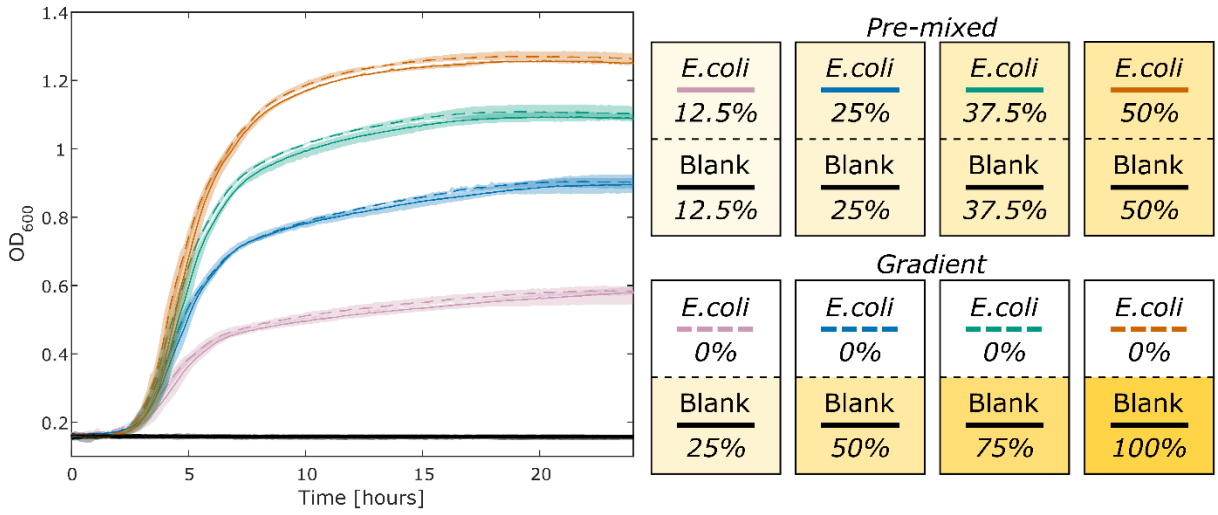

Figure 5.2: Real-time diffusion of metabolites across a membrane.

One side of each co-culture chamber was inoculated with E. coli, as seen in the pictorial legend on the right, each box represents a chamber with a black dashed line representing the membrane. The terms 'pre-mixed' and 'gradient' describe the initial media conditions. The gradient condition was loaded with LB on one side and 1x DPBS on the other. The pre-mixed condition was loaded with LB that was diluted in half with DPBS to simulate complete diffusion of LB across the membrane. These two conditions were tested with four initial concentrations of LB, 25%, 50%, 75%, and 100%, all diluted using 1x DPBS. The final pre-mixed concentration of the medium for each well was 12.5%, 25%, 37.5%, and 50% LB. This experiment was cultured as described in the methods for 24 hours. This experiment was conducted in triplicate (n = 3).

The data for Figure 5.2 was generated in triplicate such that there were 24 individual co-culture chambers inoculated on one side of the membrane only. Of these 24 individual cases, the optical density of the negative control side was measured to test that the membrane serves as a sufficient barrier to *E. coli* crossing from one well to the other. We never observed *E. coli* contamination from one well to another, therefore the design of the plate and size of the pores in the membrane (Figure 5.1D) are sufficient to maintain complete physical separation between the two sides of each chamber and yet allow for the exchange of nutrients and small molecules to support growth without a notable defect in the associated growth dynamics for the conditions we tested. Pictures of the plate can be seen with co-cultures at the end point in the Supplemental (Figure S5.2).

One potential application for this co-culture plate is the characterization of growth dynamics for two different species on either side of the membrane. To determine the basic characteristics of co-culture between competing cultures, we cultured *E. coli* in isolation on one side of the chamber for one condition and two *E. coli* populations were cultured in adjacent wells separated by the membrane and thus competing for nutrients (Figure 5.3). Both of these conditions were assessed at 50% LB (diluted with 1x DPBS) and 100% LB. The condition in which *E. coli* is isolated on just one side of the co-culture chamber acts as a reference point compared to the case in which two *E. coli* populations are competing. For the condition in which *E. coli* is competing and cultured with 100% LB, the growth characteristics are similar to those observed when *E. coli* is isolated and cultured in 50% LB. These data indicate that the isolated and competing conditions with a certain microbe and media condition can act as an

approximation for the hypothetical case in which two different species in co-culture on either side are in complete metabolic competition with each other. In this context, complete metabolic competition means that the cultures on either side have the same metabolic requirements, this is only the case when the same species are on both sides of the membrane. The growth curve representing complete metabolic competition can be used in tandem with the isolated condition in which there is no metabolic competition for a phenotypic assessment of interactions between two different species in co-culture across the membrane.

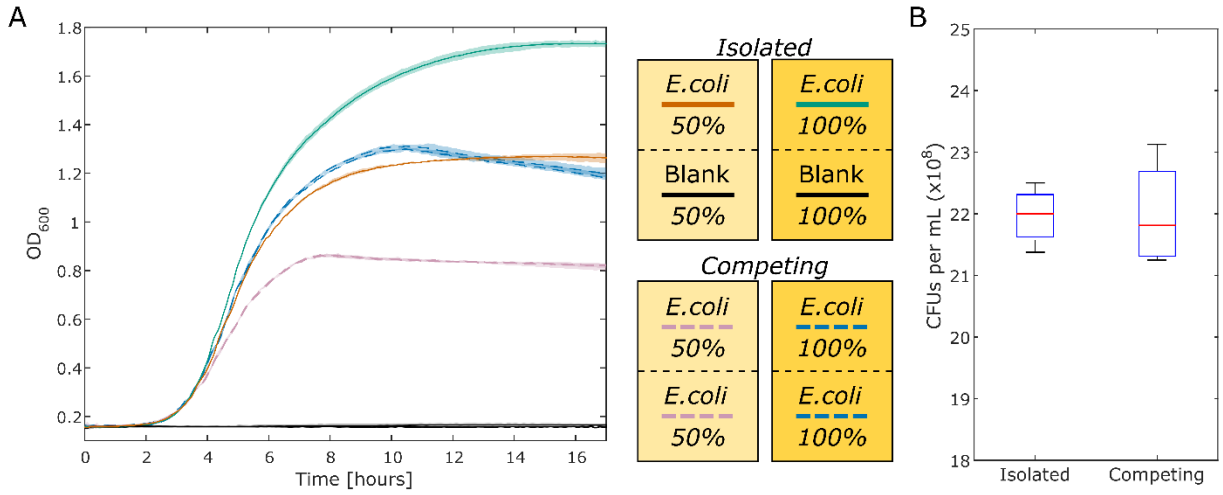

Figure 5.3. Comparison of isolated versus competing cultures.

(A) The green (100% LB) and red (50% LB) lines are the isolated culture condition that have E. coli cultured on only one side of the membrane with blank media on the other. The OD for the side of the well that is not inoculated is plotted in black (it maintains the original OD; there is no growth, as expected). In this condition, E. coli has access to all of the nutrients on both sides of the membrane, but cell growth is physically constrained to one side. The blue (100% LB) and purple (50% LB) dashed lines are the competing culture condition that have E. coli cultured on both sides of the membrane. For the competing cultures, the growth curves from both sides are plotted individually. In this condition, each E. coli population must compete for the available nutrients. The maximum and minimum values of the generated growth curves, conducted in triplicate, are displayed as shaded regions around the plotted averages. (B) The biomass produced is approximated by the CFU count of each culture. The CFU counts for the isolated condition as displayed are divided in half to compare to the competing condition, discussed further in the text. These data are the result of four experiments. The boxplot whiskers represent +/- 2.7σ from the mean.

A follow up experiment was conducted to determine if the same number of CFUs, from both sides of the membrane, are produced in the competing versus the isolated conditions. Samples were taken from the 50% LB isolated and competing conditions at 10 hours into incubation. The 50% LB condition was chosen to limit the impact of OD non-linearity and inhibition of growth due to spatial restrictions and prioritize nutrient depletion as the major limiting factor on biomass production. The bacteria were diluted, plated, and CFUs were counted (Figure 5.3B). The CFU counts for the isolated condition were divided in half to adequately compare to one side of the competing condition. This was done because all of the biomass in the insolated case is located on one side whereas the biomass is split evenly on either side in the competing condition. It can be seen that the same total number of CFUs are present in both the competing and the isolated conditions from Figure 5.3A. The equivalence between the two conditions in this boxplot indicates that the same number of viable cells are produced in the two different conditions.

Co-culture of Multiple Species

Infection with *P. aeruginosa* (PA) is pervasive in cystic fibrosis patients (158). Co-infection with *B. cenocepacia* (BC) can lead to increased mortality rates (159). These pathogens have been shown to interact in cystic fibrosis infections (160). We used the co-culture plate to determine the growth characteristics when PA and BC in which media, nutrients, and small molecules are shared. The condition in which a microbe is competing with itself across the membrane is an approximation of complete metabolic competition. The competing and isolated conditions, as defined in Figure 5.3, can be used as points of reference when assessing the impact another species has on a culture. In this case, we can see that when PA and BC are co-cultured, BC growth is negatively impacted by the presence of PA (dashed purple), more so than when it is competing with itself (dashed red). However, it appears that PA is unaffected by the present of BC (solid purple vs. solid blue).

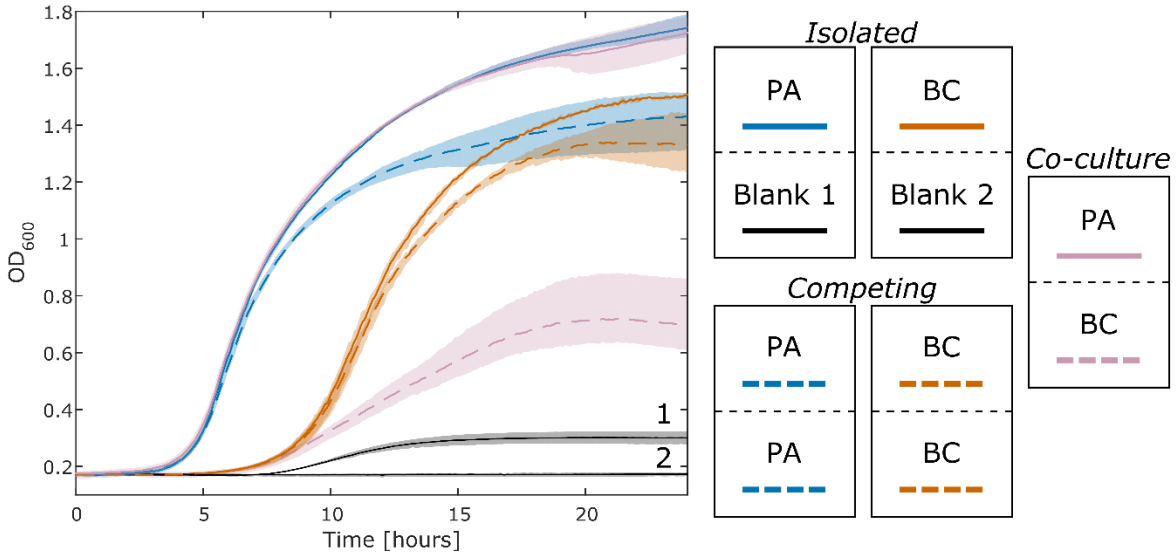

Figure 5.4. Growth curves of P. aeruginosa (PA) and B. cenocepacia (BC) in co-culture.

The culture conditions can be seen in the legend on the right side of this figure. All wells are started with 100% LB. The purple lines are gathered from the co-culture of PA and BC. The isolated PA and BC cultures are the solid blue and red lines respectively. The black lines are controls from the side of the wells that were not inoculated for the isolated PA and BC cultures. The black line slightly increases (Blank 1) as a result of pyoverdine (produced by PA) that partially absorbs at 600 nm. This result is discussed further in the Supplement (Figure S5.3). The growth curves from each of the two competing PA and BC cultures (dashed blue and red lines respectively) are nearly identical (similar to blue and purple in Figure 5.3) and thus are averaged to simplify the plot. The growth of BC (dashed purple) is negatively impacted when in co-culture with PA (solid purple).

5.5 Discussion

In this study, we present a novel tool to enable dynamic growth measurements of individual species interacting in co-culture. Mixed co-culture studies rely on a number of methods for differentiating between specific species when a semi-permeable barrier is not utilized. When applied to mixed co-culture experiments, CFU assays require that populations can be discriminated based on colony morphology (161). Similarly, flow cytometry based counting assays require discrimination by cellular morphology (162). Neither of these assays can be used to study co-cultures of morphologically similar populations. Species-specific qPCR assays can be used when genomic sequences are available

(147,163,164). However, manual sampling requires sufficient volume for DNA extraction and therefore greatly constrains possible experimental designs. This requirement of large culture volumes is a limitation shared by all methods that require periodic manual or automated sampling of the culture. Additionally, RT-qPCR assays must be developed for each species in a co-culture study while limiting nonspecific amplification. Species-specific delivery or expression of fluorescent markers are used to discriminate between microbes (161), but several experiments are required during the design of each marker to ensure specificity and stability of the marker. Additionally, genetic alteration of the microbes of interest may be undesirable. While most of these methods can be used in a broader context than batch co-culture in a liquid medium, the experimental design and optimization required for them limits throughput relative to the co-culture plate presented here.

As presented, this novel co-culture plate is able to maintain physical separation of two interacting cultures, while allowing for diffusion mediated interactions. Metabolites across the membrane appear to diffuse across at a sufficiently high rate to not be a limiting factor for growth dynamics. We are able to use the plate to investigate the co-culture of two different species with the use of self-competing controls and isolated culture controls. These controls can be used as a reference for the experimental condition of two species interacting across the membrane.

A particular strength of this co-culture plate is the ability to measure optical density data in real-time. This high temporal resolution captures complex growth dynamics that might not be observed with methods that require manual sampling of the culture. Separating the microbial cultures with a membrane eliminates the need to differentiate the individual species in co-culture. Furthermore, no genetic tools are required in order to screen microbes in this co-culture plate. One possible use of this device could be to co-culture a single species in one well with a complex community in the other well. Although it is not developed here, the wells on the co-culture plate have an adequate volume of media to allow for additional multi-omics analyses to be conducted on the cultures at the end point of the

experiment. Such analyses might involve the evaluation of concentration gradients of metabolites across the membrane, or to conduct transcriptomics of cells that are interacting with each other. Furthermore, this novel tool makes it exceptionally simple to generate phenotypic data on the dynamic interactions between two microbial species. The setup for such an experiment (e.g. Figure 5.4) requires less than two hours (See Supplement).

Although the proposed co-culture plate, in its current form, accommodates only one complete two species interaction experiment, throughput can be improved in two ways. Parallelized experiments using additional co-culture plates in conjunction with miniaturized plate readers (165) allows for the collection of endpoint metabolomics samples. As for experiments that do not require such culture volumes, the current co-culture plate design could be scaled down to a format with a greater number of smaller wells. This redesign would be optimized for rapid assays to identify biologically interesting pairs. Additional limitations of the proposed co-culture plate include the restriction to batch culture experiments, and the lack of being able to assess contact-dependent interactions due to physical separation with the membrane.

We have presented a novel co-culture plate that utilizes a vertical membrane to maintain physical separation between two cultures, yet allows for contact-independent interactions. This culture plate allows for high-throughput and high-resolution phenotypic assessment of microbial interactions. As well as interfacing with currently available plate readers, thus allowing for the rapid generation of optical density growth curves.

Availability

The parts list, technical drawings, experimental data, and code are all available in the Supplement and Supplemental Data. Supplemental Data is located at: https://github.com/csbl/CoculturePlate

Acknowledgements

Nick Anselmo for writing the CNC Machine G-code and machining the parts for the co-culture plate.

Conflict of Interest

The authors declare no conflict of interest.

Funding

TM, JCP, MB, GM, GK, and JP are supported by R01 grant GM108501 from the National Institutes of Health. GM is also supported by NIH T32LM012416. TM is also supported by National Science Foundation Graduate Research Fellowship Program.

5.6 Supplement

Parts List

The parts list for one complete co-culture plate:

1. (8) 25 mm EMD Millipore 0.1 µm Isopore polycarbonate membranes (Fisher)
2. (1) Polypropylene Stock (1/2” thickness machined to size) (McMaster-Carr, Part No. 8782K73)
3. (48) 0-80, 9/16" Fully Threaded 18-8 Stainless Steel Socket Cap Screw (McMaster-Carr)
4. (64) No. 0, 0.062" ID, 0.156" OD 18-8 Stainless Steel Flat Washer (McMaster-Carr)
5. (12) 1-64, 3/8" 18-8 Stainless Steel Socket Head Screw (McMaster-Carr)
6. (12) 1-64, 3/16" 18-8 Stainless Steel Button Head Screw (McMaster-Carr)
7. Food-Grade High-Temperature Silicone Sheet (60A) with Acrylic Adhesive Back (custom laser cut gaskets) (McMaster-Carr, Part No. 86045K67)
8. Smooth Finish, 0.02", Transparent, Impact-Resistant Polycarbonate Sheet (cut to size with waterjet) (McMaster-Carr, Part No. 85585K17)
9. (1) Breathe-Easy ® membrane, sterile (Sigma Aldrich)

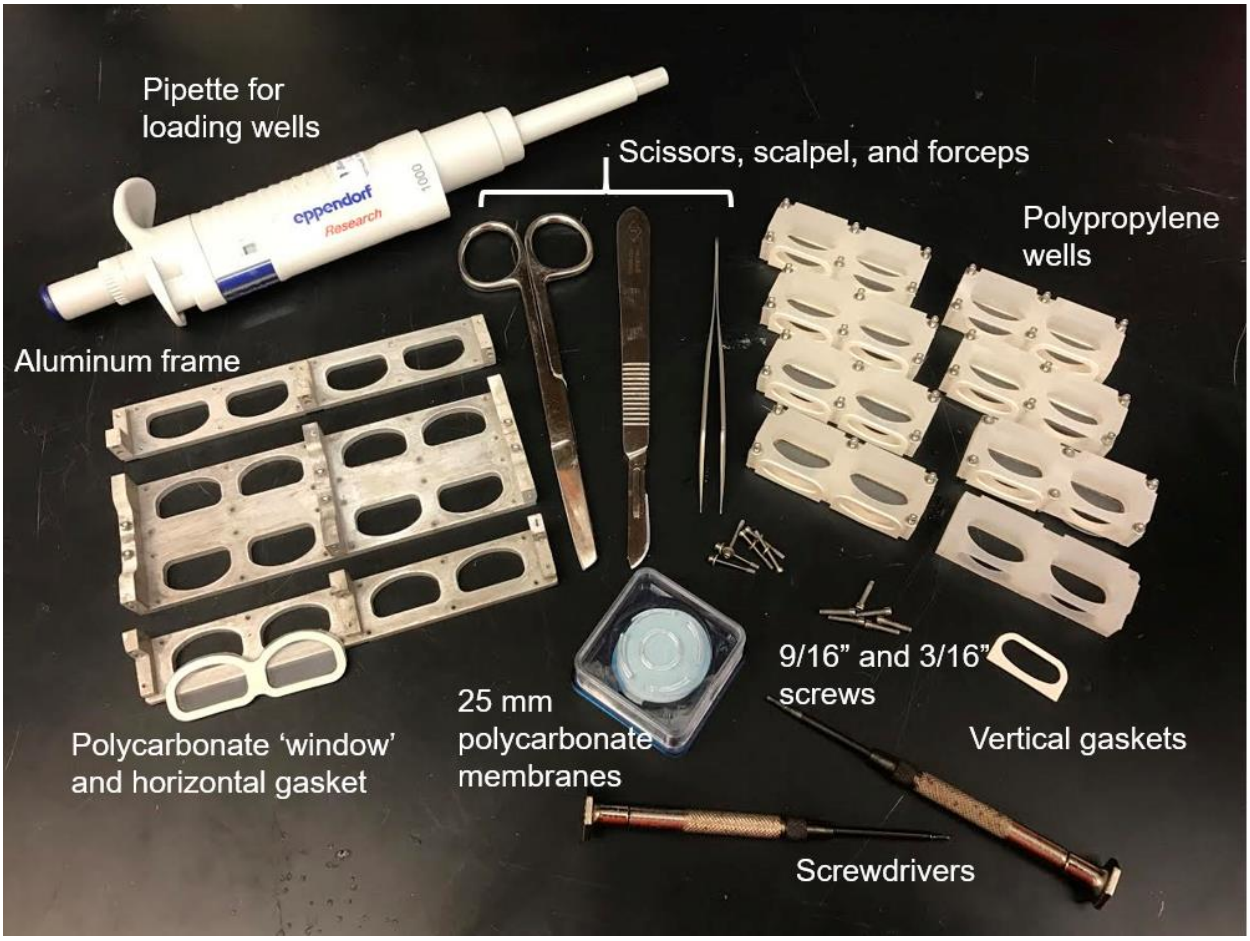

Figure S5.1. Co-culture plate parts and tools used for one complete plate.

Detailed Description of Co-culture Plate Design

Throughout this technical description, the term 'chamber' will refer to an entity consisting of two 'wells' separated by a semipermeable membrane. Thus, the fully assembled device houses 8 co-culture chambers each consisting of 2 individual wells for a total of 16 wells on the device. The disassembled device consists of 3 major parts: an 8-well central part and two 4-well side parts. Each sided part is secured to the central part by 3 stainless steel 1-64, 3/16" 18-8 stainless steel screws for a total of 6 horizontal screws (see video for visualization). The base components of the central and side parts are made of machined aluminum. Each well is made of polypropylene. All discussed parts can be autoclaved and cleaned with 70% ethanol.

During assembly, silicone gaskets are secured via acrylic adhesive around the longitudinal face of each well which uniformly clamp the polycarbonate membrane and to a clear polycarbonate well-bottoms (windows) which are placed under each well to provide a transparent bottom surface of each well for transmission based spectrophotometry. The vertically-oriented membrane is situated between 2 gaskets and secured in place when the side parts are secured to the central part. This design of the co-culture plate results in a slightly variable dimension along the short edge of the plate due to the horizontal clamping mechanism and variability in the compression of the silicone gaskets between the wells. This variation in the plate width does impact the alignment of the wells because the reading locations of the wells for a 96-well plate are within the perimeter of the co-culture plate wells.

Disassembly allows for replacement of the gaskets, when necessary, and facilitates the application of semipermeable membranes between the wells. Every part of the device is reusable with the exception of the polycarbonate membranes which need to be replaced with every use.

A video demonstrating the assembly of the co-culture plate is located at:

https://www.youtube.com/watch?v=ic3vFLgMHLo

Detailed Description of Co-culture Plate Machining

All of the SolidWorks parts and assembly files are provided in the Supplemental and at:

https://github.com/csbl/CoculturePlate

Detailed Co-culture Plate Culture Protocol

Please find a complete protocol for sterilization, assembly, and plate loading below:

I. STERILIZATION

Before each experiment:

1. Assemble plate by applying all gaskets and bolts to hold wells and well bottoms in place.
2. Assure that the vertical bolts holding the polypropylene wells to the aluminum baseplate are loose, to ensure the polypropylene does not deform in autoclave due to applied tension. Steam autoclave the central and side parts at 121°C for 60 minutes in separate autoclave bags with the gaskets facing away from each other to eliminate the possibility of the gaskets adhering to each other during the autoclaving process (the non-adhesive sides of cleaned silicone will adhere due to strong Van der Waal forces if autoclaved while in contact with each other).
3. Tools and bolts can be cleaned with 70% ethanol.
4. With clean scissors, trim approximately 4 mm from the bottom of 8 circular 25 mm membranes and place in a sterile shallow dish of 70% ethanol for 10 minutes prior to use. The flat edge of the membrane will eventually be positioned along bottom edge of the well (See video).
    a. Warning: avoid touching the central portion of the membrane to avoid damaging the area essential for allowing diffusion.
    b. Membranes were ethanol-sterilized as opposed to autoclaved because autoclaving reduces the passive diffusion through the membrane and surface hydrophobicity. Data not shown.

II. ASSEMBLY

Under biosafety hood:

1. Allow to cool and remove parts from autoclave packaging. Using proper sterile technique, uniformly tighten vertical bolts around wells to create seal with bottom gaskets. Ensure each part is placed on a sterile surface (such as the inside surface of the autoclave bag after the plastic covering has been removed).
2. Using tweezers, remove membranes from ethanol dish and place on side gaskets such that the straight cut edge aligns with the bottom of the well.
3. Carefully align and clamp side part on with 1-64, 3/8" 18-8 stainless steel socket head cap machine screws (6 total for both sides). Repeat with the other side.
4. Notice that the membranes extend above the height of the device, these will interfere with the Breathe-Easy membrane. Using the tweezers to apply slight tension to the membranes, use a scalpel to trim the membranes to be flush with the tops of the wells. This will allow the Breathe-Easy membrane to be secured to the top face of the device with minimal discontinuities. Inspect membranes and gaskets for any deformity and adjust if necessary.

5. Let ethanol evaporate from membranes (approximately 10 minutes) and proceed to plate loading.

III. LOADING

The ideal volume for each well is 2 mL to prevent contact with the Breathe-Easy membrane and formation of bubbles. Wells can then be inoculated with cell according to standard microbiology protocols. The Breathe-Easy membrane then stuck to the top surface avoiding wrinkles. The membrane is slit using a scalpel blade for each well to avoid suctioning of the membrane and contact with the below culture. Care must be taken to ensure no cross-contamination occurs as a result of making the slits. The blade can be clean with 70% ethanol when necessary between wells. The co-culture plate can then be placed in a standard 96 well plate reader. The total setup time for an experiment take approximately 2 hours accounting for autoclave time.

Growth in the Co-culture plate

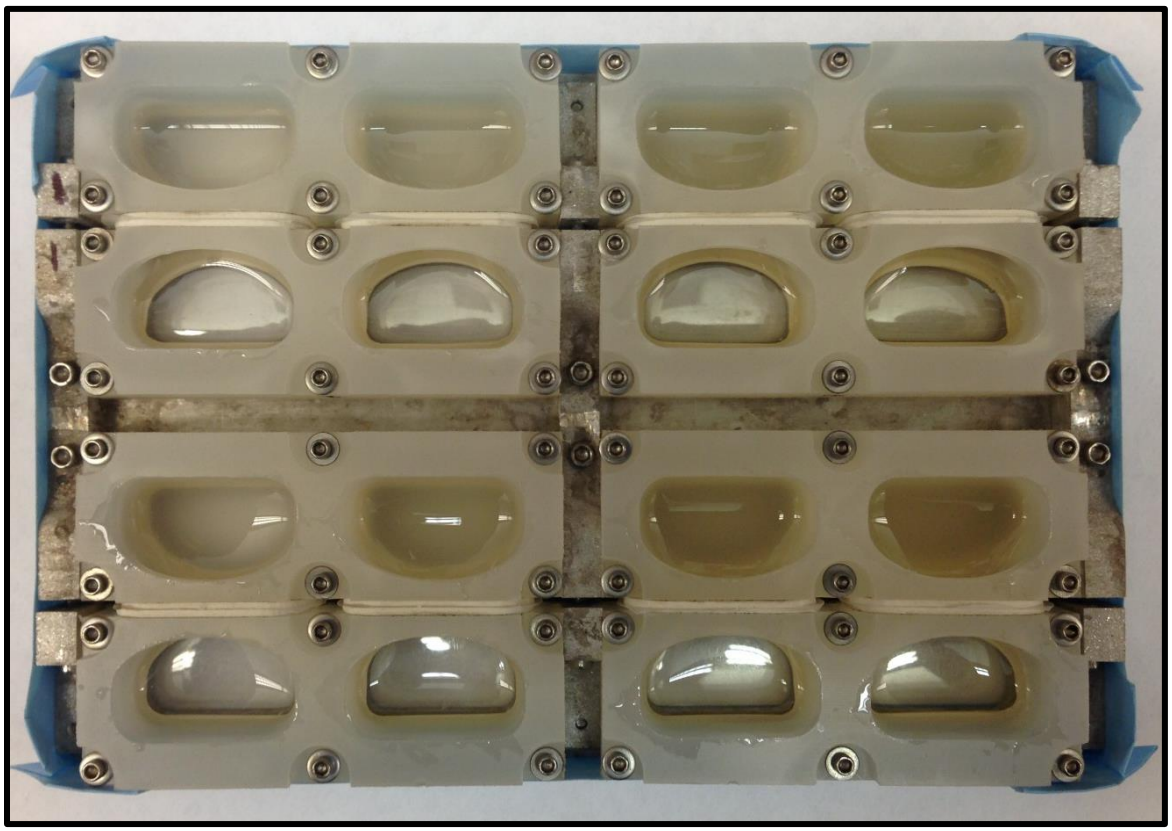

Figure S5.2. Endpoint image of co-culture plate after representative experiment from Figure 5.2. *Note that the lower wells are all void of bacterial growth, while the well on the other side of the membrane is inoculated with an active culture of E. coli. Sterility of the wells is maintained by the membranes.*

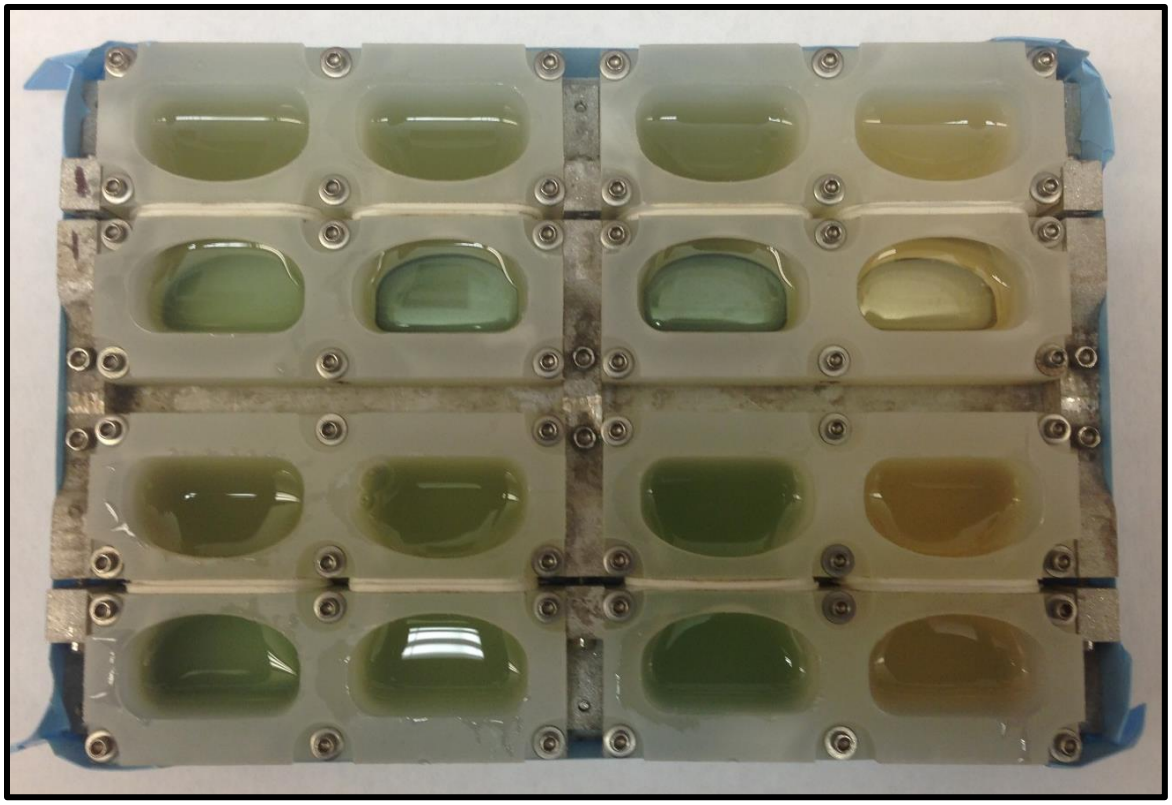

Figure S5.3. Co-culture of P. aeruginosa and B. Cenocepacia. *Well 1a is PA, 1b is BC, 5a and 5b are a technical replicate of that, these are the experimental co-cultures. Wells 3a and 3b are the isolated condition of PA, 7a and 7b are the competing condition. Wells 4a and 4b are the isolated condition of BC, 8a and 8b are the competing condition. Wells 2a, 2b, 6a, and 6b are the isolated and competing conditions for PA and BC mixed, these data are not presented in the manuscript. P. aeruginosa shows clear production of pyoverdine (green pigment) in the chambers it's cultured in. The production of pyoverdine has been previously reported (166).*

Chapter 6 Contributions, Future work, and Discussion

Here I discuss each of the unique contributions I have made during my dissertation and the future work that will occur or as already occurred resulting from my efforts.

6.1 Contributions and Future Work

Chapter 2 and 3: Aim 1

In my first aim, I identified the top 12 metabolites that have the greatest potential to diagnose infants that are at risk of developing PNAC. These metabolites are readily measurable in the infant stool and will likely be identifiable via existing detection technologies that can be implemented at the point of care. The future progress of this aim may ultimately result in a diagnostic test that is used in the NICU to improve infant health outcomes. In a broader context, the concept behind this type of diagnostic test is a, surprisingly, novel technique that is not currently utilized in the NICU. There are no common diagnostic techniques that are currently used in the NICU that rely on testing stool samples. However, the NICU may be one of the best areas of medicine to implement this type of technology because the nutritional inputs for infants are tightly regulated, thus providing additional information that can be utilized when analyzing waste products.

Chapter 4: Aim 2

In my second aim, I developed a method (CANYUNs) that allows for the efficient procedural generation of GENREs. This method emphasizes the difference between a metabolic network reconstruction and context specific predictive models that can be established based on an organism specific network and the biological evidence that is available.

The next step in this line of work is to generate additional data to further extend the CANYUNs concept. Currently, CANYUNs is capable of quantifying uncertainty in reaction selection for network building when utilizing genomic data. However, transcriptomics and metabolomics data also offer a great deal more information about the reactions that may be active in a given growth condition. I have

already generating paired metabolomics and transcriptomics data for *E. coli* Nissle growing anaerobic in 9 distinct minimal media growth conditions. Each carbon source present in the media conditions is present in the mucus layer of the human GI tract. These data will allow for the extension of CANYUNs to incorporate two additional data types that are exceptionally important for understanding metabolism. All cultures were anaerobic to increase the overall mass of carbon that results as fermentation byproducts, opposed to carbon dioxide.

Chapter 5: Aim 3

In my third aim, I designed and developed an experimental tool for the pairwise co-culture of bacterial liquid cultures. This device provides a unique method for co-culturing bacteria to investigate the contact-independent interactions that occur between two different types of bacteria. We validated and demonstrated the value of this device.

Following the publication of this work, I went on to redesign the plate to make several improvements (Figure 6.1). The primary improvement I made was to reduce the number of parts required for the manufacturing of the device. Furthermore, we applied for a provisional patent application through the UVA licensing and venture group (LVG).

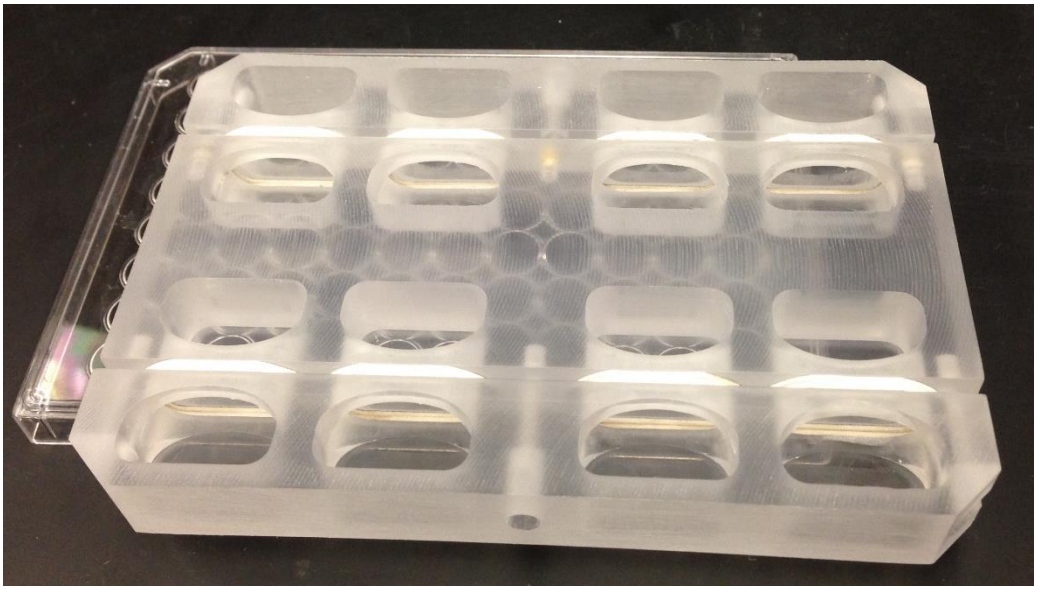

Figure 6.1: Version 2 of the Co-culture Plate.

The second version of the co-culture plate has fewer parts and requires much less time to build, clean, and assemble.

6.2 Concluding Dissertation Discussion

My dissertation has centered around my passion for developing tools that solve unique, yet important, problems. Diagnosing diseases in the NICU by utilizing waste materials, rather than limited blood samples, is a type of diagnostic technology that has yet to reach the clinic. The procedural generation of GENREs when using CANYUNs results in structurally unique metabolic networks that are designed to accelerate the field toward the generation of more accurate community modeling. Finally, the co-culture plate is a completely novel experimental tool that provides the research with unique data for studying microbial interactions, a much-needed data type for understanding microbial community dynamics. All three of my aims focus on the development of tools that will improve our understanding of human associated microbiomes.

Engineering tools: My philosophy as an engineer

Engineers create solutions for problems, often times the solution takes the form of a tool. Typically, the best way to solve a problem involves identifying the root cause and finding an optimal way

to resolve it. During the optimization process there are often times competing constraints and objectives that need to be considered. Effectively, this means that developing tools is an iterative process of design and testing providing engineers with necessary information to solve a problem.

Computational modeling has become an absolutely essential aspect of engineering. Through the use of computational power, engineers today are able to perform complex calculations that were never even dreamt of before computers were conceptualized. As student, I am able to access computational modeling tools that allow me to model and simulate the fluid dynamics of mechanic systems as complex as jets that consist of millions of individual parts. Just as we are able to model complex mechanical systems interacting with the external environment, I dream of the day when we will be able to apply computational modeling to complex biological systems with enough accuracy to be applied on an individual level in the clinic.

Pushing GENREs toward the clinic

Systems biology and specifically quantitative computational modeling are two tools that are beginning to demonstrate their utility in the medical field. Human physiology is complex and is increasingly demanding more sophisticated tools to continue progress toward eradicating diseases. An important path to engaging more engineers in the development of medical treatments and technology is, in part, developing computational modeling tools to predict how biological systems behave.

GENREs are tools that will provide direct utility in the clinic for diagnosing complex diseases. Metabolism is one of the most foundational aspects of life; the study of how metabolites are enzymatically broken down and then utilized for the building blocks of life. The study of prokaryotic organisms is a logical starting point for designing GENRE tools and methods because the governing objectives of single cellular life is far simpler than mammalian cells. It is often enough to assume that a bacterial population is metabolizing a nutrient source in order to maximize growth, the production of

cellular biomass. The complexity of studying bacteria comes from trying to understand how they are behaving as an ecosystem in the context of human health. There is beauty in the fact that the most genetically complex 'organ' in the human body may also be the access point through which GENREs and systems biology are introduced to clinical medicine.

An Ode to Systems Biology

I think it is fitting to end this dissertation by exploring why the concept of systems biology has captured my attention for the past 5 years. As a biomedical engineer with a deep interest in the GI microbiome, I identified that the field of systems biology encompasses many existing tools that have been designed to turn complex biological data into interpretable knowledge about biology. There appear two distinct phases of biology that have dominated the field through history. First the characterization of organisms that have evolved across the ecosystems of the globe, and second the study of biological mechanisms through reductionism. The application of advanced mathematics such as optimization, graph theory, and machine learning have connected the two foci of biology. We are now able to leverage all of the known foundational biological information that was painstakingly collected via reductionist techniques to better understand the governing mechanisms of complex biological systems. These techniques, when paired with high-throughput data collection, are a fruitful path forward for solving some of the greatest evolutionary challenges the humanity has faced for millennia. I feel fortunate to have happened upon constraints-based computational modeling. Within systems biology, the logical framework that I have established for this area of study seems to be a powerful way of viewing biology in general. Evolution is functionally an optimization problem; there is great potential and utility in trying to understand the constraints and objectives that govern the evolution of organisms.

6.3 Publications

Moutinho TJ Jr, Papin JA, Powers DA, Levy S, Baveja R, Hefner I, Mohamed M, Abdelghani A, Baker R, Moore SR, Hourigan SK. Stool metabolome early predictors of infants who will develop parenteral

nutrition associated cholestasis. Journal of Pediatric Gastroenterology and Nutrition. (July 2021 Submission).

Moutinho TJ Jr, Neubert BC, Jenior ML, Papin JA. Quantifying cumulative phenotypic and genomic evidence for the presence of biochemical reactions in predictive prokaryotic metabolic network models. PLOS Computational Biology. (July 2021 Submission).

Luzader DH, Fawad JA, **Moutinho TJ Jr,** Mitchell PG, Brown-Steinke K, Zhao JY, Rosselot AE, McKinney CA, Hong CI, Chou CJ, Papin JA, Moore SR. Histone deacetylase inhibition by gut microbe-generated short chain fatty acids entrains intestinal epithelial circadian rhythms. Gastroenterology. (Submitted 2020).

Moutinho TJ Jr, Neubert BC, Jenior ML, Carey MA, Medlock GL, Kolling GL, Papin JA. Functional Genome scale metabolic analysis of probiotic lactobacillus species. BioRxiv. (2019)

Jenior ML, **Moutinho TJ Jr**, Dougherty BV, Papin JA. Transcriptome-guided parsimonious flux analysis improves predictions with metabolic networks in complex environments. PLOS Computational Biology. (2020).

Moutinho TJ Jr*, Hourigan S*, Berenz A, Papin JA, Guha P, Bangiolo L, Oliphant S, Baveja R, Baker R, Vilboux T, Levy S, Deopujari V, Nataro J, Niederhuber J, Moore SR. Gram-negative Microbiota Blooms in Premature Twins Discordant for Parenteral Nutrition-associated Cholestasis. Journal of Pediatric Gastroenterology and Nutrition. (2020). (* Co-first Authors)

Moutinho TJ Jr, Panagides JC, Biggs MB, Medlock GL, Kolling GL, Papin JA. Novel co-culture plate enables growth dynamic-based assessment of contact-independent microbial interactions. PLOS One (2017).

Moutinho TJ Jr*, Dougherty B*, Papin JA. Accelerating the drug development pipeline with genome-scale metabolic network reconstructions, in Systems Biology, ed. Stefan Hohmann, Jens Nielsen. Wiley Biotechnology. (2016). (* Co-first Authors)

Biggs MB, Medlock GL, **Moutinho TJ Jr**, Lees HJ, Swann JR, Kolling GL, Papin JA. Systems-level metabolism of the altered Schaedler flora, a complete gut microbiota. The ISME Journal. (2016). (Top Ten Article Downloads, December 2016)

References

1. Sender R, Fuchs S, Milo R. Revised Estimates for the Number of Human and Bacteria Cells in the Body. PLOS Biol. 2016 Aug 19;14(8):e1002533.

2. Savage DC. Microbial Ecology of the Gastrointestinal Tract. Annu Rev Microbiol. 1977;31(1):107–33.

3. Grice EA, Segre JA. The skin microbiome. Nat Rev Microbiol. 2011 Apr;9(4):244–53.

4. Romero R, Hassan SS, Gajer P, Tarca AL, Fadrosh DW, Nikita L, et al. The composition and stability of the vaginal microbiota of normal pregnant women is different from that of non-pregnant women. Microbiome. 2014 Feb 3;2(1):4.

5. Cui L, Morris A, Huang L, Beck JM, Twigg HL, von Mutius E, et al. The Microbiome and the Lung. Ann Am Thorac Soc. 2014 Aug 1;11(Supplement 4):S227–32.

6. Moffatt MF, Cookson WO. The lung microbiome in health and disease. Clin Med. 2017 Dec;17(6):525–9.

7. Tierney BT, Yang Z, Luber JM, Beaudin M, Wibowo MC, Baek C, et al. The landscape of genetic content in the gut and oral human microbiome. Cell Host Microbe. 2019;26(2):283–95.

8. Gaci N, Borrel G, Tottey W, O'Toole PW, Brugère J-F. Archaea and the human gut: New beginning of an old story. World J Gastroenterol WJG. 2014 Nov 21;20(43):16062–78.

9. Cui L, Morris A, Ghedin E. The human mycobiome in health and disease. Genome Med. 2013 Jul 30;5(7):63.

10. Kramer P, Bressan P. Humans as Superorganisms: How Microbes, Viruses, Imprinted Genes, and Other Selfish Entities Shape Our Behavior. Perspect Psychol Sci. 2015 Jul 1;10(4):464–81.

11. Peisl BYL, Schymanski EL, Wilmes P. Dark matter in host-microbiome metabolomics: Tackling the unknowns–A review. Anal Chim Acta. 2018 Dec 11;1037:13–27.

12. Group TNHW, Peterson J, Garges S, Giovanni M, McInnes P, Wang L, et al. The NIH Human Microbiome Project. Genome Res. 2009 Dec 1;19(12):2317–23.

13. Turnbaugh PJ, Ley RE, Hamady M, Fraser-Liggett CM, Knight R, Gordon JI. The Human Microbiome Project. Nature. 2007 Oct;449(7164):804–10.

14. Garmaeva S, Sinha T, Kurilshikov A, Fu J, Wijmenga C, Zhernakova A. Studying the gut virome in the metagenomic era: challenges and perspectives. BMC Biol. 2019 Oct 28;17(1):84.

15. Lozupone CA, Stombaugh JI, Gordon JI, Jansson JK, Knight R. Diversity, stability and resilience of the human gut microbiota. Nature. 2012 Sep 13;489(7415):220–30.

16. Qin J, Li R, Raes J, Arumugam M, Burgdorf KS, Manichanh C, et al. A human gut microbial gene catalogue established by metagenomic sequencing. Nature. 2010 Mar;464(7285):59–65.

17. Schnorr SL, Sankaranarayanan K, Lewis CM, Warinner C. Insights into human evolution from ancient and contemporary microbiome studies. Curr Opin Genet Dev. 2016 Dec 1;41:14–26.

18. Escherich Th. The Intestinal Bacteria of the Neonate and Breast-Fed Infant. Rev Infect Dis. 1988 Nov 1;10(6):1220–5.

19. Baquero F, Nombela C. The microbiome as a human organ. Clin Microbiol Infect. 2012;18(s4):2–4.

20. Clarke G, Stilling RM, Kennedy PJ, Stanton C, Cryan JF, Dinan TG. Minireview: Gut Microbiota: The Neglected Endocrine Organ. Mol Endocrinol. 2014 Aug 1;28(8):1221–38.

21. Flint HJ, Scott KP, Duncan SH, Louis P, Forano E. Microbial degradation of complex carbohydrates in the gut. Gut Microbes. 2012 Jul 14;3(4):289–306.

22. Rey FE, Gonzalez MD, Cheng J, Wu M, Ahern PP, Gordon JI. Metabolic niche of a prominent sulfate-reducing human gut bacterium. Proc Natl Acad Sci. 2013 Aug 13;110(33):13582–7.

23. Bernalier-Donadille A. Fermentative metabolism by the human gut microbiota. Gastroentérologie Clin Biol. 2010 Sep 1;34:S16–22.

24. Magnúsdóttir S, Heinken A, Kutt L, Ravcheev DA, Bauer E, Noronha A, et al. Generation of genome-scale metabolic reconstructions for 773 members of the human gut microbiota. Nat Biotechnol. 2017 Jan;35(1):81–9.

25. Bäckhed F, Ding H, Wang T, Hooper LV, Koh GY, Nagy A, et al. The gut microbiota as an environmental factor that regulates fat storage. Proc Natl Acad Sci. 2004 Nov 2;101(44):15718–23.

26. Wu H-J, Wu E. The role of gut microbiota in immune homeostasis and autoimmunity. Gut Microbes. 2012 Jan 1;3(1):4–14.

27. Buffie CG, Pamer EG. Microbiota-mediated colonization resistance against intestinal pathogens. Nat Rev Immunol. 2013 Nov;13(11):790–801.

28. Cani PD. Gut microbiota — at the intersection of everything? Nat Rev Gastroenterol Hepatol. 2017 Jun;14(6):321–2.

29. Paone P, Cani PD. Mucus barrier, mucins and gut microbiota: the expected slimy partners? Gut. 2020 Dec 1;69(12):2232–43.

30. Levy M, Kolodziejczyk AA, Thaiss CA, Elinav E. Dysbiosis and the immune system. Nat Rev Immunol. 2017 Apr;17(4):219–32.

31. Tremaroli V, Bäckhed F. Functional interactions between the gut microbiota and host metabolism. Nature. 2012 Sep;489(7415):242–9.

32. Wahlström A, Sayin SI, Marschall H-U, Bäckhed F. Intestinal Crosstalk between Bile Acids and Microbiota and Its Impact on Host Metabolism. Cell Metab. 2016 Jul 12;24(1):41–50.

33. Wouw M van de, Boehme M, Lyte JM, Wiley N, Strain C, O'Sullivan O, et al. Short-chain fatty acids: microbial metabolites that alleviate stress-induced brain–gut axis alterations. J Physiol. 2018;596(20):4923–44.

34. Cani PD, Delzenne NM. The Role of the Gut Microbiota in Energy Metabolism and Metabolic Disease. Curr Pharm Des. 2009 May 1;15(13):1546–58.

35. Wichmann A, Allahyar A, Greiner TU, Plovier H, Lundén GÖ, Larsson T, et al. Microbial Modulation of Energy Availability in the Colon Regulates Intestinal Transit. Cell Host Microbe. 2013 Nov 13;14(5):582–90.

36. Visconti A, Le Roy CI, Rosa F, Rossi N, Martin TC, Mohney RP, et al. Interplay between the human gut microbiome and host metabolism. Nat Commun. 2019;10(1):1–10.

37. Makki K, Deehan EC, Walter J, Bäckhed F. The Impact of Dietary Fiber on Gut Microbiota in Host Health and Disease. Cell Host Microbe. 2018 Jun 13;23(6):705–15.

38. Cryan JF, Dinan TG. Mind-altering microorganisms: the impact of the gut microbiota on brain and behaviour. Nat Rev Neurosci. 2012 Oct;13(10):701–12.

39. David LA, Maurice CF, Carmody RN, Gootenberg DB, Button JE, Wolfe BE, et al. Diet rapidly and reproducibly alters the human gut microbiome. Nature. 2014 Jan 23;505(7484):559–63.

40. Kelly CR, Ihunnah C, Fischer M, Khoruts A, Surawicz C, Afzali A, et al. Fecal Microbiota Transplant for Treatment of Clostridium difficile Infection in Immunocompromised Patients. Am J Gastroenterol. 2014 Jul;109(7):1065–71.

41. Redondo-Useros N, Nova E, González-Zancada N, Díaz LE, Gómez-Martínez S, Marcos A. Microbiota and Lifestyle: A Special Focus on Diet. Nutrients. 2020 Jun;12(6):1776.

42. Conlon MA, Bird AR. The Impact of Diet and Lifestyle on Gut Microbiota and Human Health. Nutrients. 2015 Jan;7(1):17–44.

43. Glowacki RWP, Martens EC. In sickness and health: Effects of gut microbial metabolites on human physiology. PLOS Pathog. 2020 Apr 9;16(4):e1008370.

44. Shaw L, Klein N. The Microbiome—The Explanation for (Almost) Everything? Pediatr Infect Dis J. 2019 Apr;38(4):e69.

45. Soo I, Madsen KL, Tejpar Q, Sydora BC, Sherbaniuk R, Cinque B, et al. VSL#3 probiotic upregulates intestinal mucosal alkaline sphingomyelinase and reduces inflammation. Can J Gastroenterol. 2008 Mar;22(3):237–42.

46. Durack J, Lynch SV. The gut microbiome: Relationships with disease and opportunities for therapy. J Exp Med. 2018 Oct 15;216(1):20–40.

47. Walsh J, Griffin BT, Clarke G, Hyland NP. Drug–gut microbiota interactions: implications for neuropharmacology. Br J Pharmacol. 2018;175(24):4415–29.

48. Modi SR, Collins JJ, Relman DA. Antibiotics and the gut microbiota. J Clin Invest. 2014 Oct 1;124(10):4212–8.

49. Lembcke, Kist, Lentze, Bruns, Gesche, Herrmann, et al. Antibiotic-Associated Diarrhea: Incidence, Risk Factors of Antibiotics and Patients, Pathophysiology and Differential Diagnosis – an Interdisciplinary Approach to a Common Problem. Praxis. 2003 Apr 1;92(16):751–9.

50. Hornung B, Martins dos Santos VAP, Smidt H, Schaap PJ. Studying microbial functionality within the gut ecosystem by systems biology. Genes Nutr. 2018 Mar 6;13(1):5.

51. Palsson B. Systems biology. Cambridge university press; 2015.

52. Larrañaga P, Calvo B, Santana R, Bielza C, Galdiano J, Inza I, et al. Machine learning in bioinformatics. Brief Bioinform. 2006 Mar 1;7(1):86–112.

53. Mathé E, Hays JL, Stover DG, Chen JL. The Omics Revolution Continues: The Maturation of High-Throughput Biological Data Sources. Yearb Med Inform. 2018 Aug;27(1):211–22.

54. Jenior ML, Jr TJM, Dougherty BV, Papin JA. Transcriptome-guided parsimonious flux analysis improves predictions with metabolic networks in complex environments. PLOS Comput Biol. 2020 Apr 16;16(4):e1007099.

55. Oberhardt MA, Palsson BØ, Papin JA. Applications of genome-scale metabolic reconstructions. Mol Syst Biol. 2009 Nov 3;5(1).

56. Diener C, Gibbons SM, Resendis-Antonio O. MICOM: Metagenome-Scale Modeling To Infer Metabolic Interactions in the Gut Microbiota. mSystems. 2020 Jan 21;5(1):e00606-19.

57. Sen P, Orešič M. Metabolic Modeling of Human Gut Microbiota on a Genome Scale: An Overview. Metabolites. 2019 Feb;9(2):22.

58. Ashley EA. Towards precision medicine. Nat Rev Genet. 2016 Sep;17(9):507–22.

59. Nielsen J. Systems Biology of Metabolism: A Driver for Developing Personalized and Precision Medicine. Cell Metab. 2017 Mar 7;25(3):572–9.

60. Braid S. The Basics of Molecular Genetic Testing in the NICU. Neonatal Netw. 2019 Oct 23;38(5):274–7.

61. Bouatra S, Aziat F, Mandal R, Guo AC, Wilson MR, Knox C, et al. The Human Urine Metabolome. PLOS ONE. 2013 Sep 4;8(9):e73076.

62. Zhgun ES, Ilina EN. Fecal Metabolites As Non-Invasive Biomarkers of Gut Diseases. Acta Naturae. 2020 Apr 1;12(2):4–14.

63. Schlaberg R. Microbiome Diagnostics. Clin Chem. 2020 Jan 1;66(1):68–76.

64. Maranas CD, Zomorrodi AR. Optimization methods in metabolic networks. John Wiley & Sons; 2016.

65. Venturelli OS, Carr AV, Fisher G, Hsu RH, Lau R, Bowen BP, et al. Deciphering microbial interactions in synthetic human gut microbiome communities. Mol Syst Biol. 2018;14(6):e8157.

66. Kim A-Y, Lim R-K, Han Y-M, Park K-H, Byun S-Y. Parenteral Nutrition-Associated Cholestasis in Very Low Birth Weight Infants: A Single Center Experience. Pediatr Gastroenterol Hepatol Nutr. 2016 Mar 22;19(1):61–70.

67. Satrom K, Gourley G. Cholestasis in Preterm Infants. Clin Perinatol. 2016 Jun 1;43(2):355–73.

68. Mangalat N, Bell C, Graves A, Imseis EM. Natural history of conjugated bilirubin trajectory in neonates following parenteral nutrition cessation. BMC Pediatr. 2014 Dec 10;14(1):298.

69. Christensen RD, Henry E, Wiedmeier SE, Burnett J, Lambert DK. Identifying patients, on the first day of life, at high-risk of developing parenteral nutrition-associated liver disease. J Perinatol Off J Calif Perinat Assoc. 2007 May;27(5):284–90.

70. Park HW, Lee NM, Kim JH, Kim KS, Kim S-N. Parenteral Fish Oil–Containing Lipid Emulsions May Reverse Parenteral Nutrition–Associated Cholestasis in Neonates: A Systematic Review and Meta-Analysis. J Nutr. 2015 Feb 1;145(2):277–83.

71. Cahova M, Bratova M, Wohl P. Parenteral Nutrition-Associated Liver Disease: The Role of the Gut Microbiota. Nutrients. 2017 Sep 7;9(9):987.

72. Li Y, Tang R, Leung PSC, Gershwin ME, Ma X. Bile acids and intestinal microbiota in autoimmune cholestatic liver diseases. Autoimmun Rev. 2017 Sep 1;16(9):885–96.

73. Lee WS, Sokol RJ. Intestinal Microbiota, Lipids, and the Pathogenesis of Intestinal Failure–Associated Liver Disease. J Pediatr. 2015 Sep 1;167(3):519–26.

74. Bajaj JS, Heuman DM, Hylemon PB, Sanyal AJ, White MB, Monteith P, et al. Altered profile of human gut microbiome is associated with cirrhosis and its complications. J Hepatol. 2014 May 1;60(5):940–7.

75. Tang R, Wei Y, Li Y, Chen W, Chen H, Wang Q, et al. Gut microbial profile is altered in primary biliary cholangitis and partially restored after UDCA therapy. Gut. 2018 Mar 1;67(3):534–41.

76. Wang P, Wang Y, Lu L, Yan W, Tao Y, Zhou K, et al. Alterations in intestinal microbiota relate to intestinal failure-associated liver disease and central line infections. J Pediatr Surg. 2017 Aug 1;52(8):1318–26.

77. Khalil S, Shah D, Faridi MMA, Kumar A, Mishra K. Prevalence and Outcome of Hepatobiliary Dysfunction in Neonatal Septicaemia. J Pediatr Gastroenterol Nutr. 2012 Feb;54(2):218–222.

78. Sieniawska M, Wróblewska-Kaluzewska M, Nalecz A, Korniszewska J, Tolloczko I, Wierzbowska-Lange B. Hyperbilirubinemia in infants with urinary tract infection. Pol Med Sci Hist Bull. 1976 Jan 1;15(1):79–81.

79. Repa A, Lochmann R, Unterasinger L, Weber M, Berger A, Haiden N. Aggressive nutrition in extremely low birth weight infants: impact on parenteral nutrition associated cholestasis and growth. PeerJ. 2016 Sep 20;4:e2483.

80. Fawaz R, Baumann U, Ekong U, Fischler B, Hadzic N, Mack CL, et al. Guideline for the Evaluation of Cholestatic Jaundice in Infants: Joint Recommendations of the North American Society for Pediatric Gastroenterology, Hepatology, and Nutrition and the European Society for Pediatric Gastroenterology, Hepatology, and Nutrition. J Pediatr Gastroenterol Nutr. 2017 Jan;64(1):154–168.

81. Rothschild D, Weissbrod O, Barkan E, Kurilshikov A, Korem T, Zeevi D, et al. Environment dominates over host genetics in shaping human gut microbiota. Nature. 2018 Mar;555(7695):210–5.

82. Callahan BJ, McMurdie PJ, Rosen MJ, Han AW, Johnson AJA, Holmes SP. DADA2: High-resolution sample inference from Illumina amplicon data. Nat Methods. 2016 Jul;13(7):581–3.

83. Callahan BJ, McMurdie PJ, Holmes SP. Exact sequence variants should replace operational taxonomic units in marker-gene data analysis. ISME J. 2017 Dec;11(12):2639–43.

84. Wang Q, Garrity GM, Tiedje JM, Cole JR. Naïve Bayesian Classifier for Rapid Assignment of rRNA Sequences into the New Bacterial Taxonomy. Appl Env Microbiol. 2007 Aug 15;73(16):5261–7.

85. McMurdie PJ, Holmes S. phyloseq: An R Package for Reproducible Interactive Analysis and Graphics of Microbiome Census Data. PLOS ONE. 2013 Apr 22;8(4):e61217.

86. Wickham H. ggplot2: Elegant Graphics for Data Analysis. Springer; 2016. 266 p.

87. Harris JK, Kasmi KCE, Anderson AL, Devereaux MW, Fillon SA, Robertson CE, et al. Specific Microbiome Changes in a Mouse Model of Parenteral Nutrition Associated Liver Injury and Intestinal Inflammation. PLOS ONE. 2014 Oct 20;9(10):e110396.

88. Kasirer Y, Bin-Nun A, Raveh A, Schorrs I, Mimouni FB, Hammerman C. SMOFlipid Protects Preterm Neonates against Perinatal Nutrition-Associated Cholestasis. Am J Perinatol. 2019 Nov;36(13):1382–6.

89. Casson C, Nguyen V, Nayak P, Channabasappa N, Berris K, Panczuk J, et al. A Comparison of Smoflipid® and Intralipid® in the Early Management of Infants with Intestinal Failure. J Pediatr Surg. 2020 Jan;55(1):153–7.

90. Hourigan SK, Moutinho TJ, Berenz A, Papin J, Guha P, Bangiolo L, et al. Gram-negative microbiota blooms in premature twins discordant for parenteral nutrition associated cholestasis. J Pediatr Gastroenterol Nutr. 2020 May;70(5):640–4.

91. Bock J, Liebisch G, Schweimer J, Schmitz G, Rogler G. Exogenous sphingomyelinase causes impaired intestinal epithelial barrier function. World J Gastroenterol WJG. 2007 Oct 21;13(39):5217–25.

92. Qi Y, Jiang C, Cheng J, Krausz KW, Li T, Ferrell JM, et al. Bile acid signaling in lipid metabolism: Metabolomic and lipidomic analysis of lipid and bile acid markers linked to anti-obesity and anti-diabetes in mice. Biochim Biophys Acta. 2015 Jan;1851(1):19–29.

93. Kurek K, Łukaszuk B, Piotrowska DM, Wiesiołek P, Chabowska AM, Żendzian-Piotrowska M. Metabolism, Physiological Role, and Clinical Implications of Sphingolipids in Gastrointestinal Tract. BioMed Res Int. 2013 Sep 5;2013:e908907.

94. Loftfield E, Vogtmann E, Sampson JN, Moore SC, Nelson H, Knight R, et al. Comparison of Collection Methods for Fecal Samples for Discovery Metabolomics in Epidemiologic Studies. Cancer Epidemiol Prev Biomark. 2016 Nov 1;25(11):1483–90.

95. Zierer J, Jackson MA, Kastenmüller G, Mangino M, Long T, Telenti A, et al. The fecal metabolome as a functional readout of the gut microbiome. Nat Genet. 2018 Jun;50(6):790–5.

96. Evans AM, Bridgewater B, Liu Q, Mitchell M, Robinson R, Dai H, et al. High resolution mass spectrometry improves data quantity and quality as compared to unit mass resolution mass spectrometry in high-throughput profiling metabolomics. Metabolomics. 2014;4(2):1.

97. Ford L, Kennedy AD, Goodman KD, Pappan KL, Evans AM, Miller LAD, et al. Precision of a Clinical Metabolomics Profiling Platform for Use in the Identification of Inborn Errors of Metabolism. J Appl Lab Med. 2020 Mar 1;5(2):342–56.

98. Evans AM, DeHaven CD, Barrett T, Mitchell M, Milgram E. Integrated, nontargeted ultrahigh performance liquid chromatography/electrospray ionization tandem mass spectrometry platform for the identification and relative quantification of the small-molecule complement of biological systems. Anal Chem. 2009;81(16):6656–67.

99. DeHaven CD, Evans AM, Dai H, Lawton KA. Organization of GC/MS and LC/MS metabolomics data into chemical libraries. J Cheminformatics. 2010;2(1):1–12.

100. Clemente JC, Ursell LK, Parfrey LW, Knight R. The Impact of the Gut Microbiota on Human Health: An Integrative View. Cell. 2012 Mar 16;148(6):1258–70.

101. Galland L. The Gut Microbiome and the Brain. J Med Food. 2014 Dec;17(12):1261–72.

102. Gopalakrishnan V, Helmink BA, Spencer CN, Reuben A, Wargo JA. The Influence of the Gut Microbiome on Cancer, Immunity, and Cancer Immunotherapy. Cancer Cell. 2018 Apr 9;33(4):570–80.

103. Zhu B, Wang X, Li L. Human gut microbiome: the second genome of human body. Protein Cell. 2010 Aug 1;1(8):718–25.

104. Nicholson JK, Holmes E, Kinross J, Burcelin R, Gibson G, Jia W, et al. Host-Gut Microbiota Metabolic Interactions. Science. 2012 Jun 8;336(6086):1262–7.

105. Orth JD, Thiele I, Palsson BØ. What is flux balance analysis? Nat Biotechnol. 2010 Mar;28(3):245–8.

106. Thiele I, Vlassis N, Fleming RMT. fastGapFill: efficient gap filling in metabolic networks. Bioinformatics. 2014 Sep 1;30(17):2529–31.

107. Machado D, Andrejev S, Tramontano M, Patil KR. Fast automated reconstruction of genome-scale metabolic models for microbial species and communities. Nucleic Acids Res. 2018 Sep 6;46(15):7542–53.

108. Mundy M, Mendes-Soares H, Chia N. Mackinac: a bridge between ModelSEED and COBRApy to generate and analyze genome-scale metabolic models. Bioinformatics. 2017 Aug 1;33(15):2416–8.

109. Seaver SMD, Liu F, Zhang Q, Jeffryes J, Faria JP, Edirisinghe JN, et al. The ModelSEED Biochemistry Database for the integration of metabolic annotations and the reconstruction, comparison and analysis of metabolic models for plants, fungi and microbes. Nucleic Acids Res. 2021 Jan 8;49(D1):D575–88.

110. Thiele I, Palsson BØ. A protocol for generating a high-quality genome-scale metabolic reconstruction. Nat Protoc. 2010 Jan;5(1):93–121.

111. Kumar VS, Maranas CD. GrowMatch: an automated method for reconciling in silico/in vivo growth predictions. PLoS Comput Biol. 2009;5(3).

112. King B, Farrah T, Richards MA, Mundy M, Simeonidis E, Price ND. ProbAnnoWeb and ProbAnnoPy: probabilistic annotation and gap-filling of metabolic reconstructions. Bioinformatics. 2018 May 1;34(9):1594–6.

113. Schellenberger J, Park JO, Conrad TM, Palsson BØ. BiGG: a Biochemical Genetic and Genomic knowledgebase of large scale metabolic reconstructions. BMC Bioinformatics. 2010;11(1):213.

114. Norsigian CJ, Pusarla N, McConn JL, Yurkovich JT, Dräger A, Palsson BO, et al. BiGG Models 2020: multi-strain genome-scale models and expansion across the phylogenetic tree. Nucleic Acids Res. 2020 Jan 8;48(D1):D402–6.

115. Schmidt BJ, Ebrahim A, Metz TO, Adkins JN, Palsson BØ, Hyduke DR. GIM3E: condition-specific models of cellular metabolism developed from metabolomics and expression data. Bioinformatics. 2013 Nov 15;29(22):2900–8.

116. Gama-Castro S, Salgado H, Santos-Zavaleta A, Ledezma-Tejeida D, Muñiz-Rascado L, García-Sotelo JS, et al. RegulonDB version 9.0: high-level integration of gene regulation, coexpression, motif clustering and beyond. Nucleic Acids Res. 2016 Jan 4;44(D1):D133–43.

117. Monk JM, Lloyd CJ, Brunk E, Mih N, Sastry A, King Z, et al. iML1515, a knowledgebase that computes Escherichia coli traits. Nat Biotechnol. 2017 Oct 11;35(10):904–8.

118. Keseler IM, Mackie A, Santos-Zavaleta A, Billington R, Bonavides-Martínez C, Caspi R, et al. The EcoCyc database: reflecting new knowledge about Escherichia coli K-12. Nucleic Acids Res. 2017 Jan 4;45(D1):D543–50.

119. Keseler IM, Collado-Vides J, Santos-Zavaleta A, Peralta-Gil M, Gama-Castro S, Muñiz-Rascado L, et al. EcoCyc: a comprehensive database of Escherichia coli biology. Nucleic Acids Res. 2011 Jan;39(Database issue):D583–90.

120. González-Pech RA, Stephens TG, Chan CX. Commonly misunderstood parameters of NCBI BLAST and important considerations for users. Bioinformatics. 2019 Aug 1;35(15):2697–8.

121. Pearson WR. An Introduction to Sequence Similarity ("Homology") Searching. Curr Protoc Bioinforma. 2013;42(1):3.1.1-3.1.8.

122. Gibbons TR, Mount SM, Cooper ED, Delwiche CF. Evaluation of BLAST-based edge-weighting metrics used for homology inference with the Markov Clustering algorithm. BMC Bioinformatics. 2015 Jul 10;16(1):218.

123. Lewis NE, Hixson KK, Conrad TM, Lerman JA, Charusanti P, Polpitiya AD, et al. Omic data from evolved E. coli are consistent with computed optimal growth from genome-scale models. Mol Syst Biol. 2010 Jul 27;6:390.

124. Leatham MP, Banerjee S, Autieri SM, Mercado-Lubo R, Conway T, Cohen PS. Precolonized Human Commensal Escherichia coli Strains Serve as a Barrier to E. coli O157:H7 Growth in the Streptomycin-Treated Mouse Intestine. Infect Immun. 2009 Jul 1;77(7):2876–86.

125. Altenhoefer A, Oswald S, Sonnenborn U, Enders C, Schulze J, Hacker J, et al. The probiotic Escherichia coli strain Nissle 1917 interferes with invasion of human intestinal epithelial cells by different enteroinvasive bacterial pathogens. FEMS Immunol Med Microbiol. 2004 Apr 1;40(3):223–9.

126. Maltby R, Leatham-Jensen MP, Gibson T, Cohen PS, Conway T. Nutritional Basis for Colonization Resistance by Human Commensal Escherichia coli Strains HS and Nissle 1917 against E. coli O157:H7 in the Mouse Intestine. PLOS ONE. 2013 Jan 17;8(1):e53957.

127. Fritzemeier CJ, Hartleb D, Szappanos B, Papp B, Lercher MJ. Erroneous energy-generating cycles in published genome scale metabolic networks: Identification and removal. PLOS Comput Biol. 2017 Apr 18;13(4):e1005494.

128. Xavier JB. Social interaction in synthetic and natural microbial communities. Mol Syst Biol. 2011 Jan 1;7(1):483.

129. Braga RM, Dourado MN, Araújo WL. Microbial interactions: ecology in a molecular perspective. Braz J Microbiol. 2016 Dec;47, Supplement 1:86–98.

130. Ponomarova O, Patil KR. Metabolic interactions in microbial communities: untangling the Gordian knot. Curr Opin Microbiol. 2015 Oct;27:37–44.

131. Wright C j., Burns L h., Jack A a., Back C r., Dutton L c., Nobbs A h., et al. Microbial interactions in building of communities. Mol Oral Microbiol. 2013 Apr 1;28(2):83–101.

132. Ramsey MM, Rumbaugh KP, Whiteley M. Metabolite Cross-Feeding Enhances Virulence in a Model Polymicrobial Infection. PLOS Pathog. 2011 Mar 31;7(3):e1002012.

133. Oliveira NM, Niehus R, Foster KR. Evolutionary limits to cooperation in microbial communities. Proc Natl Acad Sci U S A. 2014 Dec 16;111(50):17941–6.

134. Goers L, Freemont P, Polizzi KM. Co-culture systems and technologies: taking synthetic biology to the next level. J R Soc Interface. 2014 Jul 6;11(96):20140065.

135. Hibbing ME, Fuqua C, Parsek MR, Peterson SB. Bacterial competition: surviving and thriving in the microbial jungle. Nat Rev Microbiol. 2010 Jan;8(1):15–25.

136. Wintermute EH, Silver PA. Dynamics in the mixed microbial concourse. Genes Dev. 2010 Dec 1;24(23):2603–14.

137. Francis MB, Allen CA, Sorg JA. Muricholic Acids Inhibit Clostridium difficile Spore Germination and Growth. PLOS ONE. 2013 Sep 9;8(9):e73653.

138. Miller MB, Bassler and BL. Quorum Sensing in Bacteria. Annu Rev Microbiol. 2001;55(1):165–99.

139. Phelan VV, Liu W-T, Pogliano K, Dorrestein PC. Microbial metabolic exchange—the chemotype-to-phenotype link. Nat Chem Biol. 2012 Jan;8(1):26–35.

140. Morris BEL, Henneberger R, Huber H, Moissl-Eichinger C. Microbial syntrophy: interaction for the common good. FEMS Microbiol Rev. 2013 May 1;37(3):384–406.

141. Linares JF, Gustafsson I, Baquero F, Martinez JL. Antibiotics as intermicrobial signaling agents instead of weapons. Proc Natl Acad Sci. 2006 Dec 19;103(51):19484–9.

142. Wintermute EH, Silver PA. Emergent cooperation in microbial metabolism. Mol Syst Biol. 2010 Jan 1;6(1):407.

143. Biggs MB, Medlock GL, Moutinho TJ, Lees HJ, Swann JR, Kolling GL, et al. Systems-level metabolism of the altered Schaedler flora, a complete gut microbiota. ISME J. 2017 Feb;11(2):426–38.

144. Traxler MF, Watrous JD, Alexandrov T, Dorrestein PC, Kolter R. Interspecies Interactions Stimulate Diversification of the Streptomyces coelicolor Secreted Metabolome. mBio. 2013 Aug 30;4(4):e00459-13.

145. Liu A, Archer AM, Biggs MB, Papin JA. Growth-altering microbial interactions are responsive to chemical context. PLOS ONE. 2017 Mar 20;12(3):e0164919.

146. Stadie J, Gulitz A, Ehrmann MA, Vogel RF. Metabolic activity and symbiotic interactions of lactic acid bacteria and yeasts isolated from water kefir. Food Microbiol. 2013 Sep;35(2):92–8.

147. Savichtcheva O, Joris B, Wilmotte A, Calusinska M. Novel FISH and quantitative PCR protocols to monitor artificial consortia composed of different hydrogen-producing Clostridium spp. Int J Hydrog Energy. 2011 Jul;36(13):7530–42.

148. Bustin SA, Beaulieu J-F, Huggett J, Jaggi R, Kibenge FS, Olsvik PA, et al. MIQE précis: Practical implementation of minimum standard guidelines for fluorescence-based quantitative real-time PCR experiments. BMC Mol Biol. 2010;11:74.

149. Boyden S. The chemotactic effect of mixtures of antibody and antigen on polymorphonuclear leucocytes. J Exp Med. 1962;115(3):453–466.

150. Nurmikko V. Microbiological Determination of Vitamins and Amino Acids Produced by Microorganisms, Using the Dialysis Cell. Appl Microbiol. 1957 May;5(3):160–5.

151. Dalgaard P, Ross T, Kamperman L, Neumeyer K, McMeekin TA. Estimation of bacterial growth rates from turbidimetric and viable count data. Int J Food Microbiol. 1994 Nov 1;23(3):391–404.

152. Jung PP, Christian N, Kay DP, Skupin A, Linster CL. Protocols and Programs for High-Throughput Growth and Aging Phenotyping in Yeast. PLOS ONE. 2015 Mar 30;10(3):e0119807.

153. Mytilinaios I, Bernigaud I, Belot V, Lambert R j. w. Microbial growth parameters obtained from the analysis of time to detection data using a novel rearrangement of the Baranyi–Roberts model. J Appl Microbiol. 2015 Jan 1;118(1):161–74.

154. Nakagawa A, Minami H, Kim J-S, Koyanagi T, Katayama T, Sato F, et al. A bacterial platform for fermentative production of plant alkaloids. Nat Commun. 2011 May 24;2:326.

155. Cope EK, Goldstein-Daruech N, Kofonow JM, Christensen L, McDermott B, Monroy F, et al. Regulation of Virulence Gene Expression Resulting from Streptococcus pneumoniae and Nontypeable Haemophilus influenzae Interactions in Chronic Disease. PLOS ONE. 2011 Dec 5;6(12):e28523.

156. Zhou K, Qiao K, Edgar S, Stephanopoulos G. Distributing a metabolic pathway among a microbial consortium enhances production of natural products. Nat Biotechnol. 2015 Apr;33(4):377–83.

157. Chen C-Y, Nace GW, Irwin PL. A 6×6 drop plate method for simultaneous colony counting and MPN enumeration of Campylobacter jejuni, Listeria monocytogenes, and Escherichia coli. J Microbiol Methods. 2003 Nov;55(2):475–9.

158. Govan JR, Deretic V. Microbial pathogenesis in cystic fibrosis: mucoid Pseudomonas aeruginosa and Burkholderia cepacia. Microbiol Rev. 1996 Sep 1;60(3):539–74.

159. Jones AM, Dodd ME, Govan JRW, Barcus V, Doherty CJ, Morris J, et al. Burkholderia cenocepacia and Burkholderia multivorans: influence on survival in cystic fibrosis. Thorax. 2004 Nov 1;59(11):948–51.

160. Eberl L, Tümmler B. Pseudomonas aeruginosa and Burkholderia cepacia in cystic fibrosis: genome evolution, interactions and adaptation. Int J Med Microbiol. 2004 Sep 24;294(2–3):123–31.

161. Schwarz S, West TE, Boyer F, Chiang W-C, Carl MA, Hood RD, et al. Burkholderia Type VI Secretion Systems Have Distinct Roles in Eukaryotic and Bacterial Cell Interactions. PLOS Pathog. 2010 Aug 26;6(8):e1001068.

162. Hanly TJ, Urello M, Henson MA. Dynamic flux balance modeling of S. cerevisiae and E. coli co-cultures for efficient consumption of glucose/xylose mixtures. Appl Microbiol Biotechnol. 2012 Mar 1;93(6):2529–41.

163. Salimi F, Mahadevan R. Characterizing metabolic interactions in a clostridial co-culture for consolidated bioprocessing. BMC Biotechnol. 2013;13:95.

164. Junicke H, Abbas B, Oentoro J, Loosdrecht M van, Kleerebezem R. Absolute Quantification of Individual Biomass Concentrations in a Methanogenic Coculture. AMB Express. 2014 Apr 12;4(1):35.

165. Jensen PA, Dougherty BV, Moutinho TJ, Papin JA. Miniaturized Plate Readers for Low-Cost, High-Throughput Phenotypic Screening. J Lab Autom. 2015 Feb 1;20(1):51–5.

166. Schalk IJ, Guillon L. Pyoverdine biosynthesis and secretion in Pseudomonas aeruginosa: implications for metal homeostasis. Environ Microbiol. 2013 Jun;15(6):1661–73.